N70-18330

Gulf General Atomic
Incorporated

GA-9909

# STUDY OF RADIATION EFFECTS IN SILICON SOLAR CELLS

---

ANNUAL REPORT

by

J. A. Naber, B. C. Passenheim, and R. A. Berger

Prepared under
Contract 952387
for the
California Institute of Technology
Jet Propulsion Laboratory
4800 Oak Grove Drive
Pasadena, California 91103

CA FILE COPY

January 23, 1970

**Gulf General Atomic**
Incorporated
*P.O. Box 608, San Diego, California 92112*

GA-9909

# STUDY OF RADIATION EFFECTS IN SILICON SOLAR CELLS

---

ANNUAL REPORT

by

J. A. Naber, B. C. Passenheim, and R. A. Berger

Prepared under
Contract 952387
for the
California Institute of Technology
Jet Propulsion Laboratory
4800 Oak Grove Drive
Pasadena, California 91103

This work was performed for the Jet Propulsion Laboratory, California Institute of Technology, as sponsored by the National Aeronautics and Space Administration under Contract NAS7-100.

Gulf General Atomic Project 6105

January 23, 1970

## FOREWORD

This report contains information prepared by Gulf General Atomic Incorporated under Jet Propulsion Laboratory subcontract. Its contents are not necessarily endorsed by the Jet Propulsion Laboratory, California Institute of Technology, or the National Aeronautics and Space Administration.

## ABSTRACT

Radiation effects in lithium-diffused bulk silicon have been studied to ascertain the nature of the defects responsible for the degradation in output of silicon devices (solar cells) irradiated by space radiation.

Results of neutron activation analysis for lithium were inconclusive for lightly diffused silicon but generally indicate greater lithium concentrations in heavily diffused silicon than had been inferred from resistivity measurements.

Minority-carrier lifetime temperature dependence measurements were performed before and after irradiation with 30-MeV electrons and fission neutrons and after anneal. These measurements indicate that lightly diffused silicon has two irradiation-induced recombination centers, one located near $E_c$ - 0.17 eV and one deeper than 0.35 eV from a band edge. These centers were found to anneal at different rates. At high electron fluences, trapping centers were observed. No irradiation temperature dependence of the degradation rate was observed between 115 and 300°K.

No impurity dependence was observed for the degradation rate of samples irradiated with fission neutrons. Nearly all the neutron damage was annealed by first-order kinetics between 300 and 380°K. An activation energy of 0.67±0.03 eV was determined, which compares with 0.66±0.05 eV for lithium diffusion in silicon. The effective frequency factor of $10^7$ $sec^{-1}$ indicates long-range migration.

An electron spin resonance investigation of the Si-G7 (divacancy) and Si-G8 (phosphorus-vacancy) centers in electron-irradiated lithium-diffused silicon indicated exceptionally low production rates. The low divacancy production rate was verified by infrared absorption measurements.

CONTENTS

CONTENTS (Continued)



FIGURES

FIGURES (Continued)

FIGURES (Continued)



TABLES

# 1. INTRODUCTION

The purpose of the present program is to ascertain the nature of the degradation and annealing of the minority-carrier lifetime in silicon irradiated with high-energy electrons and fission neutrons. The defects formed by this type of irradiation are expected to be similar to those produced by electrons, protons, and neutrons, which cause the degradation of silicon solar cells exposed to natural and artificial space radiation. In recent years, investigators at Gulf General Atomic Incorporated (GGA) have carried out basic research programs in an attempt to determine whether the degradation is caused by primary radiation-induced defects or by an association of these primary defects with impurities. The annealing properties of these defects have also been studied. In these programs, lithium-diffused silicon solar cells have shown promise of being superior to other types of silicon solar cells in a radiation environment.

Previous work by other investigators on lithium-diffused silicon solar cells was concentrated on determining the effects of irradiation and annealing, with various starting materials and lithium concentrations and cells produced by various manufacturers. These programs showed the general characteristics of the irradiation and annealing response of these cells. However, many important questions concerning the behavior of these cells in a radiation environment remain unanswered.

There are two approaches to determining the feasibility of using lithium-diffused silicon solar cells in space applications. One is the direct approach, in which the output characteristics of the cells are measured as a function of type of irradiation particle, fluence, lithium concentration, time, and temperature. This approach is time-consuming,

since it requires long-term experiments to measure the cell output characteristics after an irradiation. In addition, the number of parameters to be studied and the various environments to be considered make this approach cumbersome. The second approach is the basic-mechanisms approach. Its objective is to obtain an understanding of the physical, microscopic nature of the defects and their annealing. Once these are understood, the response of the cells in various environments can be predicted. This understanding can also lead to recommendations for improving the performance of the cells in an irradiation environment. The basic-mechanisms approach can complement the direct approach by suggesting experiments and pointing out important parameters that may otherwise have been overlooked. Used together, the two approaches will minimize the need for long-term experiments.

In the basic-mechanisms approach, data from silicon solar cells are sometimes difficult to interpret because of problems inherent in the use of lithium-diffused silicon solar cells. These problems include: high field effects in the depletion region; large concentration gradients of lithium near the junction (i.e., the actual lithium conentration within a diffusion length of the junction); effects of irradiation on contacts; and aging of contacts. Therefore, at GGA we have concentrated on the electrical properties of <u>bulk</u> lithium-diffused silicon, measuring the effects of irradiation with 30-MeV electrons and fission neutrons and subsequent annealing behavior. Special emphasis has been placed on minority-carrier lifetime measurements, since solar cell efficiency depends strongly on this parameter.

Studies to determine the nature of the recombination centers in lithium-diffused silicon for preirradiation and postirradiation and preanneal and postanneal conditions indicate recombination center densities and energy levels and their annealing characteristics. These studies have been carried out for samples with varied lithium concentrations.

Electron spin resonance (ESR) measurements yield additional detailed information about radiation-induced defects which may be responsible for lifetime degradation. Under favorable conditions this technique may separately determine the centers observed in minority-carrier lifetime studies. The ESR technique was previously used to study the production and annealing of the oxygen-vacancy (Si-B1) center in lithium-diffused silicon. In the present investigation this technique has been extended to include the study of the production and annealing of the divacancy (Si-G7), the phosphorus-vacancy (Si-G8), and an (as yet) unidentified center in lithium-diffused silicon. These results may be compared with the previous results on the B1 center.

Infrared absorption techniques have been used to augment the findings of ESR measurements. Infrared absorption measurements are less sensitive than ESR measurements, but unlike ESR can generally be used to observe defects regardless of their charge state.

Neutron activation analysis has been used in conjunction with electrical conductivity measurements in an effort to verify the lithium concentration estimated from the resistivity measurements. There has been considerable uncertainty regarding the presence or absence of precipitated lithium regions in lithium-diffused silicon.

Electrical resistivity measurements were used to determine the lithium concentration and to help determine the position of the Fermi level for the ESR and minority-carrier lifetime studies.

## 2. IRRADIATION FACILITIES

Most of the irradiations for the present program were performed at the GGA electron linear accelerator (Linac) facility. This facility contains an L-band traveling-wave electron accelerator capable of producing electrons with energies between 3 and 45 MeV, pulse widths from 0.01 to 5 μsec, and peak currents of approximately 700 mA. This machine was used both as the source of displacement radiation and as the ionizing radiation source needed to obtain excess carriers in the lifetime experiments. The intensity and pulse widths were reduced for the ionization pulses to minimize displacement damage that would occur as a result of these pulses.

A second source of ionizing pulses for the lifetime experiments was a GGA flash X-ray source. This machine delivers a 120-nsec pulse of 600-keV X-rays.

The GGA Accelerator Pulsed Fast Assembly (APFA) was the fission neutron source for minority-carrier lifetime studies. The APFA is a 7-in.-diameter uranium (93% $U^{235}$) unreflected fast reactor which can be operated as either a steady-state reactor or a repetitively pulsed (up to 720 pps) subcritical fast neutron source. The APFA offers easy accessibility for positioning of test samples. These may be located inside a 3/4-in.-diameter hole in the reactor or adjacent to the core. Once the test samples are in position, the reactor is brought to the desired reactivity configuration and (if desired) pulsed.

## 3. SAMPLE PREPARATION

In previous work with lithium-diffused silicon performed by GGA,[1] the samples were prepared by NASA/Goddard; Centralab, Semiconductor Division, Globe Union, Inc.; and Radio Corporation of America. Under the present contract, in order to save time and ensure that our sample requirements were met, we produced our own lithium-diffused samples. Silicon was diffused by two techniques: lithium-oil paint-on and lithium-tin bath diffusion.

### 3.1. PAINT-ON DIFFUSION

In the lithium-oil paint-on technique, a lithium mixture consisting of a 10:1 volume ratio of (99.9%) lithium to (high-purity, powdered) $Al_2O_3$ was blended to paste consistency with mineral oil. This blend was applied to one or both flat sides of a disk-shaped sample. Two-millimeter-thick samples of $10^4$-ohm-cm, high-purity, vacuum-float-zone n-type silicon and 0.5-ohm-cm, phosphorus-doped float-zone n-type silicon were diffused at 450°C. After diffusion, the lithium paste was removed and the lithium redistributed at 450°C. On samples diffused from one side only, redistribution was continued until the same resistivity was measured on each side of the slab. Lithium concentrations ranging from $5 \times 10^{14}$ to $2 \times 10^{17}$ $cm^{-3}$ were obtained.

### 3.2. LITHIUM-TIN BATH DIFFUSION

In the lithium-tin bath diffusion technique, two lithium-doped tin baths were prepared by mixing approximately 1:1000 weight ratios of (99.9%) lithium metal powder with (99.98%) tin metal pellets (40 mesh)

and melting the mixture. The "as-received" tin was somewhat oxidized, and this oxide was removed by dripping the melt through small glass orifices. Emission spectroscopy analysis indicated the baths contained 0.2% and 1% lithium by weight. These concentrations permitted the application of published data[2] for lithium-diffusing of silicon. Vacuum-float-grown samples were prepared with resistivities ranging from 0.25 to about 11 ohm-cm, corresponding to estimated lithium concentrations ranging from about $5 \times 10^{14}$ $cm^{-3}$ to about $5 \times 10^{16}$ $cm^{-3}$.

The principal advantage found in this technique was the ability to produce uniform samples with resistivities from 1 to 11 ohm-cm. The main difficulty encountered was keeping the baths clean. During the year, both baths discolored. The discoloration is thought to be oxidation and appears to be confined to the surface. It may be noted that the discoloration formed even though the baths were stored under a vacuum during and between diffusions. They were opened to ambient air only when samples were inserted or removed. The surface discoloration did not seem to alter the effectiveness of the baths. For diffusion, the cleaned and etched silicon slabs were forced under the surface of the molten bath by a quartz weight and diffused from all sides. Lithium concentrations were estimated after diffusion from room temperature (300°K) resistivity measurements and verified by neutron activation analysis.

### 3.3. UNIFORMITY OF LITHIUM DIFFUSION

Resistivity profiles were determined by a four-probe technique for both samples lithium-diffused by the paint-on technique and samples prepared by the lithium-tin bath technique. These measurements indicated the uniformity of lithium diffused into the silicon. For example, one of the samples lithium-diffused with the lithium-tin bath was originally 6.4 x 8.7 x 2 mm. After diffusion, the resistivity of each side was measured; then 0.25 mm was lapped off one side and the resistivity of

both sides was remeasured. This process was repeated, with about 0.25 mm being removed from the same side each time, until the sample thickness was reduced to about 1 mm. Our four-probe instrument has 1-mm probe spacing, so the measured resistivity was corrected for the diminishing sample thickness according to the method of Valdes.[3] Figure 1 shows the corrected resistivity versus sample thickness for the 11-ohm-cm sample. Other samples ranging from 0.052 to 11.5 ohm-cm were similarly investigated and were found to be uniform.

The lithium paint-on technique was most suitable for producing the highly diffused (low resisitivity) samples needed for neutron activation analysis and ESR samples. Some difficulty was experienced in producing uniform samples, and samples were occasionally found to be pitted after a lithium paint-on diffusion. This difficulty has been mentioned by many other investigators.[4] Samples which were found to be nonuniform were discarded.

The samples used for minority-carrier lifetime studies were produced mainly by the lithium-tin bath technique. Uniform samples were obtained by this method with little difficulty.

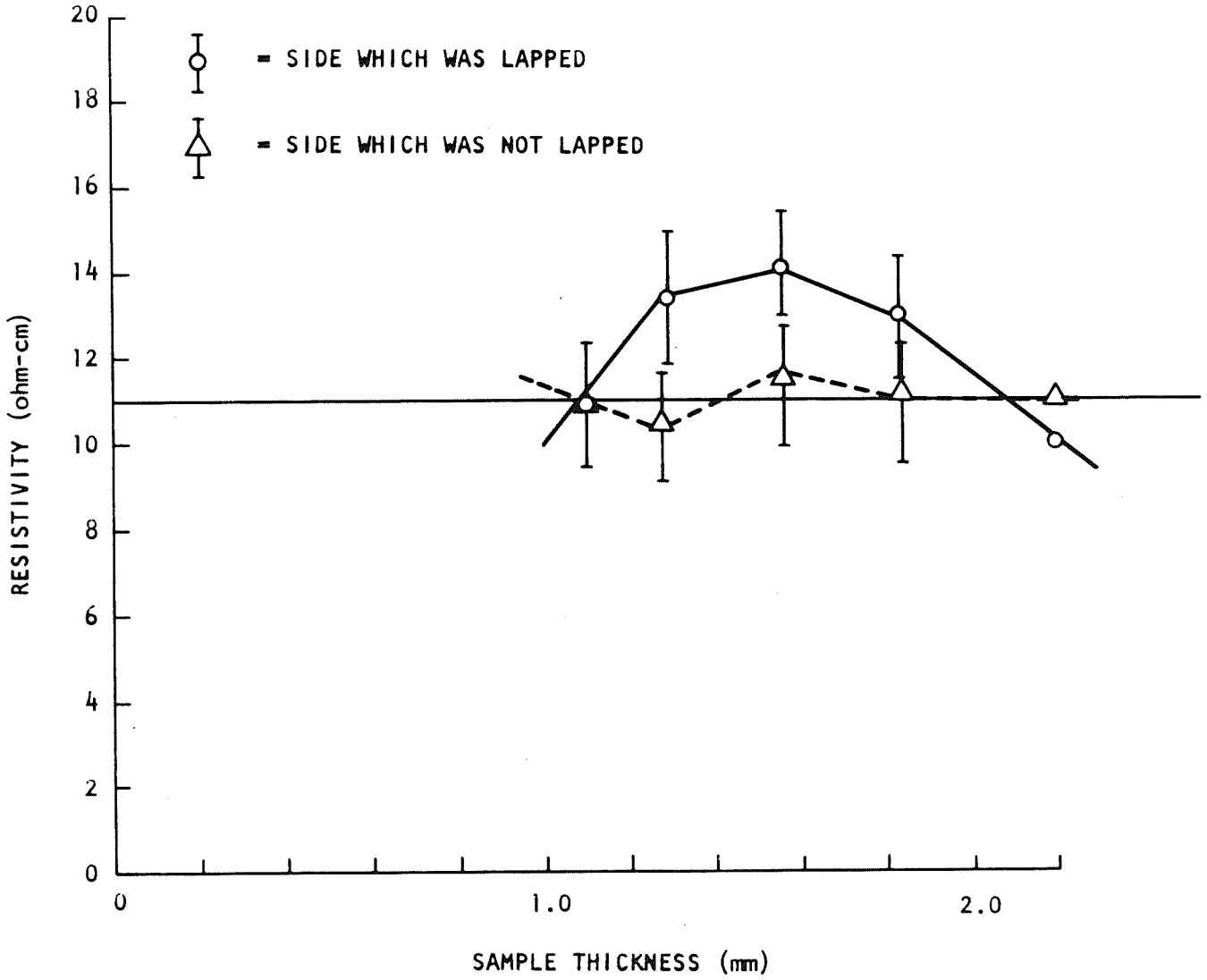


Fig. 1. Resistivity versus sample thickness for 11-ohm-cm lithium-diffused silicon

# 4. NEUTRON ACTIVATION ANALYSIS

## 4.1. PURPOSE

Electrical resistivity and Hall-effect measurements have been used to estimate the lithium density in lithium-diffused silicon samples.[1] Resistivity profiles were used to determine the relative lithium profile. It is usually assumed that each lithium atom is present as a singly ionized donor. Neutron activation analysis (NAA) was used as an independent means to estimate the lithium density in silicon. By comparing resistivity measurements and NAA results, we hoped to establish whether lithium was present as a precipitate.

An NAA method has been developed for the determination of very small amounts of lithium in various materials. A pulsing TRIGA nuclear reactor, a rapid pneumatic sample-transfer system, and a Cerenkov counter are used, respectively, to obtain high specific yields from the $Li^7(n,\gamma)Li^8$ reaction, bring the 0.84-sec half-life product radionuclide to the counter, and count the 13.1-MeV ($E_{max}$) beta particles from $Li^8$. In the absence of appreciable interferences, as little as $10^{-9}$ g of lithium can thus be detected.[5,6]

## 4.2. RESULTS AND ANALYSIS

Table 1 summarizes the results obtained for the samples which underwent activation analysis. Resistivities ranged from $10^4$ to 0.052 ohm-cm. Such resistivities would imply lithium densities ranging from less than $10^{13}$ $cm^{-3}$ to about $3 \times 10^{17}$ $cm^{-3}$.[7]

TABLE 1
COMPARISON OF LITHIUM CONTENT AS DETERMINED BY RESISTIVITY ESTIMATES AND AS MEASURED BY NEUTRON ACTIVATION ANALYSIS

| Sample Number | Resistivity (ohm-cm) | Weight (g) | Volume ($cm^3$) | Estimated Li Density | Resistivity Estimate of Total Li (μg) | NAA Results (μg) | Method of Li Diffusion |
|---|---|---|---|---|---|---|---|
| 1 | $10^4$ | 0.124 | 0.056 | $<10^{13}$ | 0.000 | 0.010 | Not diffused |
| 4 | $10^4$ | 0.123 | 0.053 | $<10^{13}$ | 0.000 | <0.066 | Not diffused |
| 2 | 11 | 0.112 | 0.050 | $5x10^{14}$ | 0.000 | <0.055 | Li-tin bath |
| 5 | 4 | 0.116 | 0.050 | $1.5x10^{15}$ | 0.001 | <0.053 | Li-tin bath |
| 3 | 0.37 | 0.108 | 0.048 | $1.5x10^{16}$ | 0.009 | 0.026 | Paint-on |
| 6 | 0.25 | 0.104 | 0.045 | $3x10^{16}$ | 0.016 | <0.060 | Paint-on |
| 9 | 0.11 | 0.270 | 0.116 | $1x10^{17}$ | 0.14 | 0.094 | Paint-on |
| 7 | 0.05 | 0.290 | 0.125 | $2.5x10^{17}$ | 0.35 | 2.65 | Paint-on |
| 8 | 0.05 | 0.260 | 0.110 | $2.5x10^{17}$ | 0.32 | 0.094 | Paint-on |

To determine the lithium content, each sample and a 26.4-μg lithium comparator standard were sequentially exposed to the 870-MW pulses in the F-ring of the TRIGA Mark I reactor. They were immediately (less than 0.6 sec) transferred to a Cerenkov counter, and the 0.84-sec $Li^8$ component of the decay curve was measured by multichannel scaling. Comparison of sample response with that of the standards provides the basis for calculating the lithium content of the samples. The actual limit of the amount of lithium measured by activation analysis appeared to be about an order of magnitude greater than the interference-free limits of detection of $10^{-9}$ g.

Limitations on the sample size somewhat restricted the measurement sensitivity. The physical size of the samples was limited by the dimensions of the special polyethylene containers used in the pneumatic system required to rapidly transfer the sample from the TRIGA reactor to the counting system. The average volume of the samples submitted was 0.07 $cm^3$. The most favorable case was a 0.125-$cm^3$ (0.052-ohm-cm) sample, which corresponds to an estimated lithium content of about $3.5 \times 10^{-7}$ g. Thus, for lightly diffused samples, the NAA determination was limited by experimental uncertainties.

For the low-lithium-concentration samples, the estimate of the lithium obtained by NAA agrees fairly well with the lithium estimate obtained from resistivity measurements. These samples were all diffused by the lithium-tin bath technique. However, for the high-lithium-content samples, the NAA estimates ranged from values equal to the resistivity estimates to values much larger than the resistivity estimates.

## 4.3. CONCLUSIONS

The NAA results tend to suggest that for the low-lithium-content (less than $10^{17}$ $cm^{-3}$) samples, the lithium is present in the samples as

singly ionized donors. For this study, the low-lithium-content samples were diffused by the lithium-tin bath technique. However, for the high-lithium-content (greater than $10^{17}$ $cm^{-3}$) samples, the NAA results show that there may be significantly more lithium present in certain samples than indicated by the resistivity measurements. These high-lithium-content samples were produced by the lithium paint-on technique.

The results for high-lithium-content samples are in agreement with those of Ferman and Swalin,[8] who found that lithium does precipitate in heavily diffused silicon. The possibility of freeing this precipitated lithium adds new possibilities to the annealing mechanisms present in lithium-diffused silicon.

## 5. STUDY OF MINORITY-CARRIER LIFETIME

### 5.1. INTRODUCTION

Minority-carrier lifetime measurements have been studied for several reasons. First, changes in minority-carrier lifetimes due to radiation-induced defects can be observed at very low fluence levels (approximately $10^{12}$ e/cm$^2$), making these measurements some of the most sensitive measurements available. Second, the temperature dependence of minority-carrier lifetime establishes the density and energy levels of recombination centers. Third, the solar cell output can be related to the minority-carrier lifetime ($\tau$). The ideal[9] voltage current characteristics of solar cells is given by

$$I = I_L - I_S \left(e^{qV/nkT} - 1\right) , \tag{1}$$

where I is the current in the load, V is the voltage across the junction, $I_S$ is the reverse saturation current, $I_L$ is the quantity proportional to light intensity, k is Boltzmann's constant, T is absolute temperature, q is the electronic charge, and n = 1. The open-circuit voltage, $V_{OC}$, where I = 0, is seen to be

$$V_{OC} = n \frac{kT}{q} \ln\left(\frac{I_L}{I_S} + 1\right) . \tag{2}$$

In a similar manner, the short-circuit current, $I_{SC}$, is

$$I_{SC} = \frac{C \sqrt{D\tau}}{\lambda + \sqrt{D\tau}} , \tag{3}$$

where C is a constant dependent on light-source intensity, $\lambda$ is the wavelength of the light source, D is the minority-carrier diffusion constant, and $\tau$ is the minority-carrier lifetime. When the resistance of the solar cell is sufficiently small, $I_{SC} = I_L$. It is evident from Eqs. (1), (2), and (3) that the minority-carrier lifetime can be directly related to the degradation and anneal of solar cell outputs.

## 5.2. MINORITY-CARRIER LIFETIME MEASUREMENT TECHNIQUES

The minority-carrier lifetimes were measured by two techniques. The first was the standard photoconductivity decay method, and the second was the steady-state photoconductivity method.

### 5.2.1. Photoconductivity Decay

The photoconductivity decay technique is described in Ref. 1. Three penetrating carrier-injection sources were employed: a filtered xenon strobe light, a 600-keV flash X-ray, and a low-level, 0.1-μsec pulse of 30-MeV electrons. Carrier-injection levels of less than 1% were generally used. The same preirradiation, low-injection-level lifetime was measured using all three injection sources. Photodecay signals were observed on an oscilloscope and photographed. When necessary, these data were reduced by a computer calculation as previously described.[10]

### 5.2.2. Steady-State Photoconductivity

The steady-state photoconductivity technique was used for the neutron irradiation experiments and some of the electron irradiation experiments. For these measurements, minority carriers were injected with a tungsten-filament light source, which was passed through a lens system, water, gallium arsenide, and silicon filters, and were chopped by a toothed wheel at $10^3$ Hz. At equilibrium, the change in conductivity is $\Delta\sigma = g\tau e\ (\mu_n + \mu_p)$, where g is the generation rate of the light source and $\mu_n$ and $\mu_p$ are the

electron and hole mobilities. The direct-current conductivity is $\sigma_0 = n_0 e \mu_n$. Thus, holding the sample current constant, one finds that

$$\left|\frac{\Delta V}{V}\right| = \frac{\Delta\sigma}{\sigma_0} = \frac{\Delta n}{n_0} = \frac{g\tau}{n_0}\left(\frac{\mu_n + \mu_p}{\mu_n}\right) \quad . \tag{4}$$

The signal observed was dc voltage (V) modulated by a $10^3$-Hz chopped signal of amplitude $\Delta V = 10^{-3}$ V. From Eq. (4), it is clear that

$$\tau = \frac{n_0}{g}\left(\frac{\mu_n}{\mu_n + \mu_p}\right)\left|\frac{\Delta V}{V}\right| = A\left|\frac{\Delta V}{V}\right| \quad . \tag{5}$$

The constant A was empirically determined for each sample by comparing the measured photodecay lifetime ($\tau$) with the amplitude of the steady-state signal ($\Delta V/V$) at one or more temperatures. Characteristically, A = 2 to 3 x $10^{-2}$ sec, depending on the light intensity. Carrier-injection levels of less than 1% were used.

## 5.3. EXPERIMENTAL

### 5.3.1. Samples

All the samples used in these lifetime investigations were fabricated from $10^4$-ohm-cm, float-zone n-type silicon. This high-purity material had a room temperature lifetime of about $10^3$ μsec before lithium diffusion. Thus, the density of recombination centers prior to diffusion was negligibly low. The samples were lithium-diffused by both the lithium-tin bath and paint-on techniques. Samples were of the standard four-lead configuration. Gold preforms were ultrasonically tacked to 1.6 x 1.6 x 10 mm samples and bonded by heating to 450°C for 7 min. Four 0.002-in. copper

leads were soft-soldered to the gold dots, and a copper-constantan thermocouple was cemented to one end of the sample with GE-7031 insulating varnish. Three types of samples were studied: 11-ohm-cm and 3.7-ohm-cm samples were made by lithium-tin bath diffusion, and a 0.4-ohm-cm sample was produced by the lithium-oil paint-on technique.

Assuming all the lithium ions are singly ionized donors, one would estimate from the resistivity an initial lithium density of $n_0 = 4.5 \times 10^{14}$ $cm^{-3}$ for the 11-ohm-cm samples and $n_0 = 1.5 \times 10^{16}$ $cm^{-3}$ for the 0.4-ohm-cm sample. Typical preirradiation, inverse temperature dependence of conductivity is shown in Figs. 2 and 3. The conductivity decrease with increasing temperature is due to the temperature dependence of lattice scattering.[11]

### 5.3.2. Sample Chambers

Samples were attached to headers which could be installed in either of the two variable-temperature chambers illustrated in Figs. 4 and 5. Figure 4 also schematically indicates the tungsten light source, lens, and chopper system used in the steady-state minority-carrier lifetime measurements. The tungsten source and chopper could be replaced with a xenon strobe lamp for photodecay measurements. This chamber was principally used where the injection source had to be filtered to remove nonpenetrating light. Water, gallium arsenide, and silicon filters were used. The silicon filter was mounted on the sample block so that it was always at the sample temperature. The cryostat shown in Fig. 5 was used when the injection source was penetrating, e.g., 30-MeV electrons or 600-keV X-rays.

## 5.4. MINORITY-CARRIER LIFETIME RECOMBINATION THEORY

The theory of recombination of excess carriers has been treated by others,[12-14] and the relation between theory and experimentally measured

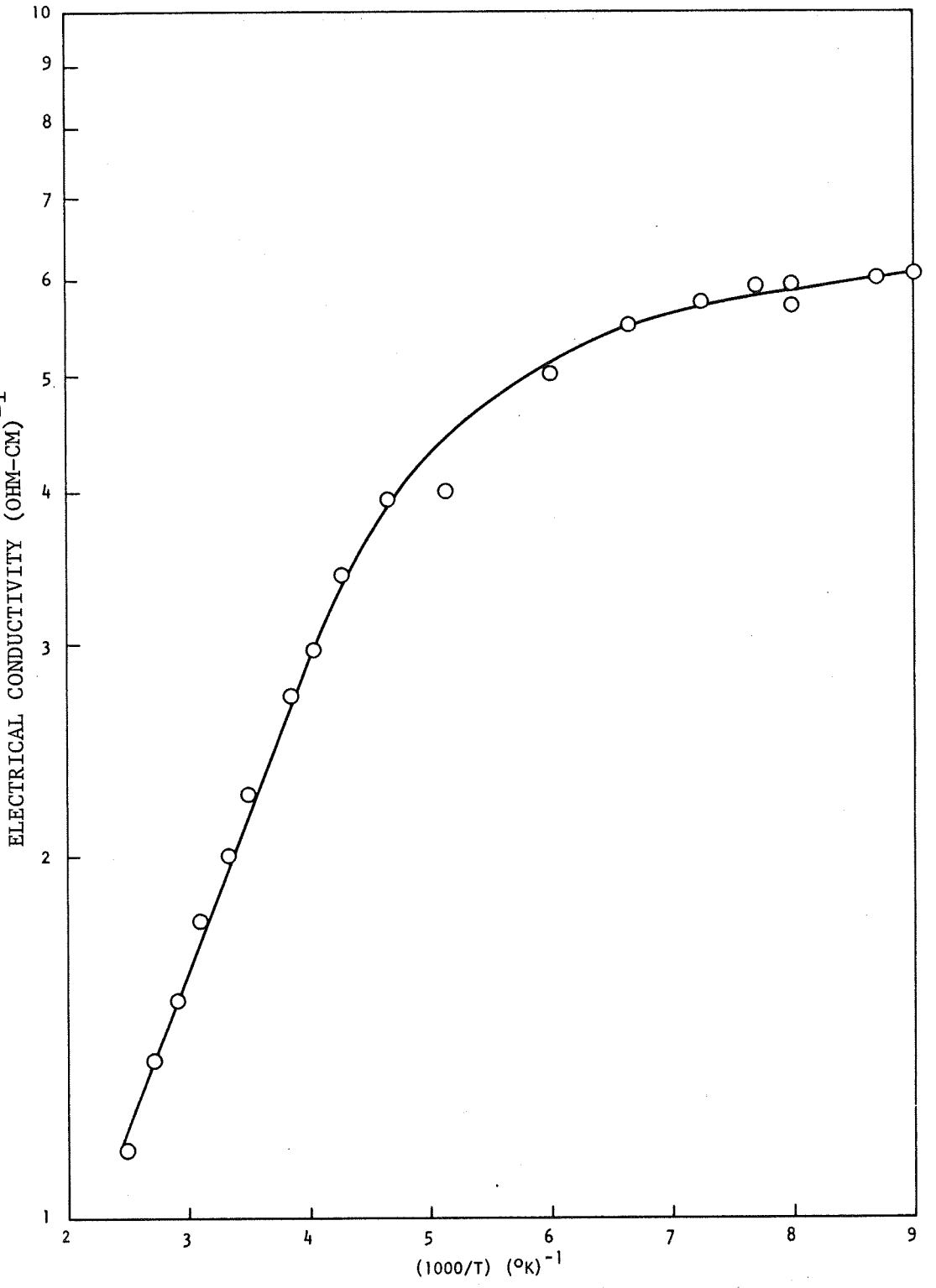


Fig. 2. Initial conductivity of 0.4-ohm-cm lithium-diffused silicon

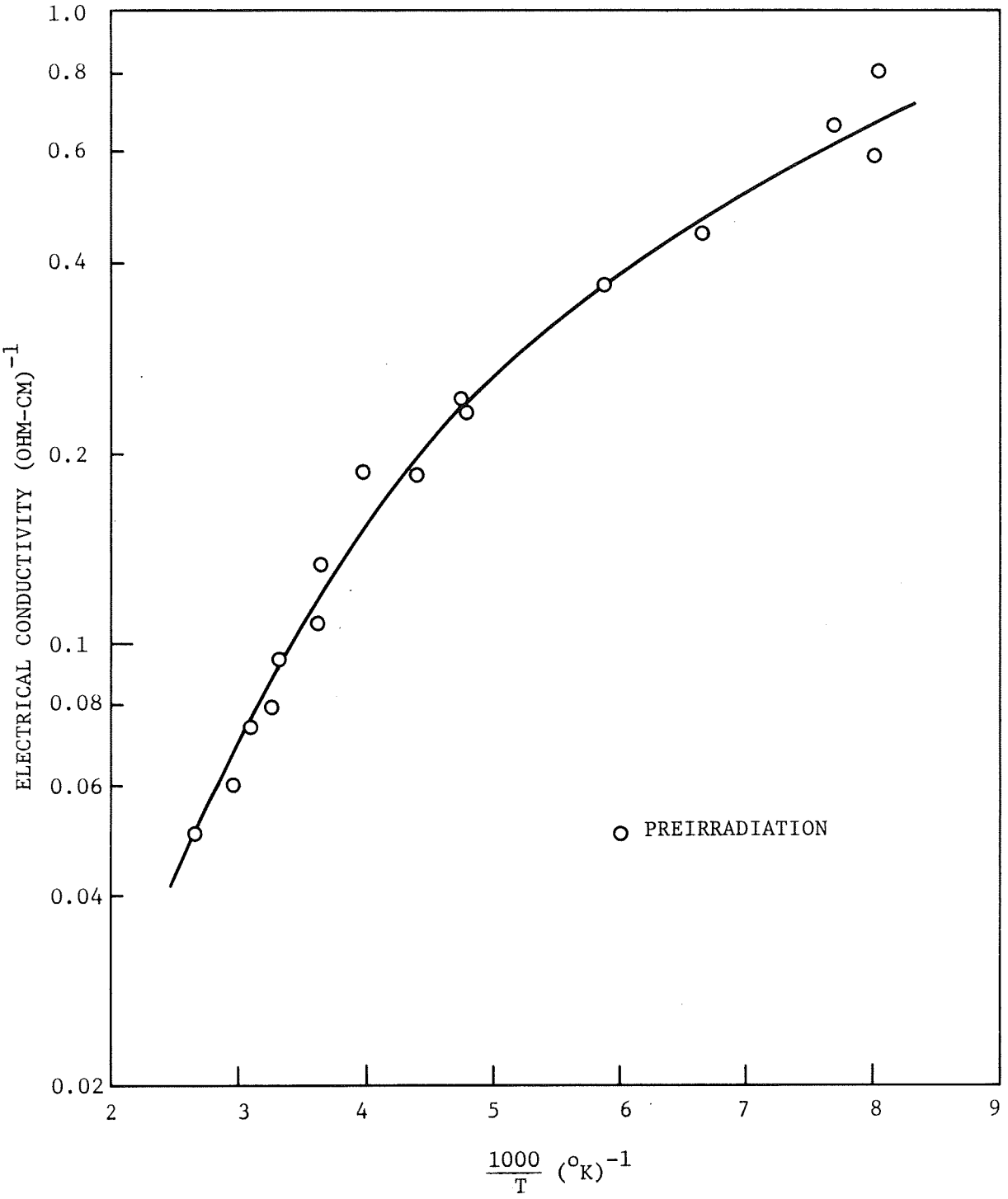


Fig. 3. Electrical conductivity as a function of 1000/T for lithium-diffused, 11-ohm-cm n-type silicon

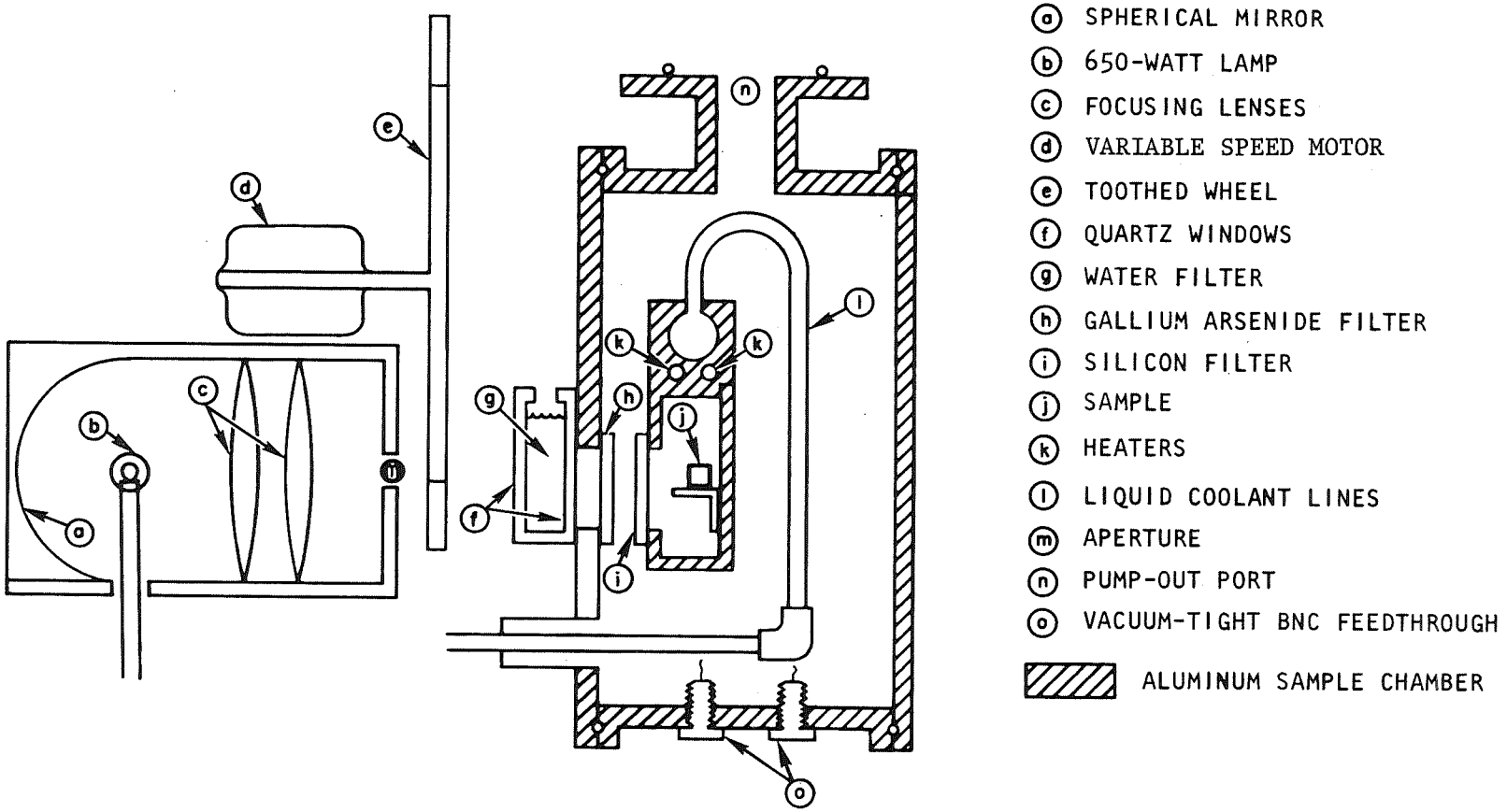


Fig. 4. Apparatus for measuring lifetime and resistivity as a function of neutron fluence (not to scale)

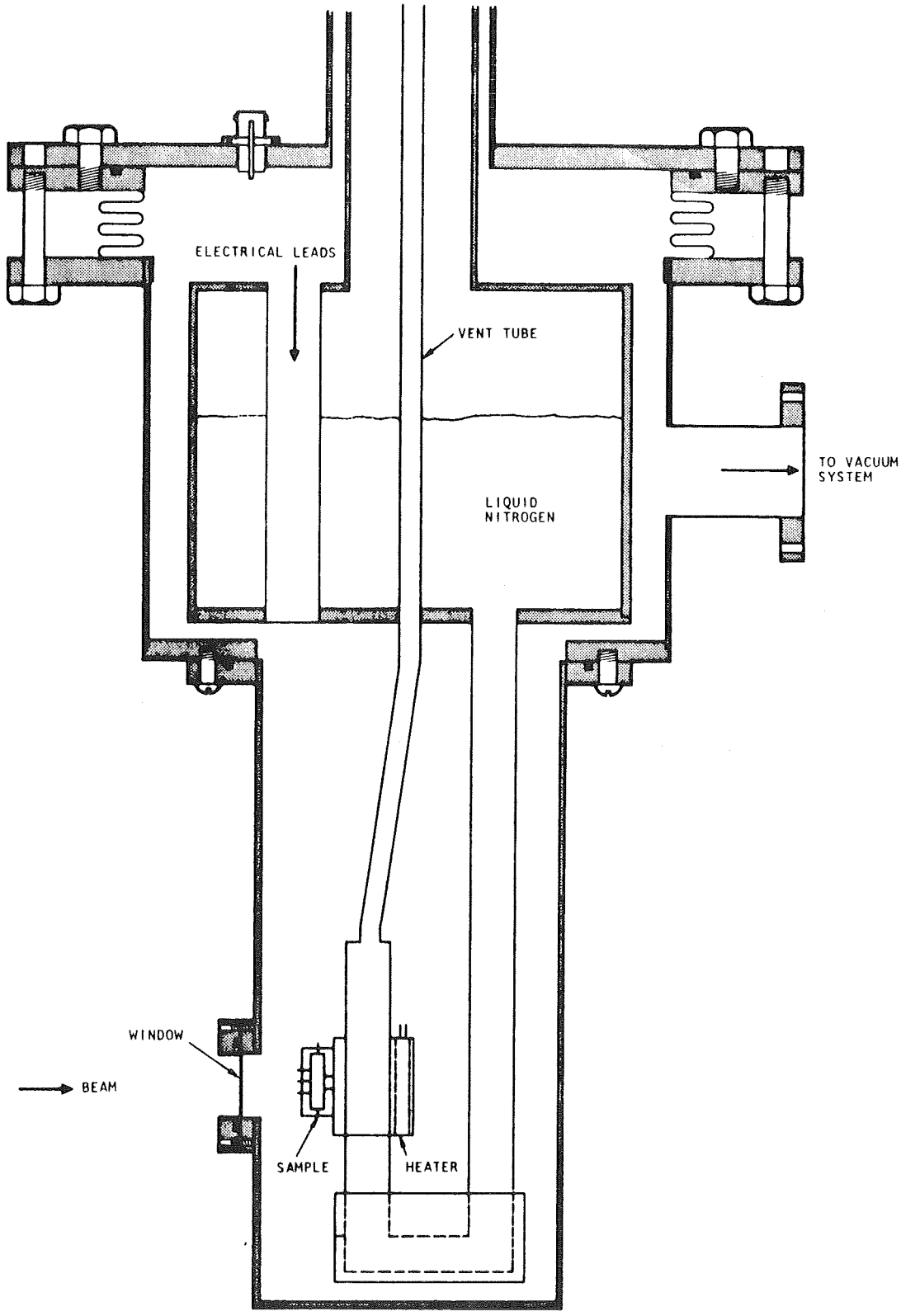


Fig. 5. Variable-temperature (50 to 500°K) cryostat used to make electrical and optical measurements

quantities has been reported earlier.[15-17] The conclusions can be summarized as follows. The Shockley-Read theory for a single-level defect assumes that the number of recombination centers is small relative to the excess-carrier density. This assumption implies that the excess electrons and holes have equal densities and lifetimes. The expression for the lifetime in this case is

$$\tau = \tau_{p_0} \left( \frac{n_0 + n_1 + \Delta n}{n_0 + p_0 + \Delta n} \right) + \tau_{n_0} \left( \frac{p_0 + p_1 + \Delta p}{n_0 + p_0 + \Delta n} \right) , \tag{6}$$

where $n_0$ and $p_0$ are the thermal equilibrium electron and hole concentrations, $n_1$ and $p_1$ are the electron and hole concentrations calculated when the Fermi level is assumed to lie at the recombination center level, $\Delta n = \Delta p$ is the excess-carrier concentration, $\tau_{n_0}$ is the lifetime for electrons in highly p-type material, and $\tau_{p_0}$ is the lifetime for holes in highly n-type material. In n-type material (for p-type, n's and p's are interchanged), where $n_0 >> p_0$, dividing by $n_0$ gives

$$\tau = \frac{\tau_{p_0} \left( 1 + \frac{n_1}{n_0} \right) + \tau_{n_0} \left( \frac{p_1}{n_0} \right) + \frac{\Delta n}{n_0} \left( \tau_{p_0} + \tau_{n_0} \right)}{1 + \frac{\Delta n}{n_0}} \tag{7}$$

or

$$\tau = \frac{\tau_\ell + \tau_h \left( \frac{\Delta n}{n_0} \right)}{1 + \frac{\Delta n}{n_0}} , \tag{8}$$

where $\tau_\ell$ (low-injection-level lifetime) and $\tau_h$ (high-injection-level lifetime) are the corresponding terms in the equations.

Our measurements were largely confined to low-injection-level measurements ($\Delta n/n_0 < 1\%$) in n-type material. The low-injection-level lifetime, $\tau_\ell = \tau_{p_0}(1 + n_1/n_0) + \tau_{n_0}(p_1/p_0)$, may be simplified in this limit for two special cases.

Case 1: When the recombination level ($E_T$) is closer to a band edge than the Fermi level ($E_F$), either

$$n_1 > n_0 > p_1 \qquad \text{or} \qquad p_1 > n_0 > n_1$$

and

$$\tau \cong \tau_{p_0}(1 + n_1/n_0) \qquad \text{or} \qquad \tau \cong \tau_{n_0}(p_1/p_0)$$

where

$$n_1 = N_C \exp(E_T - E_C)/kT \ ,$$

$$p_1 = N_V \exp(E_V - E_T)/kT \ ,$$

where $N_C$ and $N_V$ are the conduction and valence band carrier densities. Forcing the Fermi level below the recombination level contributes an exponential factor to the lifetime temperature dependence.

Case 2: When the Fermi energy is well above the recombination center level,

$$n_0 >> n_1 > p_1 \ ,$$

$$\tau \cong \tau_{p_0} \ .$$

The temperature dependence of $\tau$ is found in terms containing $\tau_{p_0}$, $\tau_{n_0}$, $n_1$, $p_1$, and $n_0$. The term $n_0$ is known, however, and can be extracted from the data. The temperature dependences of $\tau_{p_0}$ and $\tau_{n_0}$ are exhibited through the thermal velocity, $V_{th}$, of the carriers and the capture cross section, $\sigma$, where

$$\tau_{p_0} = \frac{1}{N_R V_{th} \sigma_p}$$

and

$$\tau_{n_0} = \frac{1}{N_R V_{th} \sigma_n} \quad ,$$

and where $N_R$ is the concentration of recombination centers.

Theoretical work on the temperature dependence of the cross section for neutral and attractive recombination centers has been performed by Lax.[18] A brief summary of the theory is given in Ref. 19. Figure 6 gives the temperature dependence for the cross sections of the singly charged attractive center and the neutral center.

## 5.5. MINORITY-CARRIER LIFETIME MEASUREMENTS

The experimental study of the effects of radiation and annealing on the minority-carrier lifetime was performed with both highly lithium-diffused and lightly lithium-diffused n-type silicon. The highly lithium-diffused silicon was lithium diffused by the paint-on technique. Its room temperature resistivity was about 0.4 ohm-cm. The lightly lithium-diffused silicon was lithium-diffused by the bath technique and had a room temperature resistivity near 11 ohm-cm.

It was anticipated that the two-order-of-magnitude difference in lithium concentration in the two types of samples would produce different

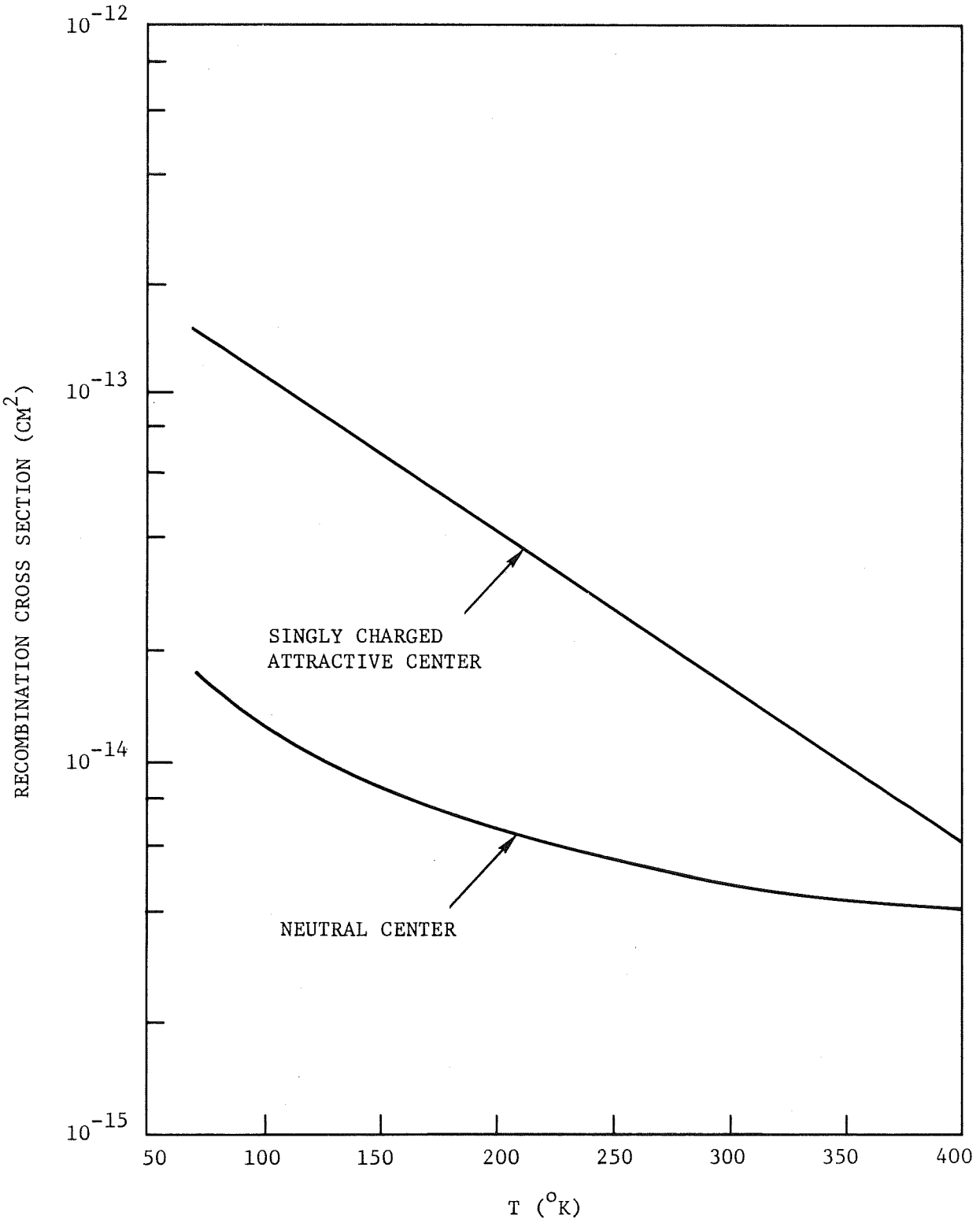


Fig. 6. Recombination cross section in silicon versus temperature

degradation and annealing results. It was also anticipated that the temperature dependence of the preirradiation, postirradiation-preanneal, and postanneal lifetime for the two different resistivities would help determine the nature of the recombination centers.

During the experimental study of the minority-carrier lifetime, 30-MeV electrons and fission neutrons were used as the irradiating particles. The use of electrons and neutrons produces both point defects and cluster damage, two types of damage produced by space irradiation.

### 5.5.1. 30-MeV Electron Irradiations of Highly Lithium-Diffused Silicon

5.5.1.1. Preirradiation Measurements. The study of the highly lithium-diffused silicon was performed mainly to check the reproducibility of data obtained in previous measurements.[1] During the previous work, the samples were lithium-diffused by sources outside of GGA, whereas the samples used during the present contract were diffused at GGA. The temperature dependence of the conductivity of the 0.4-ohm-cm sample is shown in Fig. 2. The room temperature resistivity indicates a lithium density of $1.5 \times 10^{16}$ $cm^{-3}$.[7] The low-injection-level (less than 1%) room temperature minority-carrier lifetime, measured by the photoconductivity decay technique, was 4.5 μsec.

The temperature dependence of the preirradiation minority-carrier lifetime[1] indicates that the recombination center in the highly lithium-diffused silicon was deeper in the gap than about 0.17 eV from either band edge.

5.5.1.2. Degradation. The degradation of the minority-carrier lifetime as a function of electron fluence was measured at 300°K. This datum is plotted in Fig. 7. The lifetime degradation can best be described in terms of the degradation constant, K, which is defined from

$$\frac{1}{\tau} = \frac{1}{\tau_0} + K\phi \quad , \tag{9}$$

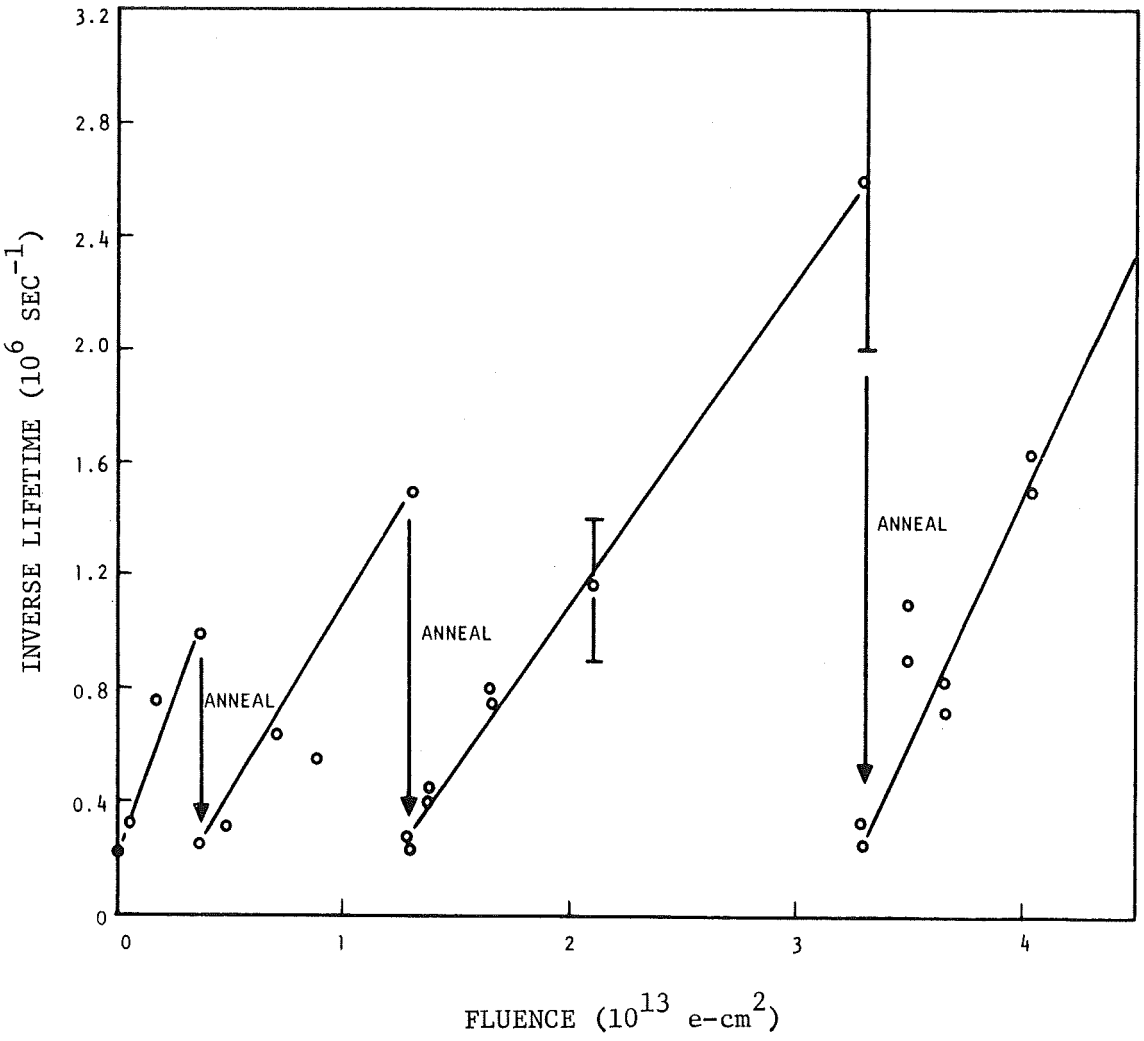


Fig. 7. Inverse lifetime versus fluence for the 0.4-ohm-cm, lithium-diffused n-type silicon irradiated with 30-MeV electrons at room temperature

where $\tau_0$ is the lifetime prior to irradiation and $\tau$ is the lifetime after a fluence $\phi$. The lifetime degradation constant for this material for fluences of approximately $10^{13}$ e/cm$^2$ is $1.8\pm0.3 \times 10^{-7}$ cm$^2$/e-sec. This degradation constant is about twice as large as observed for non-lithium-diffused silicon of equivalent resistivity.[1] The first three irradiations are shown in Fig. 7. The fourth irradiation, to $4 \times 10^{14}$ e/cm$^2$, was much larger than the first three. At the end of the fourth irradiation, the lifetime was too short to measure by the photoconductivity decay method.

5.5.1.3. Annealing. After the sample was degraded to about 0.5 μsec in each of the first three irradiations, it was annealed at 370°K for 30 min. This annealing schedule, which was selected from the previous results[1] on highly lithium-diffused silicon, was found to completely anneal all the damage apparent at room temperature; i.e., the lifetime returned to its preirradiation value. The effectiveness of this schedule in annealing all the damage was in agreement with previous results.[1]

The lifetime returned to its preirradiation value after each of the first three irradiations of about $10^{13}$ e/cm$^2$. However, following the fourth irradiation of $4 \times 10^{14}$ e/cm$^2$ and anneals of 30 min at 370°K and 30 min at 420°K, the 300°K lifetime returned to about 1.6 μsec. After this annealing, only a recombination lifetime was observed and no trapping was observed.

5.5.1.4. Analysis and Conclusions. The increased degradation constant of heavily lithium-diffused silicon relative to the degradation constant of non-lithium-diffused silicon is interpreted to indicate that the presence of lithium is effective in the production of recombination centers in lithium-diffused silicon. These recombination centers either contain lithium or are affected in their production by lithium.

The annealing of the recombination centers in lightly irradiated heavily diffused silicon is complete; i.e., all the recombination centers are annealed. The annealing times are consistent with previous results.[1] However, after extended fluences, the annealing of the recombination centers is not complete; i.e., not all the recombination centers have annealed. For example, after the electron fluence of $4 \times 10^{14}$ e/cm$^2$, the room temperature lifetime recovered to 1.6 μsec. The lifetime before irradiation was 4.5 μsec.

The density of unannealed irradiation-produced recombination centers can be calculated from the following equation:[20]

$$\frac{N_{DT}}{N_D} = \frac{\frac{1}{\tau_T} - \frac{1}{\tau_0}}{\frac{1}{\tau_f} - \frac{1}{\tau_0}} , \qquad (10)$$

where $N_{DT}$ is the recombination center density after anneal to temperature T and $N_D$ is the density of recombination centers introduced by irradiation, $\tau_0$ is the lifetime before irradiation, $\tau_f$ is the lifetime after irradiation, and $\tau_T$ is the lifetime after an anneal at temperature T. All measurements are made at the same temperature.

After the extended electron fluence of $4 \times 10^{14}$ e/cm$^2$, only 80% of the recombination centers had annealed. This implies that the previous irradiation history of the samples is important.

Of major interest in the study of the highly lithium-diffused silicon is the fact that samples which receive initially small electron fluences completely anneal, while samples which receive initially large fluences do not completely anneal. There are at least two possible reasons for this difference in annealing: (1) lithium, which is assumed to do the annealing, is depleted in the production of defects and the

annealing process and is therefore not available to produce further annealing; and (2) the nature of the recombination center which is effective at 300°K changes.

### 5.5.2. 30-MeV Electron Irradiations of Lightly Lithium-Diffused Silicon

5.5.2.1. Preirradiation Measurements. An investigation of the response of lightly diffused 11-ohm-cm ($n_0 = 4.5 \times 10^{14}$ $cm^{-3}$) silicon to 30-MeV electron irradiation was undertaken to test the supposition that the production and anneal of recombination centers depend on the lithium concentration and that extended irradiations and repeated anneals would deplete the active lithium initially present. Such depletion would eventually inhibit further degradation and annealing. Furthermore, the use of lightly diffused silicon would permit the Fermi level to move over a greater portion of the energy gap during the temperature cycling from 100 to 400°K than was the case for the heavily lithium-diffused silicon. The analysis of the temperature dependence of the minority-carrier lifetime for the lightly diffused silicon would permit the determination of the nature and position of recombination centers deeper in the energy gap than for heavily lithium-diffused silicon.

The minority-carrier lifetime temperature dependence was studied before and after irradiation and before and after annealing in order to determine the energy levels of the radiation-induced recombination centers and their annealing kinetics.

The preirradiation electrical conductivity of this 11-ohm-cm material is shown in Fig. 3. Figure 8 shows a typical preirradiation minority-carrier lifetime plotted versus 1000/T. In most cases, we could not account for the observed lifetime with the Shockley-Read[16] theory for one recombination center. The inverse temperature dependence was not exponential as expected for a center between the Fermi level and a band edge, but it was too severe to be explained by either a neutral or singly charged attractive center located deeper in the gap than the Fermi level.

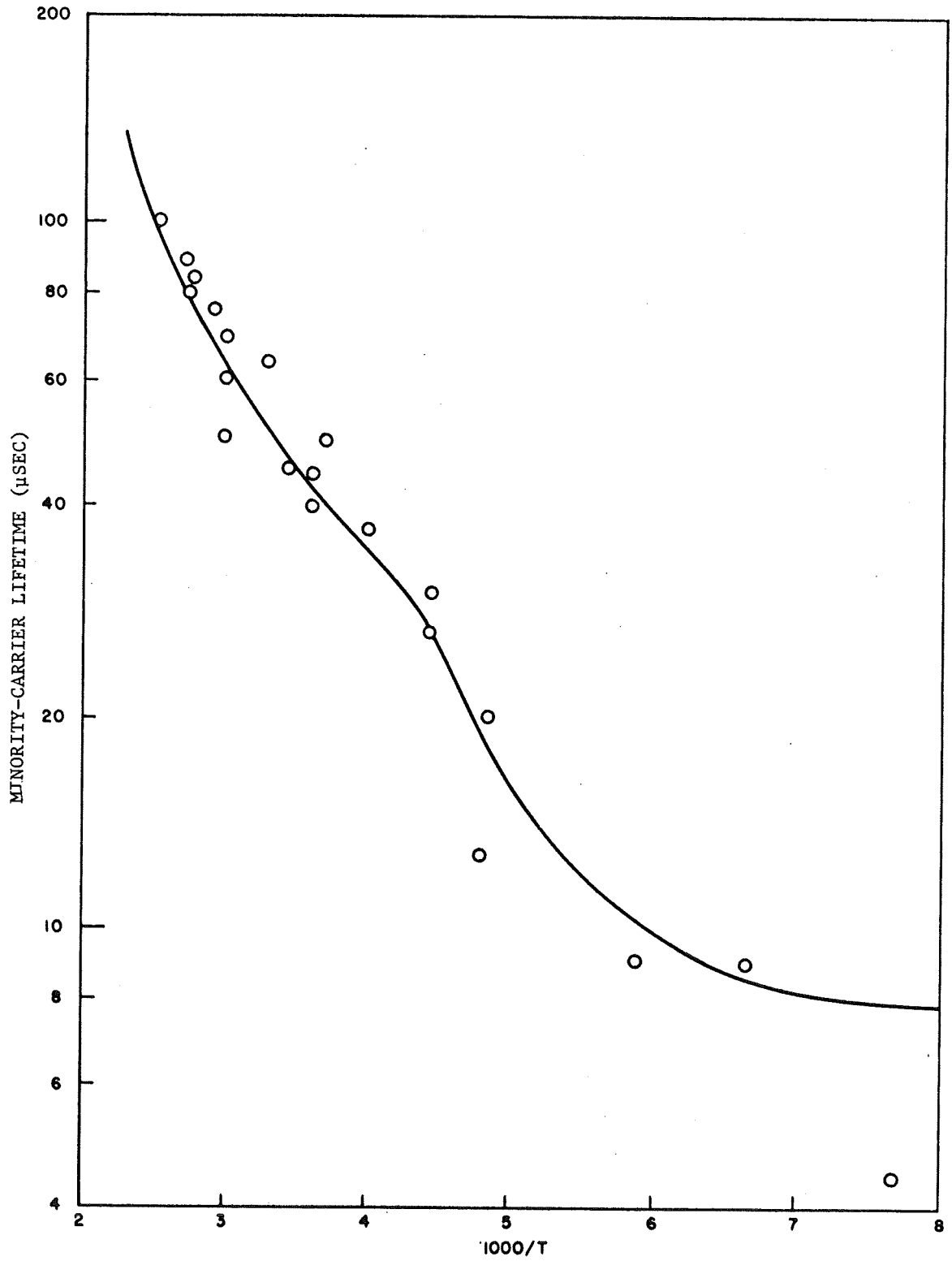


Fig. 8. Preirradiation minority-carrier lifetime versus 1000/T for lithium-diffused n-type silicon

In addition, a slight discontinuity is apparent in the inverse temperature-dependence curve near 1000/T = 4.5. Therefore, a two-recombination center model (schematically indicated in Fig. 9) was proposed to account for the preirradiation lifetime observed for 11-ohm-cm samples. In this material, the Fermi level varies from about 0.1 eV at 100°K to about 0.35 eV at 400°K. If there are N(1) recombination centers about 0.17 eV below the conduction band edge and N(2) centers deeper than 0.35 eV from either band edge, the Fermi level is always well above the deeper center and crosses the shallow center at an intermediate temperature near 200°K. At all temperatures, the lifetime (see Section 5.4) due to the deep center is

$$\tau(2) = \tau_{p_0}(2) = [N(2)v\sigma(2)]^{-1} \quad . \tag{11}$$

Similarly, at temperatures below about 200°K, the lifetime due to N(1) centers located at about $E_c$ - 0.17 eV is

$$\tau(1) = \tau_{p_0}(1) = [N(1)v\sigma(1)]^{-1} \quad , \tag{12}$$

but above about 250°K, level (1) is well above the Fermi level and

$$\tau(1) = \tau_{p_0}(1)\ [1 + n_1(1)/n_0] \quad , \tag{13}$$

where

$$n_1(1) = N_c \exp\ [E_T(1) - E_c]/kT \quad . \tag{14}$$

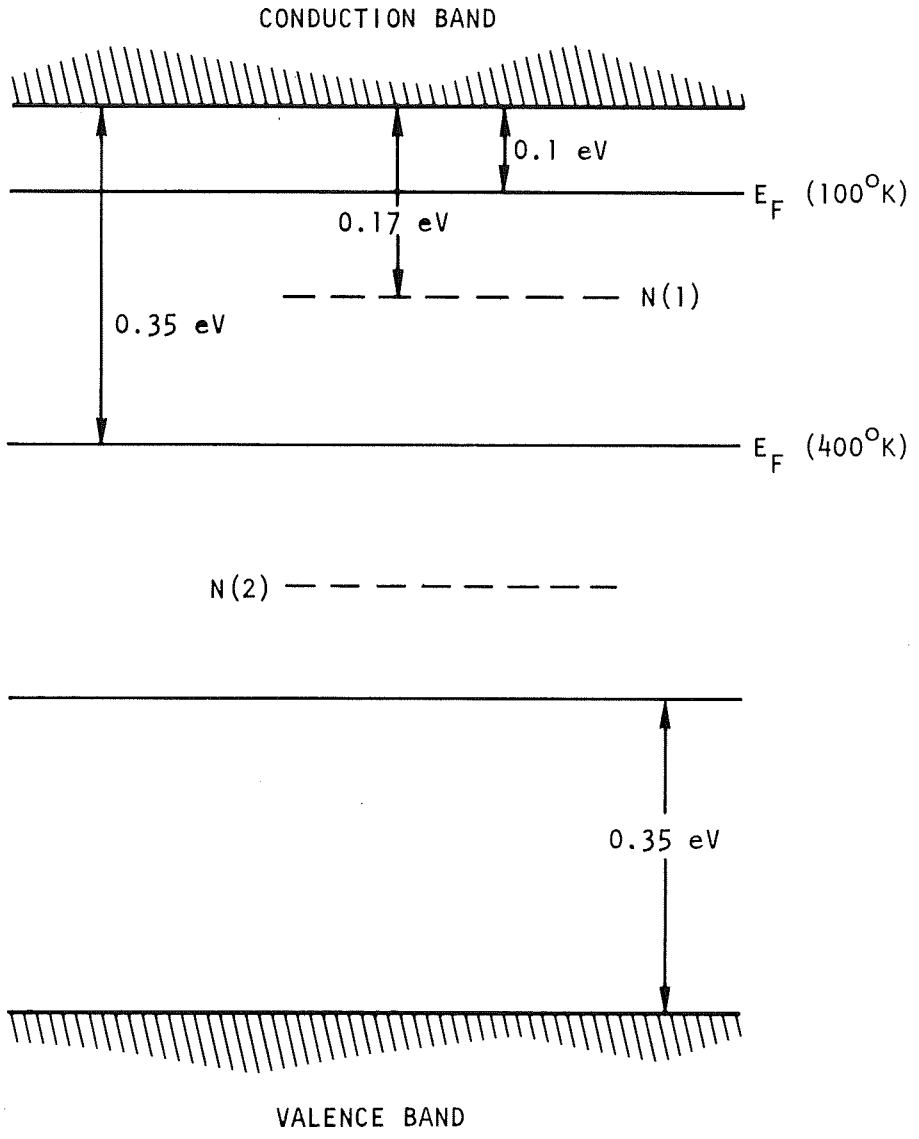


Fig. 9. Proposed energy level scheme for lightly diffused silicon before irradiation

The observed lifetime is then expected to be

$$\tau^{-1} = \tau(1)^{-1} + \tau(2)^{-1} \tag{15}$$

due to recombination through both centers. Below about 200°K, both $\tau(1)$ and $\tau(2)$ are of the form $\tau = (Nv\sigma)^{-1}$, so the composite lifetime is

$$\tau^{-1} = \tau(1)^{-1} + \tau(2)^{-1} = N(1)v\sigma(1) + N(2)v\sigma(2) \quad . \tag{16}$$

Above about 200 to 250°K, $\tau(1)$ begins to increase exponentially. Since the observed lifetime is

$$\tau = \frac{\tau(1)\tau(2)}{\tau(1) + \tau(2)} \quad , \tag{17}$$

above 200 to 250°K it is dominated by the shorter lifetime $\tau(2)$. The solid line through the data in Fig. 8 is predicted by the above two-center model with $N(1) = 10^{11}$ cm$^{-3}$ centers near $E_c$ - 0.17 eV and $N(2) = 7 \times 10^{10}$ cm$^{-3}$ attractive centers more than 0.35 eV from the band edge. The preirradiation lifetime-temperature dependence of all the 11-ohm-cm samples seemed to fit this two-lifetime model for recombination center densities ranging from $5 \times 10^{10}$ to $1.2 \times 10^{11}$ cm$^{-3}$. Similar lifetime-temperature dependences have been observed in other samples in this laboratory and in p-type silicon by other investigators.[21]

The most distinguishing characteristic of the two-center model is a break in the inverse temperature-dependence curve between temperature regions dominated by one or the other center. For all the low-lithium-density samples, this break occurred near $1000/T = 4.5$ ($200 < T < 250$°K).

5.5.2.2. 300°K Degradation and Annealing. Four samples were irradiated at 300°K, two samples were irradiated at 115°K, and one sample was irradiated at 200 and 250°K. The irradiation temperature dependence of the lifetime degradation rate was investigated from 115 to 300°K.

Figures 10 and 11 show the degradation of lifetime at 300°K versus electron fluence for two samples which were degraded and annealed a number of times. These samples were damaged by 4.5-μsec Linac pulses at fluences ranging from 0.8 to 2.5 x $10^{11}$ e/cm$^2$-pulse. Figure 12 shows the minority-carrier lifetime temperature dependence for a sample before and after irradiation at 300°K. The initial 300°K degradation constants for these samples were found to be 5.0±2.0 x $10^{-8}$ cm$^2$/e-sec for fluences up to $10^{13}$ e/cm$^2$. It would appear from Fig. 10 that the degradation rate, for fluences greater than about $10^{13}$ e/cm$^2$, decreases, approaching 3 x $10^{-8}$ cm$^2$/e-sec. The uncertainty of the degradation rate determined from these measurements is rather disappointing. However, it is clear (see Fig. 13) that the degradation rate at 300°K for this lightly diffused silicon is nearer the degradation rate for non-lithium-diffused silicon (K = 6±2 x $10^{-8}$ cm$^2$/e-sec) of the same resistivity than to the rate for highly lithium-diffused silicon (K = 1.5±0.3 x $10^{-7}$ cm$^2$/e-sec). These data confirm previous observations that the degradation rate does depend on the initial lithium concentration.

5.5.2.3. Radiation-Induced Recombination Centers. After irradiation to fluences of about $10^{12}$ e/cm$^2$ (30 MeV), two samples were immediately cooled to 115°K, and the low-injection-level postirradiation minority-carrier lifetime was then measured as the sample was gradually warmed to about 310°K. It is assumed that negligible annealing took place during these measurements at reduced temperatures. Figure 12 shows this postirradiation-preanneal lifetime, which can be attributed to recombination through both the radiation-induced recombination centers and the recombination centers present before irradiation. The contribution to the measured lifetime due only to the radiation-induced recombination centers can be determined from

$$\frac{1}{\tau} = \frac{1}{\tau_0} + \frac{1}{\tau_D} \quad , \tag{18}$$

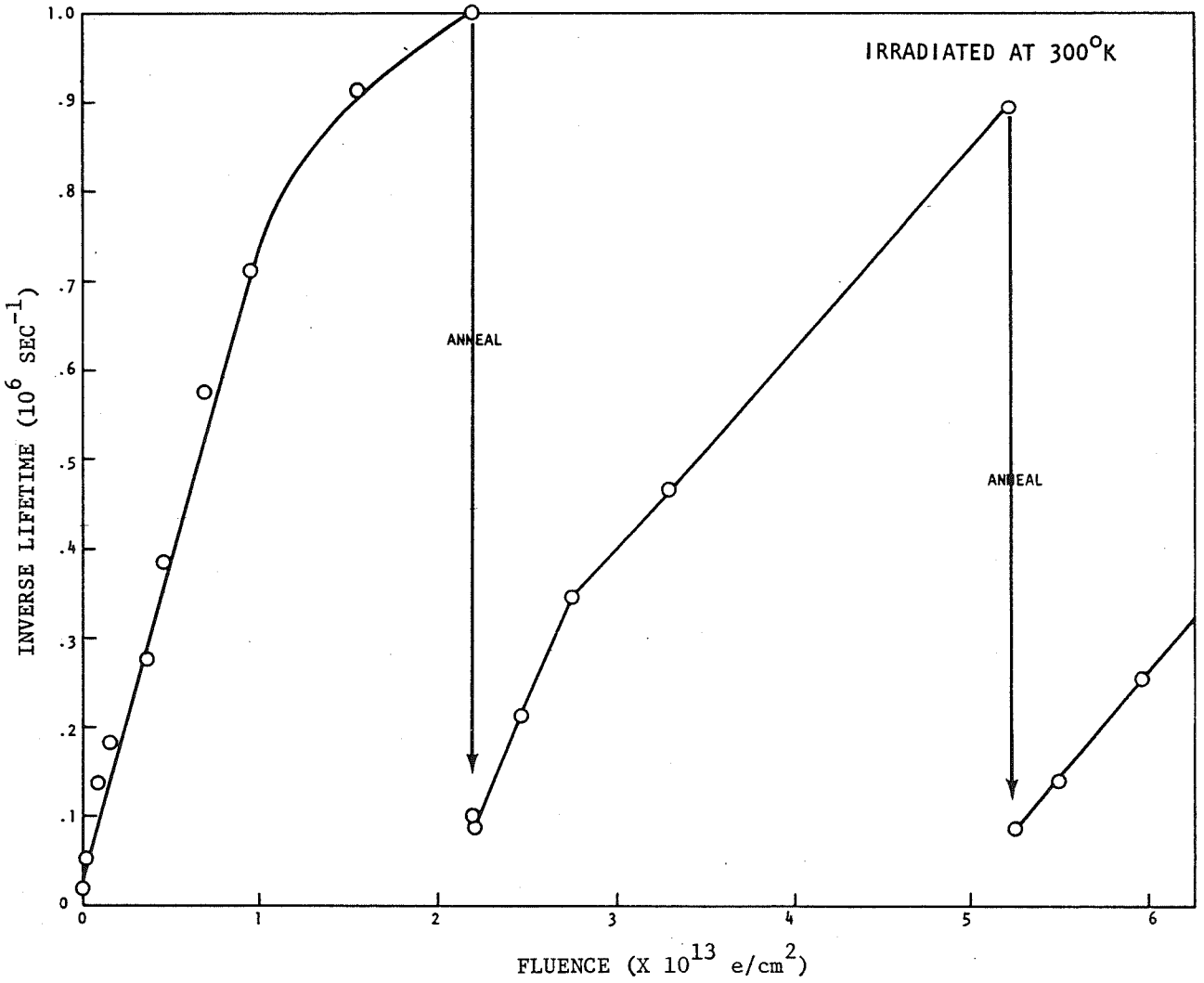


Fig. 10. Inverse lifetime versus 30-MeV electron fluence for 11-ohm-cm, lithium-diffused n-type silicon sample

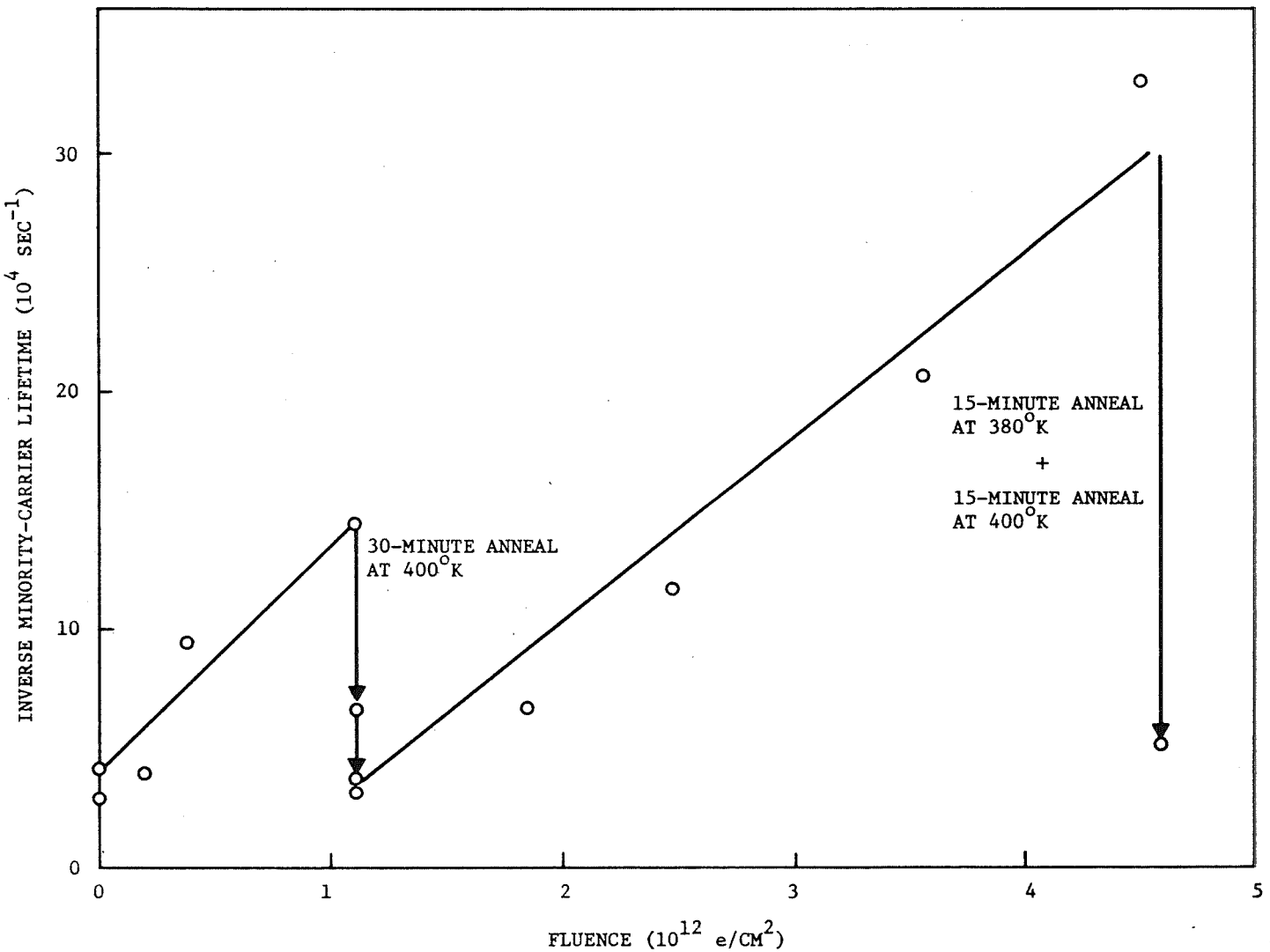


Fig. 11. Degradation of lifetime versus 30-MeV electron fluence for 11-ohm-cm, lithium-diffused n-type silicon

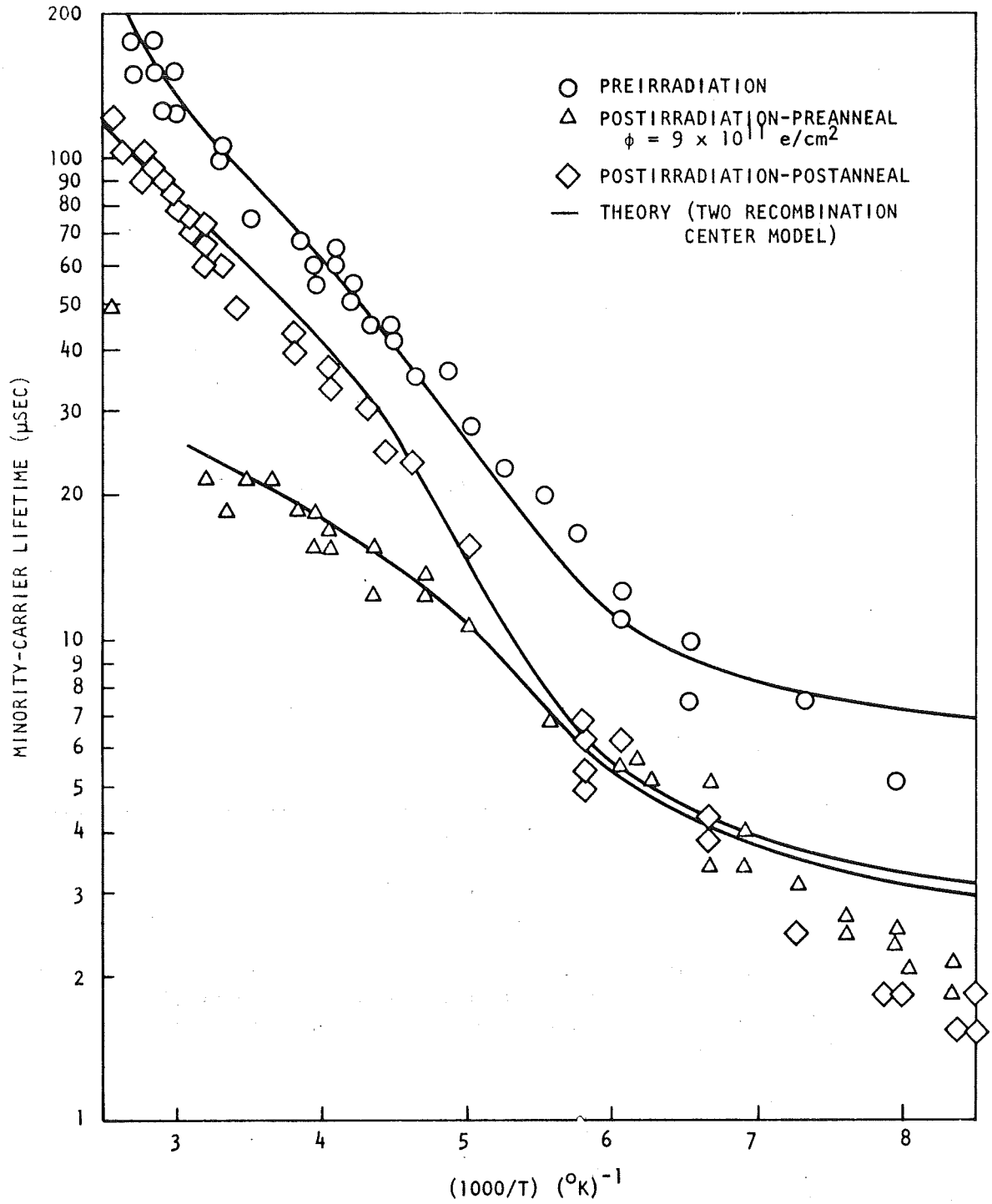


Fig. 12. Inverse temperature dependence of minority-carrier lifetime in an 11-ohm-cm lithium-diffused silicon sample exposed to 30-MeV electrons at 300°K

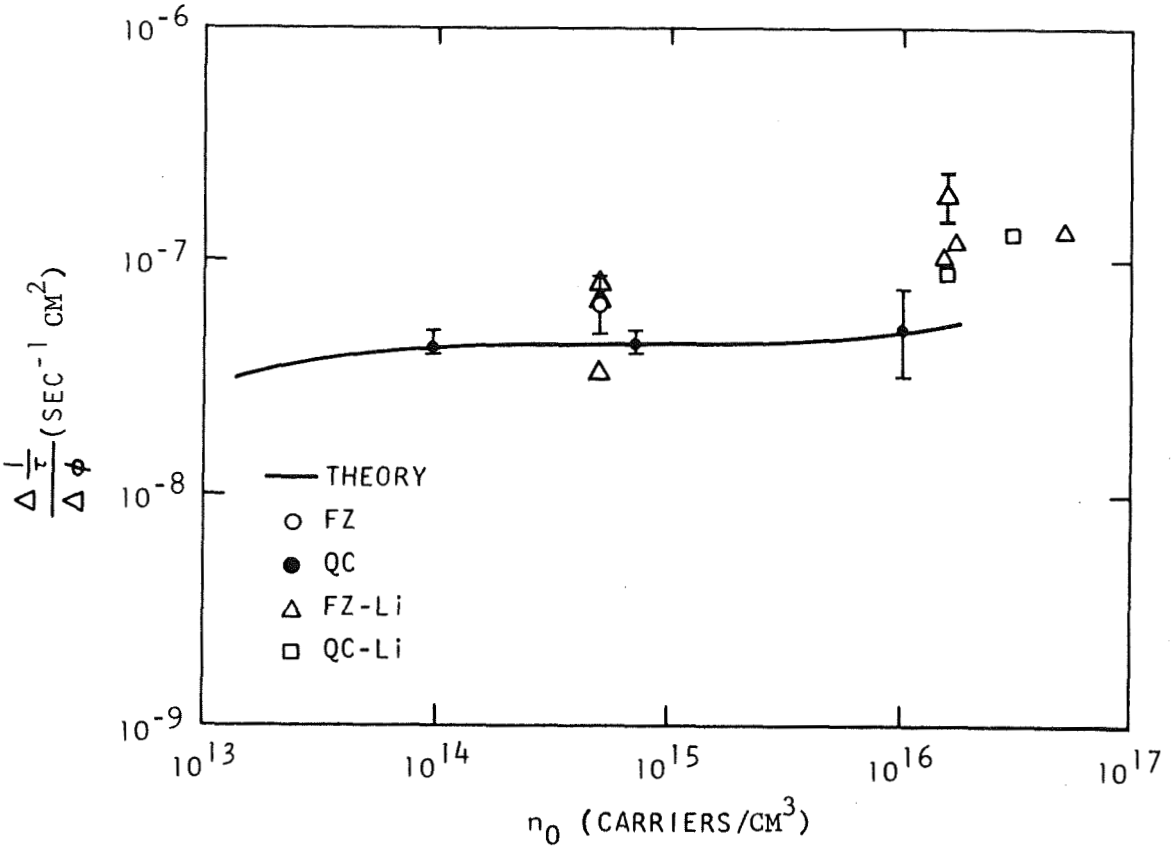


Fig. 13. Lifetime degradation constant versus majority-carrier concentration for FZ and QC n-type silicon irradiated with 30-MeV electrons at 300°K (theory curve based on analysis of work performed under a previous contract

where $\tau$ is the measured postirradiation-preanneal lifetime, $\tau_0$ is the preirradiation lifetime, and $\tau_D$ is the lifetime due to the radiation-induced recombination centers.

After the postirradiation-preanneal data had been obtained, samples were isothermally annealed for 1/2 to 1 hr at temperatures between 385 and 400°K.

Figure 12 shows the inverse temperature dependence of minority-carrier lifetime after a 300°K irradiation to $9 \times 10^{11}$ e/cm$^2$ and an isothermal anneal at 385°K for 1 hr. It is apparent from this plot that the anneal was not complete. In fact it appears that no increase in the postanneal lifetime occurred at temperatures below about 200°K (1000/T = 5). These results are qualitatively confirmed by a similar experiment (see Fig. 14) in which a similar sample was irradiated at 300°K to $1.1 \times 10^{12}$ e/cm$^2$ and measured before and after a 30-min anneal at 400°K. Assuming the postirradiation-postanneal lifetime is due to unannealed radiation-induced recombination centers and the unaltered recombination centers present before irradiation, the contribution ($\tau'$) of the unannealed radiation-induced recombination centers to the measured lifetime ($\tau$) can be determined as before from

$$1/\tau = 1/\tau_0 + 1/\tau' \quad . \tag{19}$$

Similarly, the lifetime due to those centers which were annealed may be determined from

$$1/\tau_{\substack{\text{annealed} \\ \text{centers}}} = 1/\tau_{\text{preanneal}} - 1/\tau_{\text{postanneal}} \quad . \tag{20}$$

Attempts were made to analyze the lifetimes of the radiation-induced and annealed recombination centers according to the Shockley-Read theory.

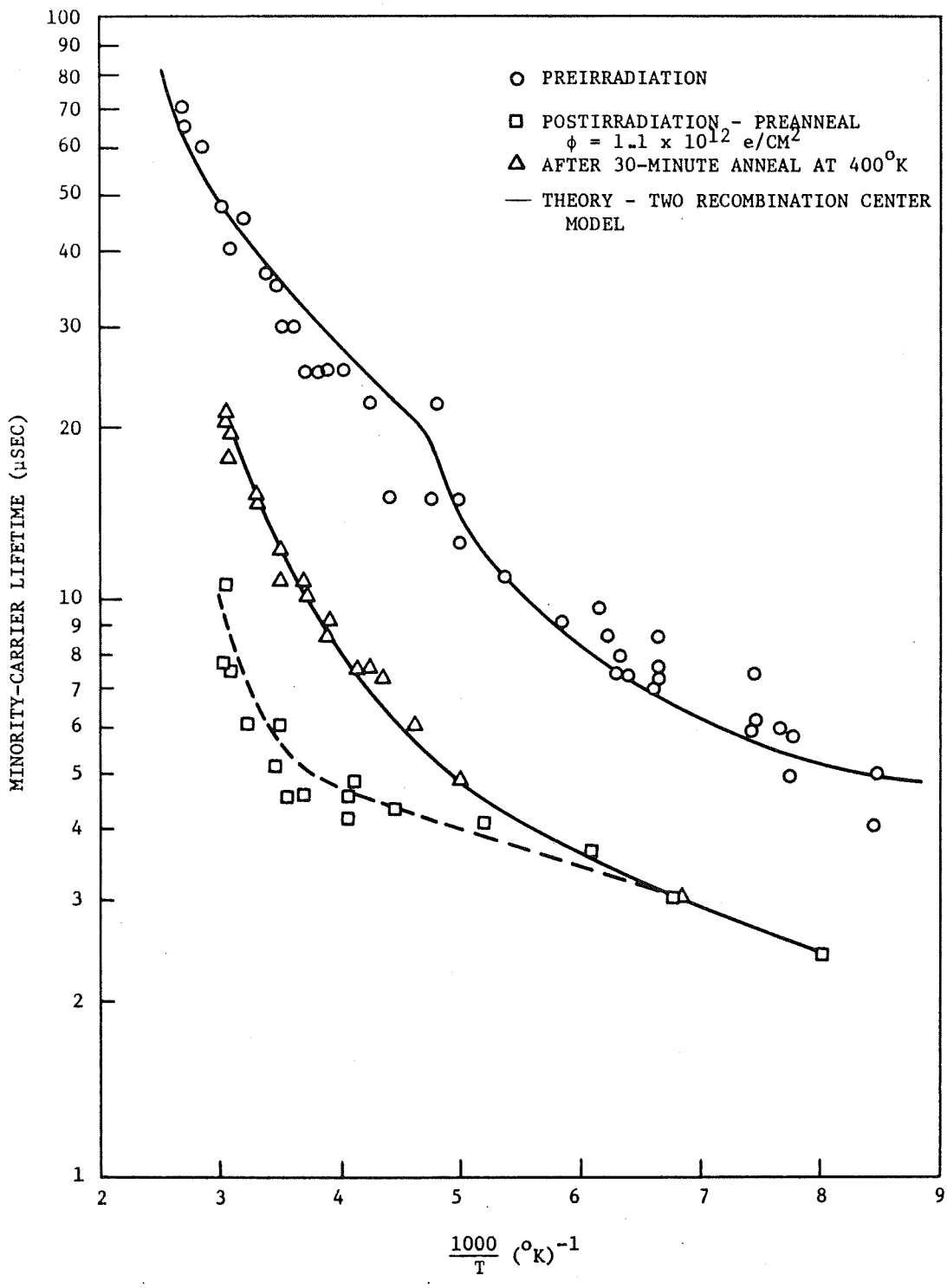


Fig. 14. Inverse temperature dependence of lifetime before and after irradiation with 30-MeV electrons to a fluence of 1.1 x $10^{12}$ e/cm$^2$ and before and after 30-min anneal at 400°K

Unfortunately, the experimental uncertainty of the minority-carrier lifetime data, as indicated by the scatter of the data in Fig. 12, prohibits an unambiguous determination of the energy level(s) and charge state(s) of the radiation-induced and annealed recombination centers by this sort of analysis alone. However, when these data are compared with some other experimental observations, a feasible model is suggested.

Other investigators,[22,23] using injection level and photoconductivity measurements, have noted the introduction of a deep ($E_c$ - 0.4 eV) defect level with 1- to 2-MeV electron irradiations, and the subsequent disappearance of this level upon annealing at 300°K. Our measurements indicate a significant increase in the observed lifetime at temperatures above about 200°K after annealing at 380 to 400°K. However, we observe no significant change in the low-temperature lifetime after this anneal. The postulate which seems most consistent with these observations and which best fits our data is that 30-MeV electron irradiations of 11-ohm-cm, lithium-diffused high-purity silicon produces two recombination centers. One of these centers is in the vicinity of $E_c$ - 0.17 eV and does not significantly anneal in 30 to 60 min at 380 to 400°K. The other center is deeper than 0.35 eV and is significantly reduced by the same annealing schedule. It is not presently known how these centers are related to the centers thought to control the preirradiation lifetime. The present minority-carrier lifetime measurements are not precise enough to distinguish the charge state of these defects. The solid curves through the postirradiation, preanneal, and postanneal data in Fig. 12 were calculated from this two-center model assuming radiation-induced defect densities from about $3 \times 10^{10}$ to about $4 \times 10^{11}$ $cm^{-3}$, depending on whether the defect was assumed to be neutral or attractive.

After the irradiated sample represented in Fig. 12 had been stored for 10 and 31 days at room temperature (300°K), the minority-carrier lifetime temperature dependence was remeasured as shown in Fig. 15. Inspection of Fig. 15 reveals considerable room temperature annealing has

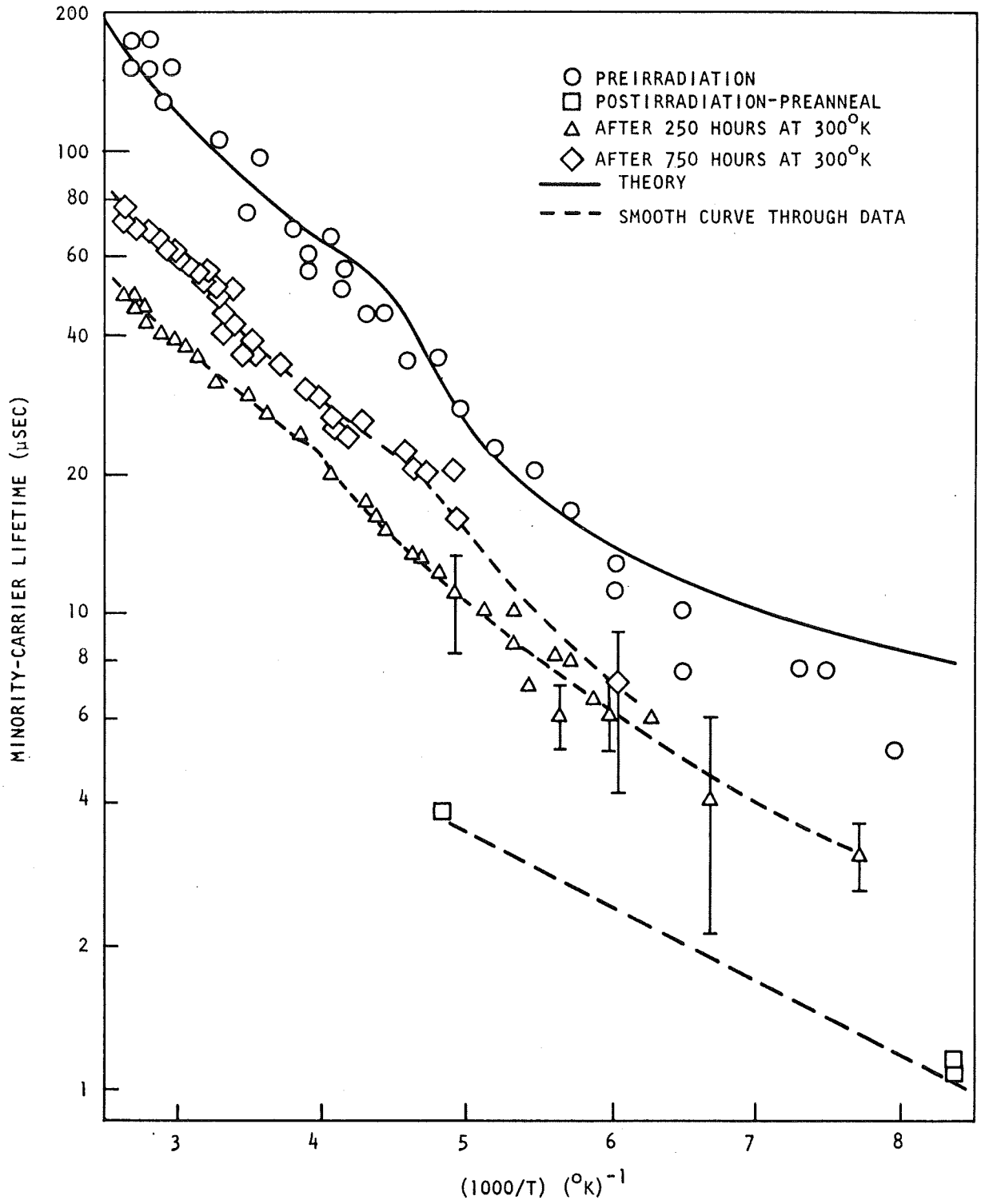


Fig. 15. Inverse temperature dependence, τ, of minority-carrier lifetime in 11-ohm-cm lithium-diffused silicon before and after irradiation to 30-MeV electrons and after approximately 250-hr anneal at about 300°K

occurred even in the 115 to 200°K temperature range (1000/T > 5). This result contrasts with the results of a 1-hr, 385 to 400°K anneal (shown in Figs. 12 and 14), where the low-temperature lifetime (1000/T > 5) was virtually unaffected. Comparison of Figs. 12 and 14 with Fig. 15 suggests that the lifetime of electron-irradiated float-zone silicon is due to at least two recombination centers: a deep one which controls carrier recombination above 1000/T $\sim$ 5, and a shallow one which dominates the recombination below 1000/T $\sim$ 5. Short (30- to 60-min) excursions to high (380 to 400°K) temperatures apparently reduces the density of the deeper center. Long periods at moderate temperatures (300°K) apparently anneal both centers. Isothermal and isochronal anneal data taken on these and more highly diffused samples suggest first-order annealing kinetics above about 360°K. At these temperatures, the lifetime is controlled by the deeper center. Such behavior suggests a single-stage annealing process. The shallow center does not significantly anneal during this process but anneals appreciably during extended storage at room temperature, perhaps suggesting a multistage annealing process.

5.5.2.4. Large Electron Fluences. When 11-ohm-cm samples were irradiated at room temperature to fluences approaching $10^{14}$ e/cm$^2$ and annealed, a trapping center was observed. Figure 16 shows postirradiation and anneal lifetime temperature dependences. The trapping center was apparent as a photodecay signal whose time constant increased with decreasing temperature. The amplitude of this signal was reduced in the presence of steady illumination, and no annealing of this trapping center was observed after holding one sample at 430°K for 66 hr. It may be significant that a trapping center is observed in the $10^4$-ohm-cm float-zone silicon (from which these samples were produced) after irradiation at room temperature to fluences of $8.2 \times 10^{10}$ e/cm$^2$.[17] Further study of this trapping center was prohibited by contacts which became rectifying at low temperatures.

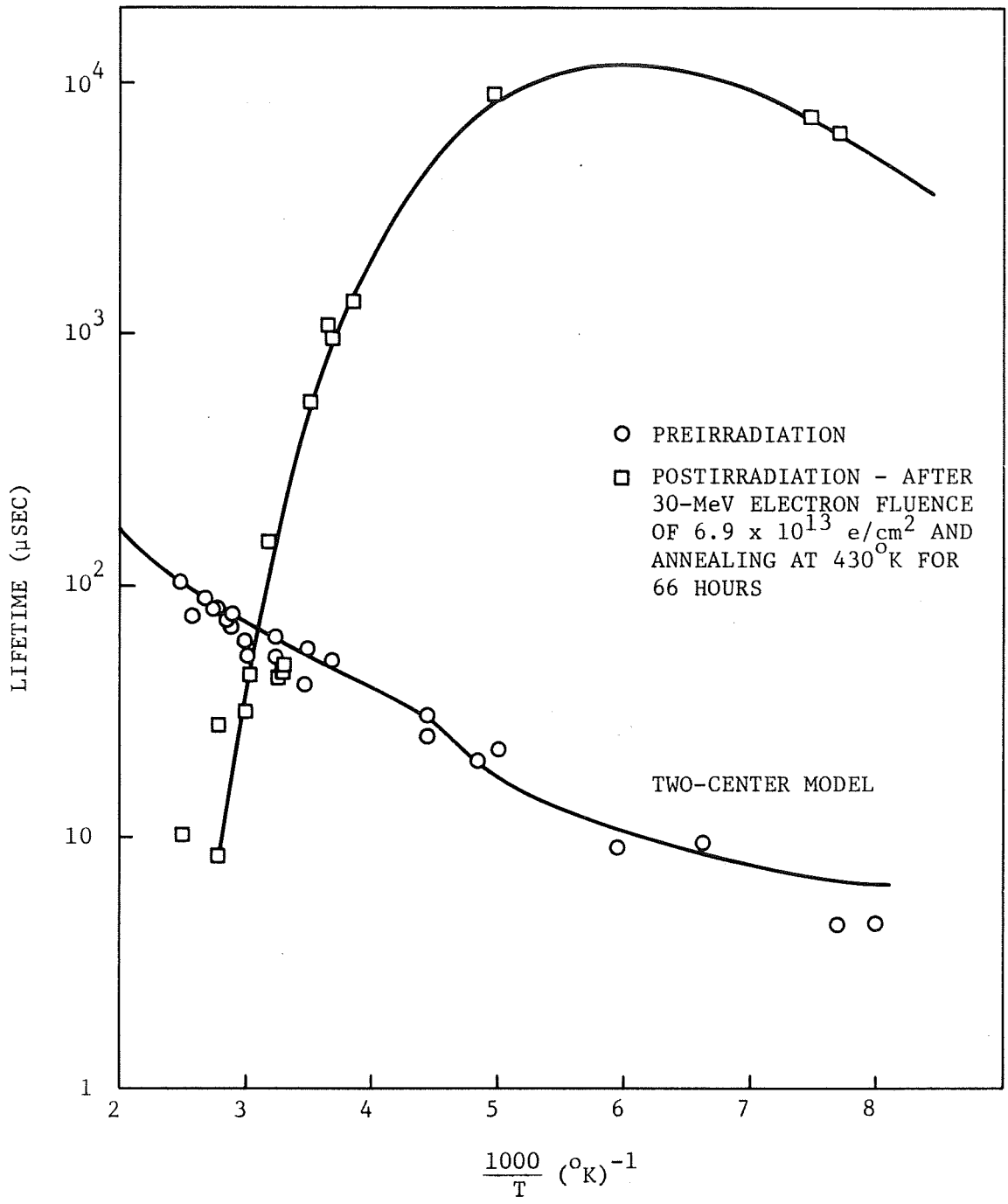


Fig. 16. Inverse temperature dependence of lifetime of 11-ohm-cm silicon

If the operation of the device is affected by the presence of trapping, special attention must be given to the introduction of traps with large electron fluences, especially since the traps do not anneal even in lithium-diffused n-type silicon.

5.5.2.5. Isothermal Anneals. After decreasing the minority-carrier lifetime at room temperature, samples were isothermally annealed for 1/2 to 1 hr at temperatures ranging from 380 to 400°K. The minority-carrier lifetime was monitored during the anneal. Because the lifetime at a particular temperature is inversely proportional to the recombination center density, the unannealed fraction of total defects as a function of annealing time was determined using Eq. (10)(see Fig. 17).

Since the isothermal annealing data displayed in Fig. 17 represent first-order annealing kinetics, one may calculate an activation energy and frequency factor.[20] For first-order kinetics, the recombination center density, N(T,t), at temperature T and time t is

$$N(T,t) = N_0 \exp [-R(T)t] \quad , \tag{21}$$

where $N_0$ is the initial recombination center density. The temperature-dependent rate constant, R(T), is

$$R(T) = \nu_e \exp(-E/kT) \quad , \tag{22}$$

where $\nu_e$ is the effective frequency factor and E is the activation energy. From the above, one may compute a temperature-dependent annealing time

$$\tau = (1/\nu_e)\, e^{E/kT} \quad . \tag{23}$$

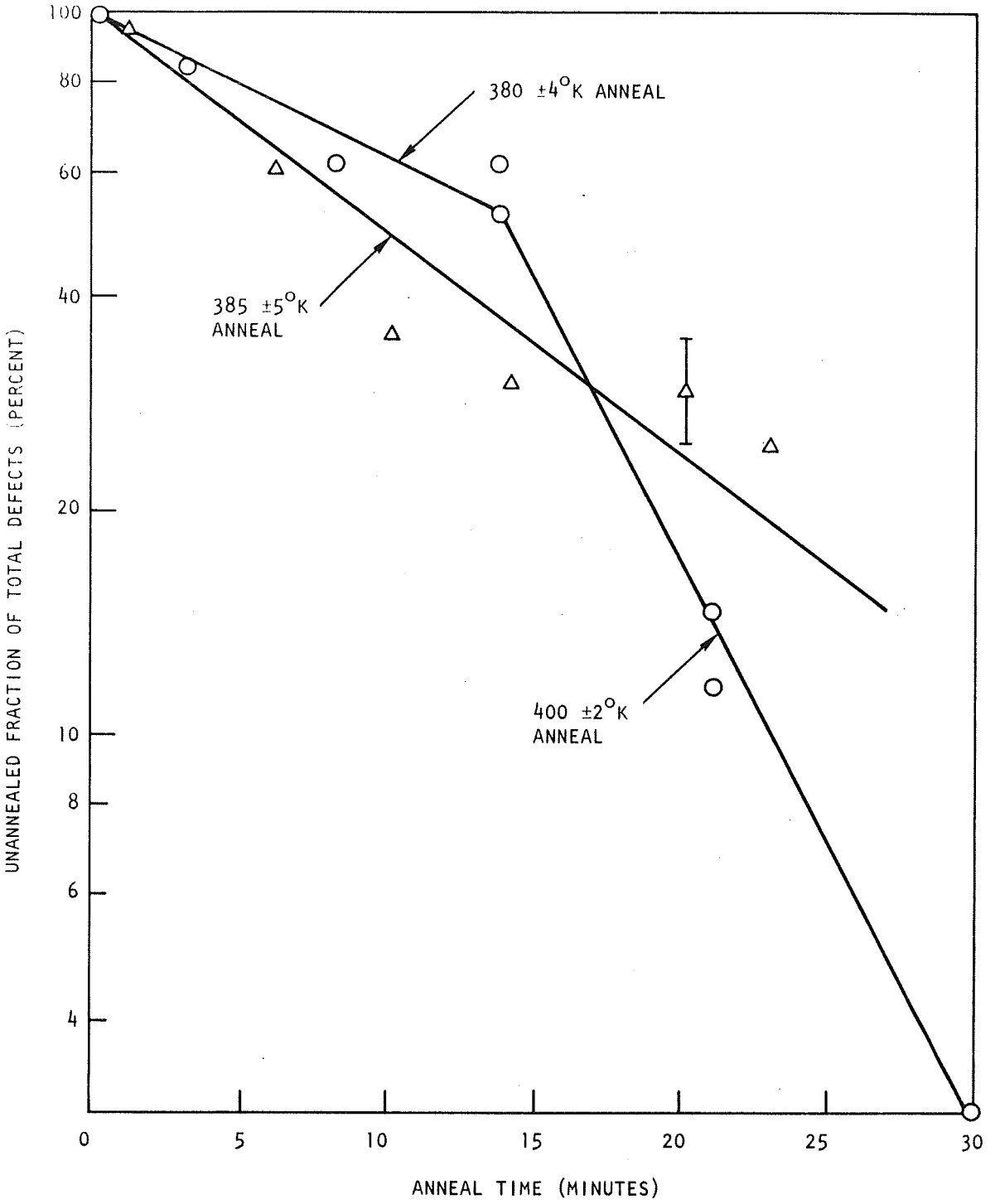


Fig. 17. Isothermal anneal of recombination centers in 11-ohm-cm, lithium-diffused n-type silicon irradiated with approximately 1 to 5 x $10^{12}$ 30-MeV electrons

The results of this calculation are displayed in Fig. 18 together with the equivalent results for low-resistivity, lithium-diffused float-zone (FZ) silicon. The similarity in slope indicates that the activation energies are similar ($E \cong 0.75 \pm 0.1$ eV) for the float-zone materials. The vertical offset results from different effective frequency factors. This is consistent with the idea that the anneal is due to lithium diffusing to the radiation-induced recombination center: the greater the lithium concentration, the shorter the migratory path and the shorter the annealing time. The comparison with the quartz crucible (QC) material is discussed in Ref. 1. From these isothermal studies, it is evident that the annealing rate depends on the amount of lithium and oxygen present in the silicon. In general, the greater the concentration of free lithium, the faster the annealing rate.

5.5.2.6. Irradiation Temperature Dependence. The introduction of temperature-dependent defects believed to be due to the irradiation production and subsequent temperature-controlled separation of metastable close-spaced vacancy interstitials has been observed in silicon irradiated at temperatures below about 125°K with low-energy electrons ($E \leq 2$ MeV)[24-26] and X-rays.[27] Temperature-independent defects introduced by these irradiations are observed to anneal near 200°K. The 11-ohm-cm lithium-diffused sample shown in Fig. 12 was also irradiated at 115°K, following which it was held at 200°K for 1 hr. No increase in lifetime during the 200°K anneal was observed in either of two 11-ohm-cm samples irradiated at 115°K with 30-MeV electrons. Within the uncertainty of our measurements, the recombination center introduction rate was the same for irradiations at 115, 200, 250, and 300°K, with measurements made at 115°K. This result is predictable for two reasons. First, the introduction of irradiation-induced temperature-dependent defects due to the competing, thermally activated processes of vacancy-interstitial separation and recombination is generally only weakly apparent at temperatures as high as 115°K. Second, the irradiation temperature-dependent process is thought to require closely spaced vacancy-interstitial pairs. Both clusters and point defects are produced by high-energy (30-MeV) electron irradiations, and only a fraction of the point defects are of the appropriate type.

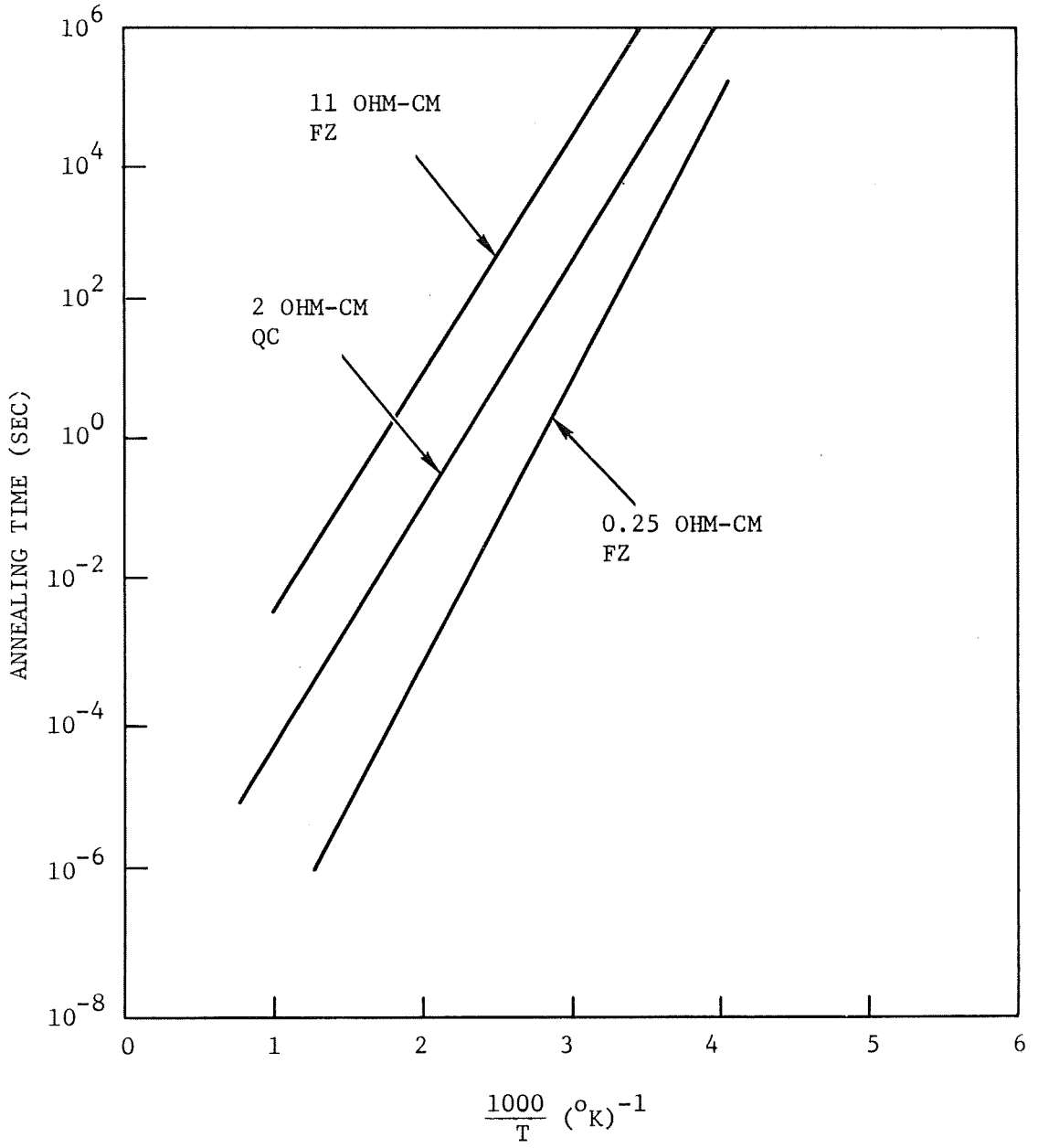


Fig. 18. Annealing time of lithium-diffused n-type silicon as a function of inverse temperature after 30-MeV electron irradiation

The above results indicate that at low fluences, the recombination center introduction rate is independent of irradiation temperature from 115 to 300°K. However, the minority-carrier lifetime degradation constant, K, measured at the irradiation temperature does depend on temperature, because the minority-carrier thermal velocity and the radiation-induced recombination center capture cross section depend on temperature. That is, if the radiation-induced recombination center density, $N_D$, introduction rate is a temperature-independent constant, C, so that $N_D = C\Phi$, and the preirradiation lifetime is

$$\tau_0 = (N_0 \, v\sigma_0)^{-1} \quad , \tag{24}$$

then after irradiation to a fluence $\Phi$, the lifetime will be

$$\tau_0 = (N_0 \, v\sigma_0 + N_D \, v\sigma_D)^{-1} \quad , \tag{25}$$

where $\sigma_D$ is the capture cross section of the radiation-induced centers. Calculation of the minority-carrier lifetime degradation rate, $K = (1/\tau - 1/\tau_0)/\Phi$, yields $K = Cv\sigma_D$. Figure 19 shows the degradation constants measured at 115, 200, 250, and 300°K.

It is evident that the degradation constant increases with decreasing temperature, and it is possible to predict the degradation constant at any temperature if the temperature dependence of v and $\sigma_D$ are known.

5.5.2.7. Conclusions. Based on the analysis of the change in minority-carrier lifetime in 11-ohm-cm lithium-diffused silicon, the following observations can be made:

1. The initial preirradiation lifetime is due to at least two centers. The temperature dependence indicates that one center is near $E_c$ - 0.17 eV, and that the other is an attractive center deeper than 0.35 eV from either band edge.

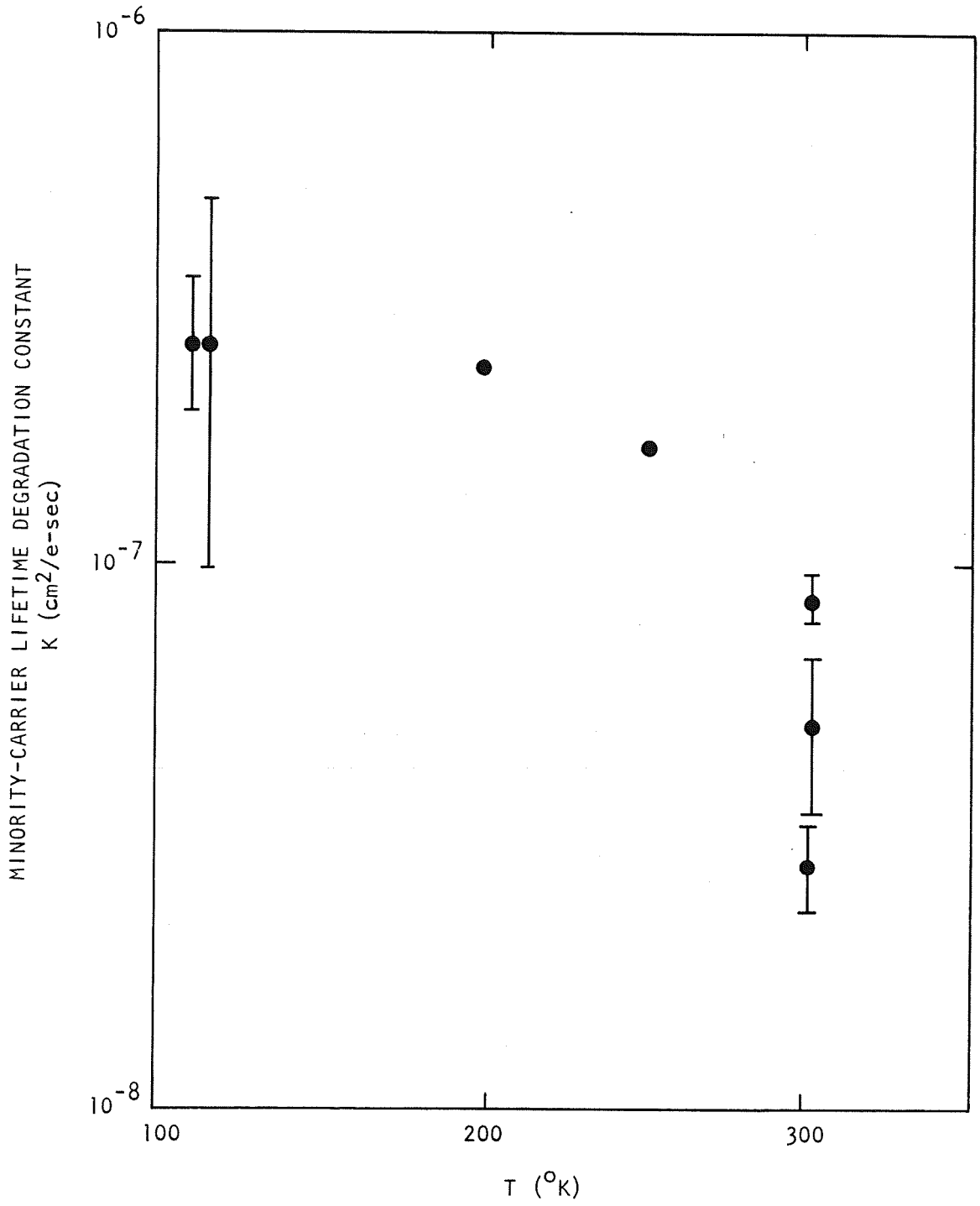


Fig. 19. Minority-carrier lifetime degradation constant for lithium-diffused silicon versus temperature of irradiation and measurement

2. At least two kinds of recombination centers are introduced in this material by the 30-MeV electron irradiation, one dominant at temperatures above 150 to 200°K and the other dominant below 150 to 200°K.

3. The dominant postirradiation-preanneal center at low temperatures has an energy level near $E_c$ - 0.17 eV.

4. The dominant postirradiation-preanneal center at high temperatures is deeper than 0.35 eV from either band edge.

5. The low-temperature center is not significantly annealed in 1 hr at 390°K for the lithium density in this material but appears to anneal, at least partially, over long periods at room temperature and to anneal completely in more highly diffused samples.

6. The high-temperature center is significantly annealed by the presence of lithium for the lithium densities present in this material.

7. The high-temperature center affects the lifetime very similarly to the center introduced in high-purity, non-lithium-diffused silicon.[17] This suggests that either (a) this center is the same in lithium-diffused and non-lithium-diffused silicon and, hence, probably does not contain lithium (although its introduction rate and annealing properties may be affected by lithium), or (b) this center and the one in the non-lithium-diffused silicon are different but have very similar recombination properties. However, there is no definite information on the nature of either the high-temperature or low-temperature center in this material.

8. Successive irradiations and anneals could shift the low-temperature portion of the curve downward and to higher temperatures. Thus, at some fluence, the dominant low-temperature center might become dominant at room temperature, perhaps changing the subsequent room temperature damage constants and annealing characteristics.

9. No irradiation temperature dependence of the recombination center introduction rate for 30-MeV electrons in the 115 to 300°K temperature range was observed.

10. The minority-carrier lifetime degradation constant for lithium-diffused samples irradiated and measured at 300°K is an order of magnitude smaller than that for samples irradiated and measured at 115°K.

5.5.3. Neutron Irradiations

Neutron irradiation of lithium-diffused silicon is of interest because of the nature of defects produced by neutrons. Neutrons are known to produce mainly clustered defects, and the introduction of these defects is independent of the impurities present in the silicon. Annealing experiments on neutron-irradiated n-type silicon containing ordinary oxygen concentrations and arsenic and phosphorus concentrations below $6 \times 10^{14}$ have indicated insignificant impurity dependence.[28]

5.5.3.1. Preirradiation and Degradation. Two identical 3.7-ohm-cm samples (designated a and b) were made from $10^4$-ohm-cm, float-zone n-type silicon by the lithium-tin bath technique. Figures 20 and 21 show the preirradiation and postirradiation conductivity versus 1000/T for these samples. Preirradiation minority-carrier lifetime ($\tau$) was

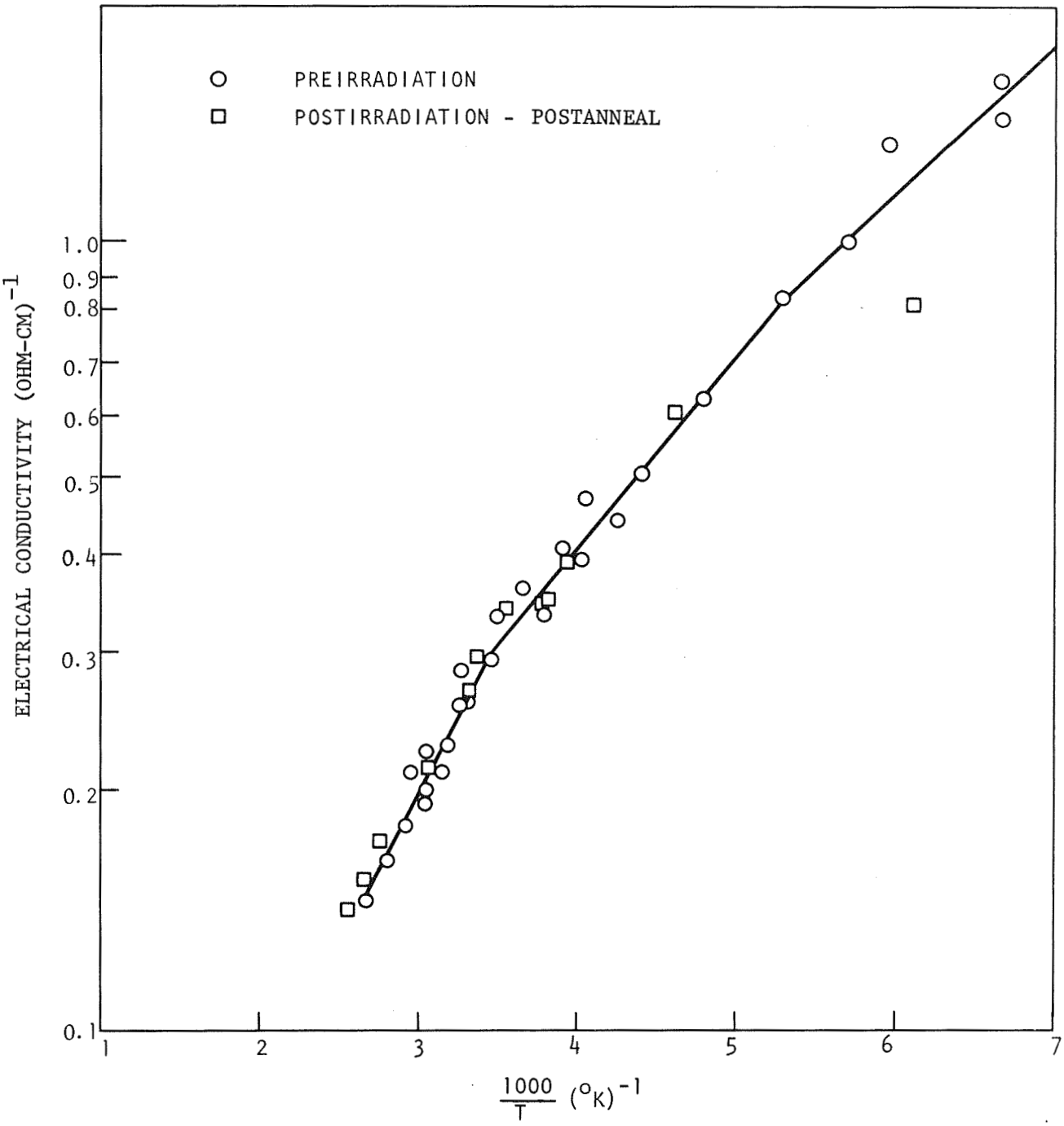


Fig. 20. Preirradiation and postirradiation conductivity versus 1000/T for sample a

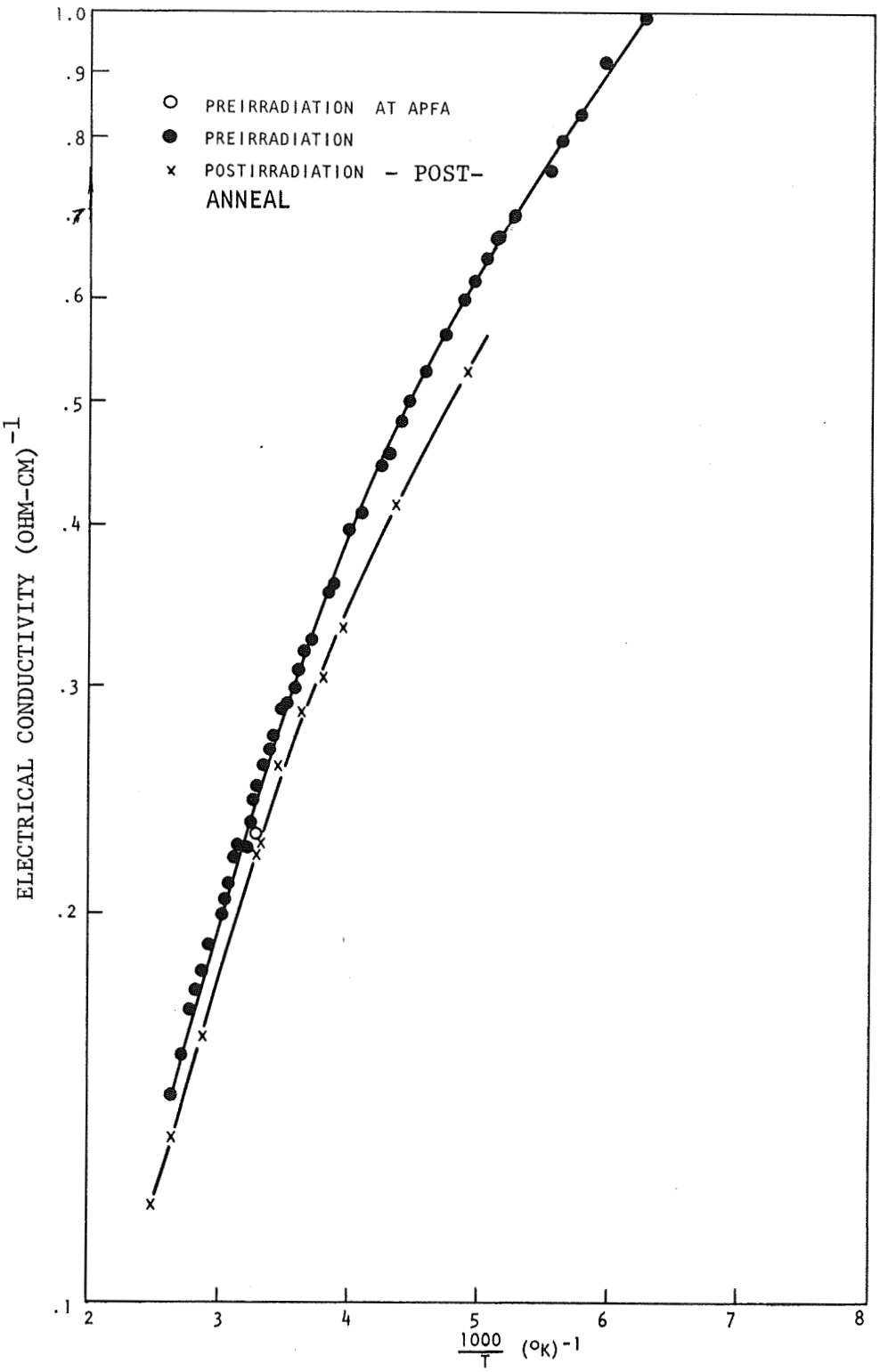


Fig. 21. Preirradiation and postirradiation electrical conductivity versus 1000/T for sample b

measured by photoconductivity decay and steady-state photoconductivity techniques as described in Sections 5.2.1 and 5.2.2. During irradiation, $\tau$ was monitored by the steady-state technique where $\tau = A|\Delta V/V|$. As with the 11-ohm-cm samples, the preirradiation lifetime (shown in Fig. 22) can best be explained by assuming two recombination centers, one at $E_c$ - 0.17 eV and the other deeper than 0.35 eV. The solid curve in Fig. 22 represents the lifetime for $1.2 \times 10^{11}$ $cm^{-3}$ shallow and $1.2 \times 10^{11}$ $cm^{-3}$ deep centers.

These samples were subjected to neutron irradiations at GGA's APFA facility. The APFA was run in the continuous mode at a neutron flux of $6.2 \times 10^{7}$ neutrons/$cm^2$-sec. Fluences were measured by extrapolation based on sulfur pellet dosimetry. Sample a was irradiated at 273°K and sample b at 302°K. Sample a had an initial 273°K lifetime of 30 μsec; this value was reduced to about 5 μsec by a fluence of $2.25 \times 10^{10}$ n/$cm^2$. The sample was isochronally annealed for 5-min periods at temperatures up to 411°K, degraded again, and isothermally annealed at 411°K. Figure 23 is a plot of $1/\tau$ versus fluence for sample a. Better than 90% of the damage introduced by the first irradiation was annealed. Apparently, all the damage introduced by the next two irradiations was annealed. The degradation constant was found to be $6.4 \pm 0.4 \times 10^{-6}$ $cm^2$/n-sec and is independent of the total fluence up to $\phi = 6.75 \times 10^{10}$ n/$cm^2$. This constant is also almost the same as that observed in non-lithium-diffused silicon,[29] which is consistent with the lack of impurity dependence for neutron damage.[30]

In an effort to detect lithium depletion, sample b was subjected to higher-fluence neutron irradiations. The sample was irradiated at room temperature (T = 302°K) to determine whether the degradation constant was a strong function of temperature. The initial room temperature lifetime of approximately 30 μsec was degraded to about 2 μsec by a fluence of $4.5 \times 10^{10}$ n/$cm^2$. The degradation constant at 302°K was found to be $K = 6.4 \pm 0.4 \times 10^{-6}$ $cm^2$/n-sec, the same degradation rate found

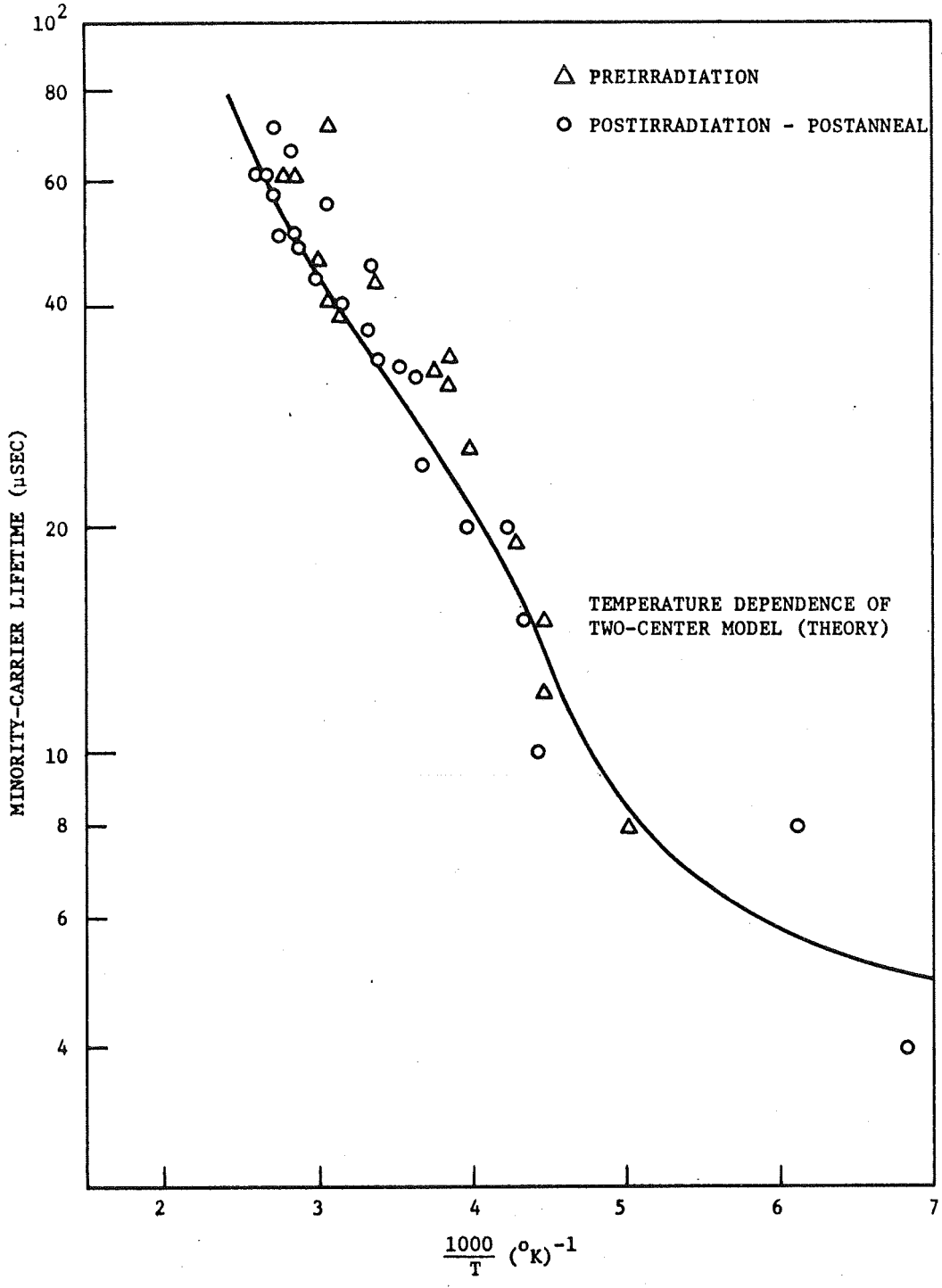


Fig. 22. Preirradiation and postirradiation minority-carrier lifetime versus 1000/T for neutron-irradiated 3.7-ohm-cm sample a

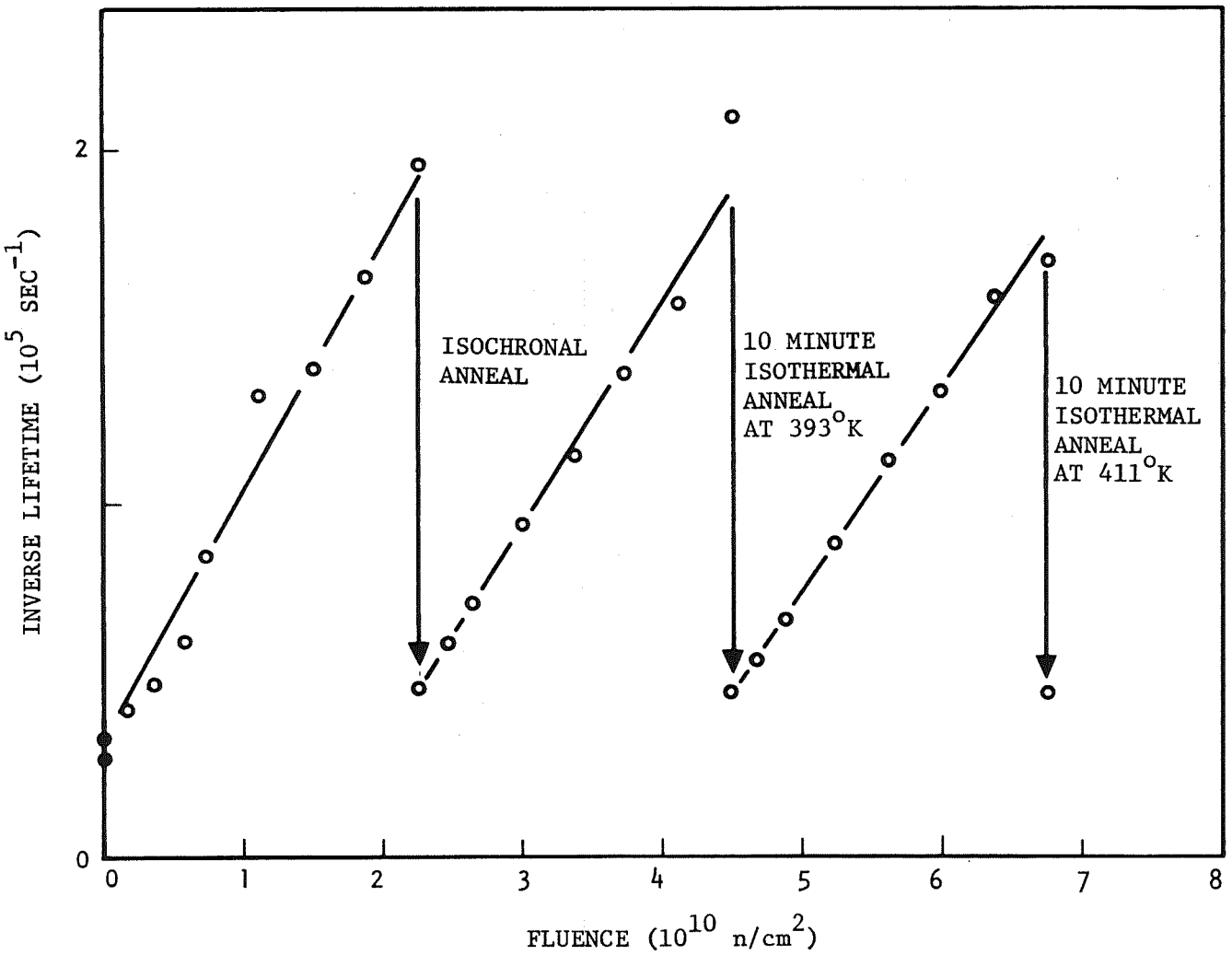


Fig. 23. Degradation of inverse lifetime as a function of fluence

for sample a at 273°K and very nearly the same as for phosphorus-doped float-zone silicon ($K \approx 5.8 \times 10^{-6}$) of equivalent resistivity.[29] Figure 24 is a plot of the inverse lifetime versus fluence for sample b. Four irradiations are represented, three to fluences of $4.5 \times 10^{10}$ n/cm$^2$ and one to $\phi \approx 1.3 \times 10^{11}$ n/cm$^2$. Between the first and second irradiations, the sample was isochronally annealed at temperatures up to 440°K. During this period, about 90% of the radiation-induced damage was annealed. Half of the remaining 10% may be due to a reverse anneal which was apparent at T > 420°K. After the other irradiations, the sample was isothermally annealed at T = 411°K. The degradation constant was $6.4 \pm 0.4 \times 10^{-6}$ cm$^2$/n-sec for all irradiations except the final and largest one, in which, at $\phi > 5 \times 10^{10}$ n/cm$^2$, the degradation constant decreased; after the final 10-min anneal at 410°K, the sample recovered only 40% of its initial lifetime. Nevertheless, this corresponds to an anneal of more than 90% of the radiation-induced defects after a total fluence of $\phi \approx 3.3 \times 10^{11}$ n/cm$^2$. Furthermore, after 2 days at room temperature, the room temperature lifetime had apparently further recovered.

5.5.3.2. Isothermal Anneal. Sample a was isothermally annealed at 393 and 411°K. Again, the sample was rapidly heated (t < 60 sec) to the anneal temperature and held there until changes in the minority-carrier lifetime (exhibited as $\Delta V/V$) were observed to cease. The annealed fraction of annealable defects is defined as

$$f_t = \frac{N_t - N_\infty}{N_0 - N_\infty} \quad , \tag{26}$$

where $N_\infty$ is the number of defects after annealing is complete, $N_t$ is the number of defects at any time t, and $N_0$ is the number of defects immediately after irradiation. Since the number of defects, in this case recombination centers, is related inversely to the minority-carrier lifetime, the annealed fraction can be written as

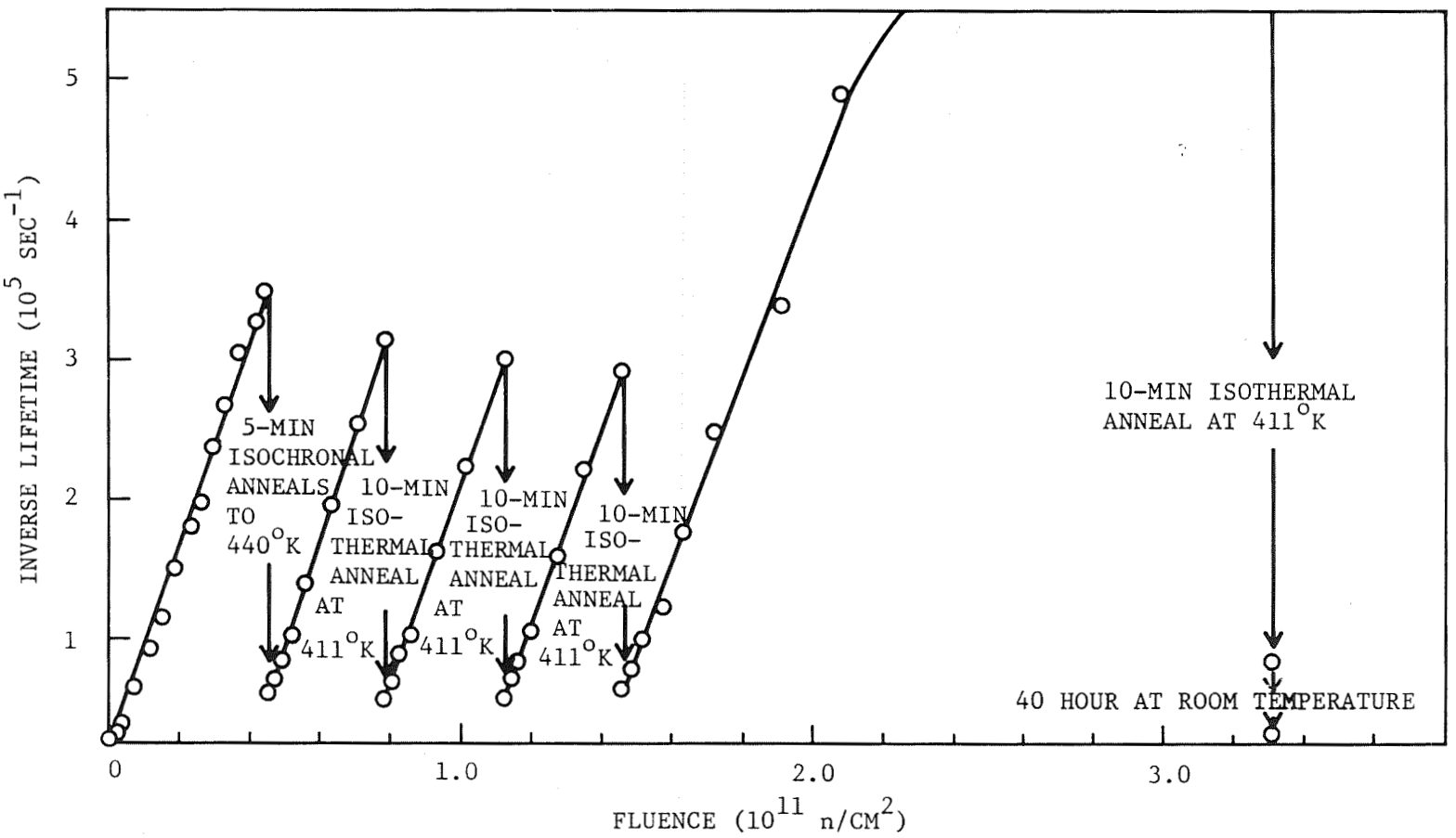


Fig. 24. Inverse lifetime versus neutron fluence for sample irradiated and measured at room temperature

$$f_t = \frac{\frac{1}{\tau_t} - \frac{1}{\tau_\infty}}{\frac{1}{\tau_0} - \frac{1}{\tau_\infty}} \quad , \tag{27}$$

and when the steady-state photoconductivity is measured,

$$f_t = \frac{\left(\frac{V}{\Delta V}\right)_t - \left(\frac{V}{\Delta V}\right)_\infty}{\left(\frac{V}{\Delta V}\right)_0 - \left(\frac{V}{\Delta V}\right)_\infty} \quad . \tag{28}$$

Figure 25 shows the annealed fraction of annealable defects as a function of time. Assuming first-order kinetics, one may determine the activation energy and the effective atomic frequency factor from any two isothermal anneals. The linearity of Fig. 25 is evidence that the annealing kinetics are, indeed, first order.

For sample a, the isothermal anneal data indicate that $E \approx 0.66 \pm 0.03$ eV and $\nu_e = 0.4 \pm 0.2 \times 10^{7}\ \text{sec}^{-1}$. These results yield an activation energy close to that of lithium diffusion in the silicon lattice.[31] The atomic frequency factor is quite low compared with the value $\nu_e = 10^{11}\ \text{sec}^{-1}$, which was observed for electron-irradiated lithium-diffused silicon.[1]

Figures 20 and 21 show the preirradiation and postirradiation conductivity of the sample. It is clear that the sample's electrical conductivity completely annealed.

For sample b, one isothermal anneal at 411°K was investigated. Figure 26 shows the unannealed fraction of annealable defects as a function of time for both samples a and b for a 411°K isothermal anneal. It is evident that the annealing rate is not significantly different for these two samples.

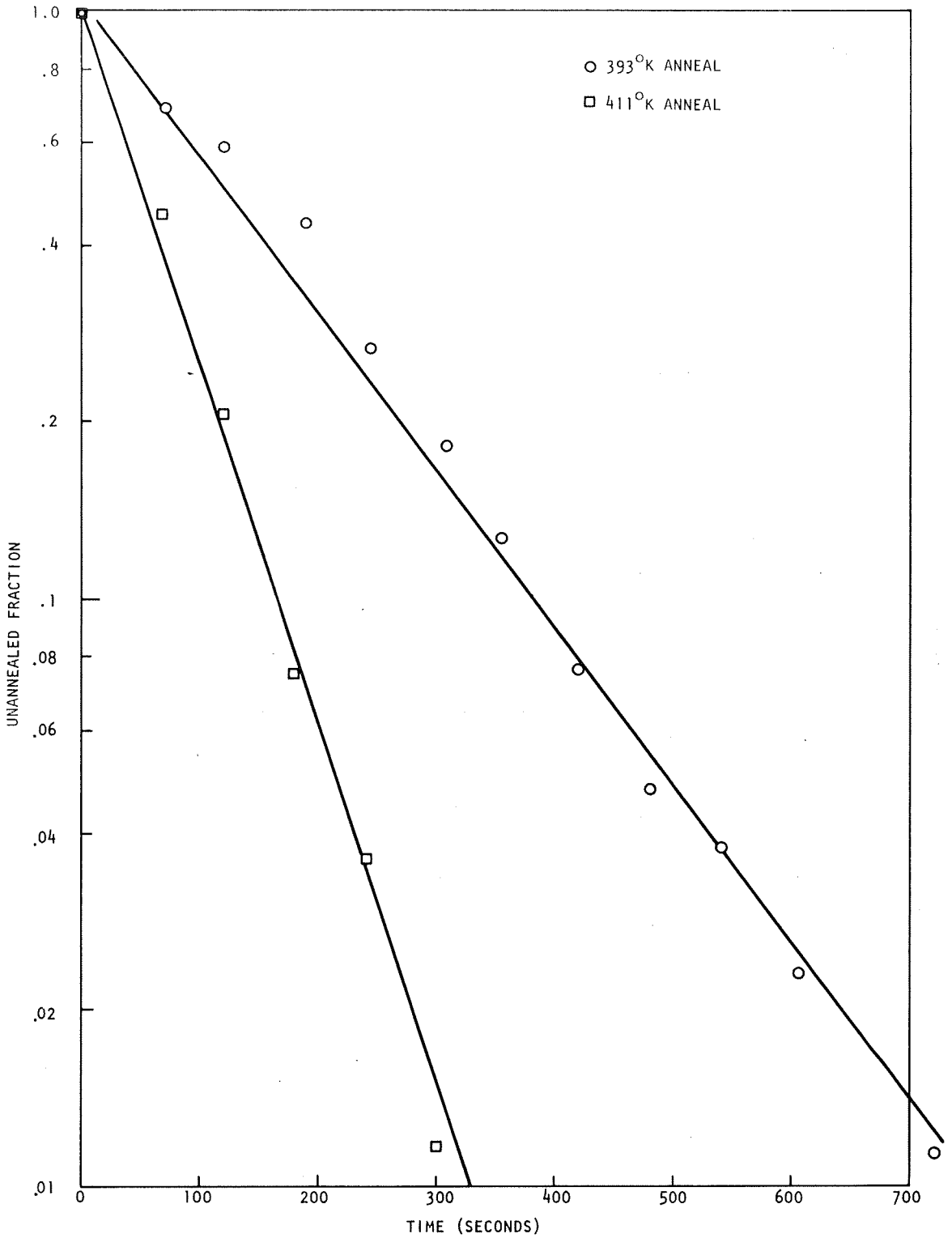


Fig. 25. Isothermal anneal of sample a

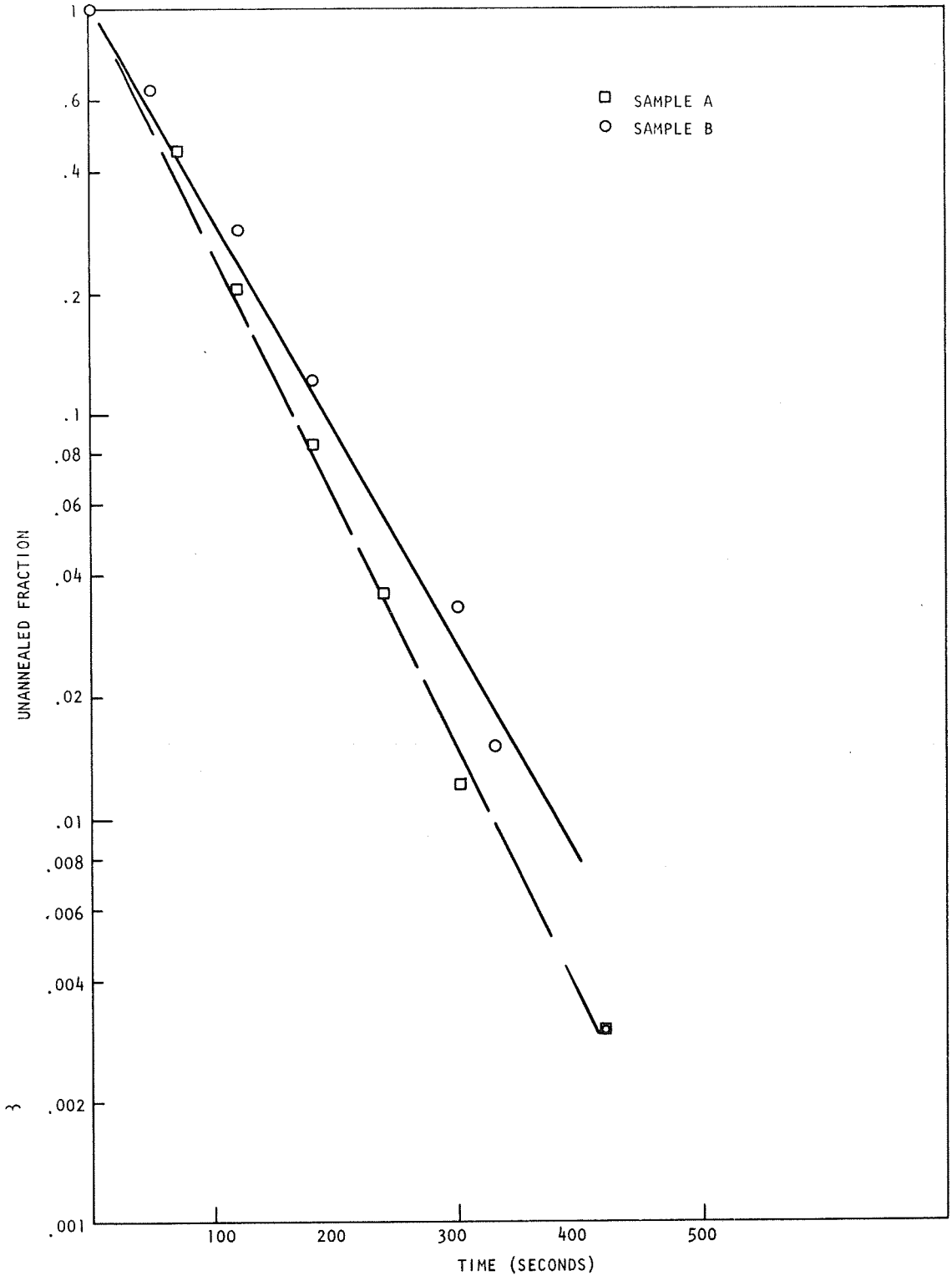


Fig. 26. Unannealed fraction of annealable defects for 411°K isothermal anneal versus time

5.5.3.3. Isochronal Anneal. Isochronal anneal data were taken by rapidly heating sample a to an elevated temperature, holding it at that temperature for 5 min, and rapidly cooling it to 273°K, where the lifetime (as evidenced by $\Delta V/V$) was remeasured.

Figure 27 shows the unannealed fraction of the total and annealable defects as a function of anneal temperature for sample a. The unannealed fraction of annealable defects is given by

$$f_T = \frac{(1/\tau_T) - (1/\tau_f)}{(1/\tau_0) - (1/\tau_f)} = \frac{(V/\Delta V)_T - (V/\Delta V)_f}{(V/\Delta V)_0 - (V/\Delta V)_f} \quad , \tag{29}$$

where $\tau_T$ is the observed lifetime at 273°K after 5-min anneal at temperature T, $\tau_0$ is the lifetime at 273°K immediately after irradiation, and $\tau_f$ is the observed lifetime after annealing has ceased.

Figure 28 is a semilogarithmic plot of $\ln(N/N_T)$ versus 1000/T, where N is the number of recombination centers prior to a 5-min anneal at temperature T, and $N_T$ is the number present after the anneal. The values of N and $N_T$ were always measured at the irradiation temperature of 273 or 302°K before and after the anneal. From the data of Fig. 28, the activation energy was found to be E = 0.69±0.02 eV. The atomic frequency factor was $\nu_0 = 1.5 \pm 0.8 \times 10^7$ sec$^{-1}$. These values are in agreement with the isothermal annealing results.

Sample b was isochronally annealed for 5-min periods at temperatures between 302 and 440°K. Figure 29 shows the unannealed fraction of damage versus temperature. The 5% annealing at room temperature is due in part to experimental uncertainty. In addition, the room temperature anneal was actually 10 min long, because possible room temperature isothermal annealing was being investigated. At 440°K, what appeared to be the beginning of a reverse anneal was observed.

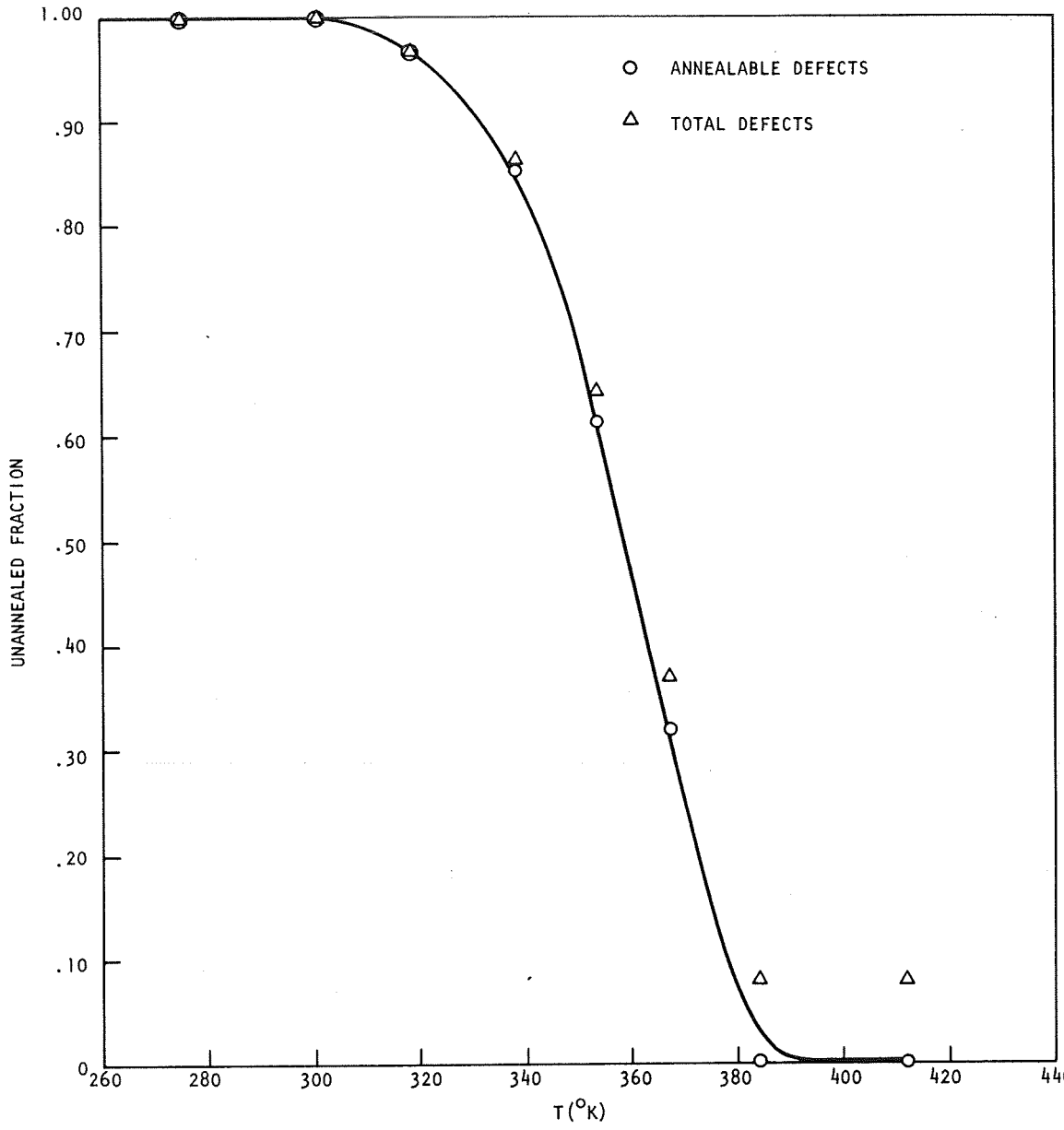


Fig. 27. Unannealed fraction of defects versus isochronal anneal temperature for neutron-irradiated 3.7-ohm-cm (sample a), lithium-diffused n-type silicon

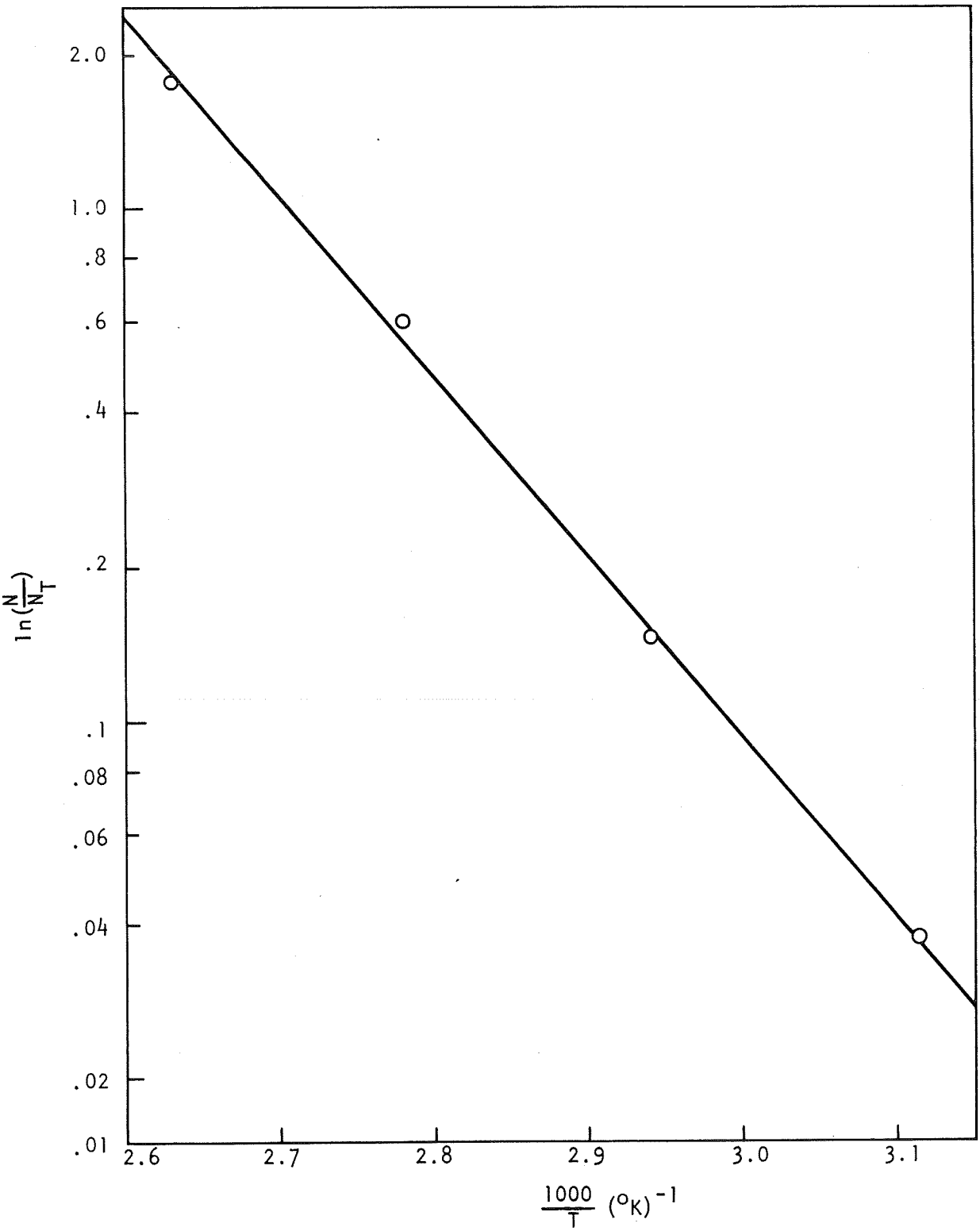


Fig. 28. Sample a isochronal anneal analysis

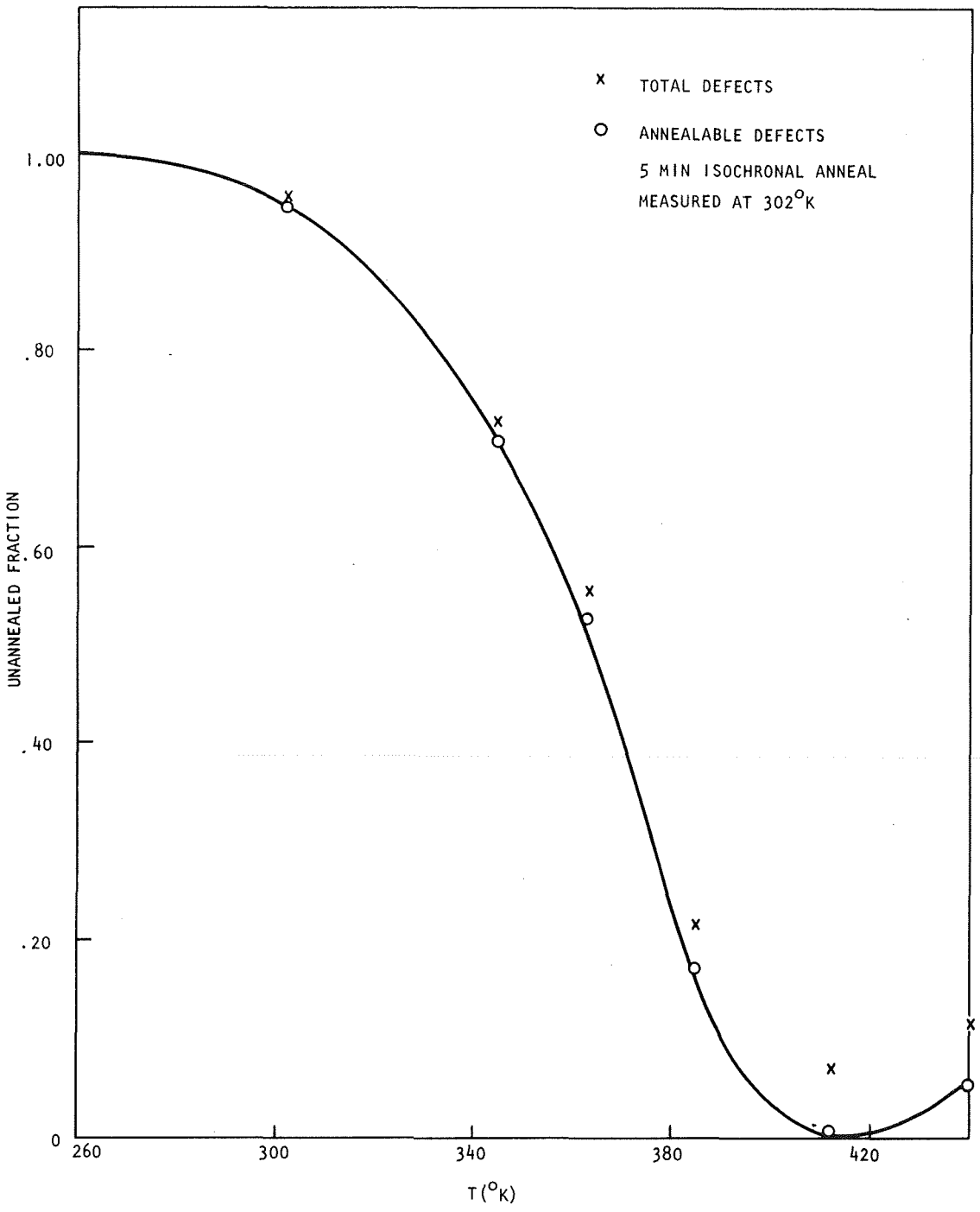


Fig. 29. Unannealed fraction versus isochronal anneal temperature for neutron-irradiated 3.7-ohm-cm sample b

5.5.3.4. Analysis and Conclusions. A number of conclusions can be made concerning the data obtained in the neutron irradiation. First, the degradation constants of this lithium-diffused n-type silicon irradiated at 273 and 302°K are equal and independent of the fluence to 2 x $10^{11}$ $n/cm^2$. This value of the degradation constant is nearly the same as for silicon which contains no lithium,[29] which is consistent with the lack of impurity dependence for neutron damage[30] and is to be contrasted with our previous observation that the degradation constant for electron-irradiated n-type silicon depends on lithium concentration.[1] These observations imply that the defects introduced by neutron irradiations are intrinsic defects, i.e., clusters, as expected. Second, more than 90% of the neutron damage was annealed at temperatures between 300 and 380°K. (From Stein's data,[29] one would expect less than 10% recovery for non-lithium-diffused n-type silicon subjected to the same annealing schedule.) This finding is in contrast to the insignificant annealing impurity dependence observed for phosphorus- and arsenic-doped n-type silicon. Third, the effective frequency factor of $\nu \sim 10^7$ $sec^{-1}$ for this annealing indicates a process involving long-range migration.[20] Finally, the activation energies determined from isothermal and isochronal anneals agree and are very close to E = 0.66±0.05 eV for the energy of lithium diffusion in silicon.[31-33] This observation strongly suggests that the anneal depends on the diffusion of lithium to the neutron-produced recombination centers.

A paper describing the above results is to be published in Radiation Effects.[34]

# 6. STUDY OF THE DETAILED NATURE OF DEFECTS

## 6.1. ELECTRON SPIN RESONANCE

### 6.1.1. Introduction

Electron spin resonance has been an important technique in the study of radiation effects in silicon, since ESR is one of the few techniques[35] which provides information about the detailed nature of the defects. At GGA, ESR has been successfully used in programs[10,19,36,37] investigating the production, annealing, and properties of various damage centers, including the Si-B1, Si-G6, Si-G7, and Si-G8 centers. Recently, the ESR technique has been used to study the effect of lithium in radiation damage. A thorough investigation of the effect of lithium on the B-1 (oxygen-vacancy) center was completed under an earlier contract.[10] This study was of particular value, since many investigators feel that the B-1 center is the predominant recombination center in silicon irradiated with 1-MeV electrons. The results of this study provided invaluable insight into the interaction of lithium with radiation-produced entities including impurity-related defects.

During the present contract period, the ESR technique was used to gain more fundamental information on the role of lithium in displacement damage processes. The first study performed was an investigation of the effects of lithium on the production and annealing of the divacancy (Si-G7). The second study was an investigation of the effects of lithium on the production and annealing of the vacancy-phosphorus (Si-G8) center.

### 6.1.2. Experimental Apparatus

To achieve the contract goals, an ESR apparatus was assembled. The microwave plumbing for the superheterodyne ESR spectrometer was

assembled as shown in Fig. 30. Microwave power from the LFE 814 stable oscillator is split at the "magic tee" into the cavity and reference arms of the spectrometer. This bridge arrangement is first nulled using the attenuator and phase shifter in the reference arm; then it is tuned away from null using only the phase shifter, thus producing a bridge sensitive to the dispersion mode. Microwave power is reflected from the reference and sample arms into the detection arm of the bridge.

The ESR signal and the local oscillator signals are fed into a magic tee balanced mixer. This unit takes the difference of the two signals and provides a 60-Mc IF signal which can be amplified electronically by the IF amplifier. This signal is then fed into a PAR 121 phase-sensitive detector, where it is demodulated from the 1-kc audiofrequency-field modulation signal and finally displayed on a strip-chart recorder.

The ESR samples were placed in an aluminum cavity operating in the $TE_{101}$ mode. The cavity was in a dewar which allowed data to be taken at 20°K.

### 6.1.3. Theory

6.1.3.1. Divacancy. The divacancy is an important damage center to study, since it is thought to be one of the recombination centers present in silicon after high-energy electron and neutron irradiation. This center is believed to have three electrical levels within the forbidden gap. These levels are located at 0.17 and 0.4 eV below the conduction band and at 0.25 eV above the valence band. If the Fermi level is (1) above 0.17 eV, the divacancy is in a double negative charge state and nonparamagnetic; (2) between 0.17 and 0.4 eV, the divacancy is in a single negative charge state and paramagnetic; and (3) below 0.4 eV, the divacancy is neutral and nonparamagnetic.[35,38] For n-type silicon, the level below the middle of the forbidden gap is always filled and

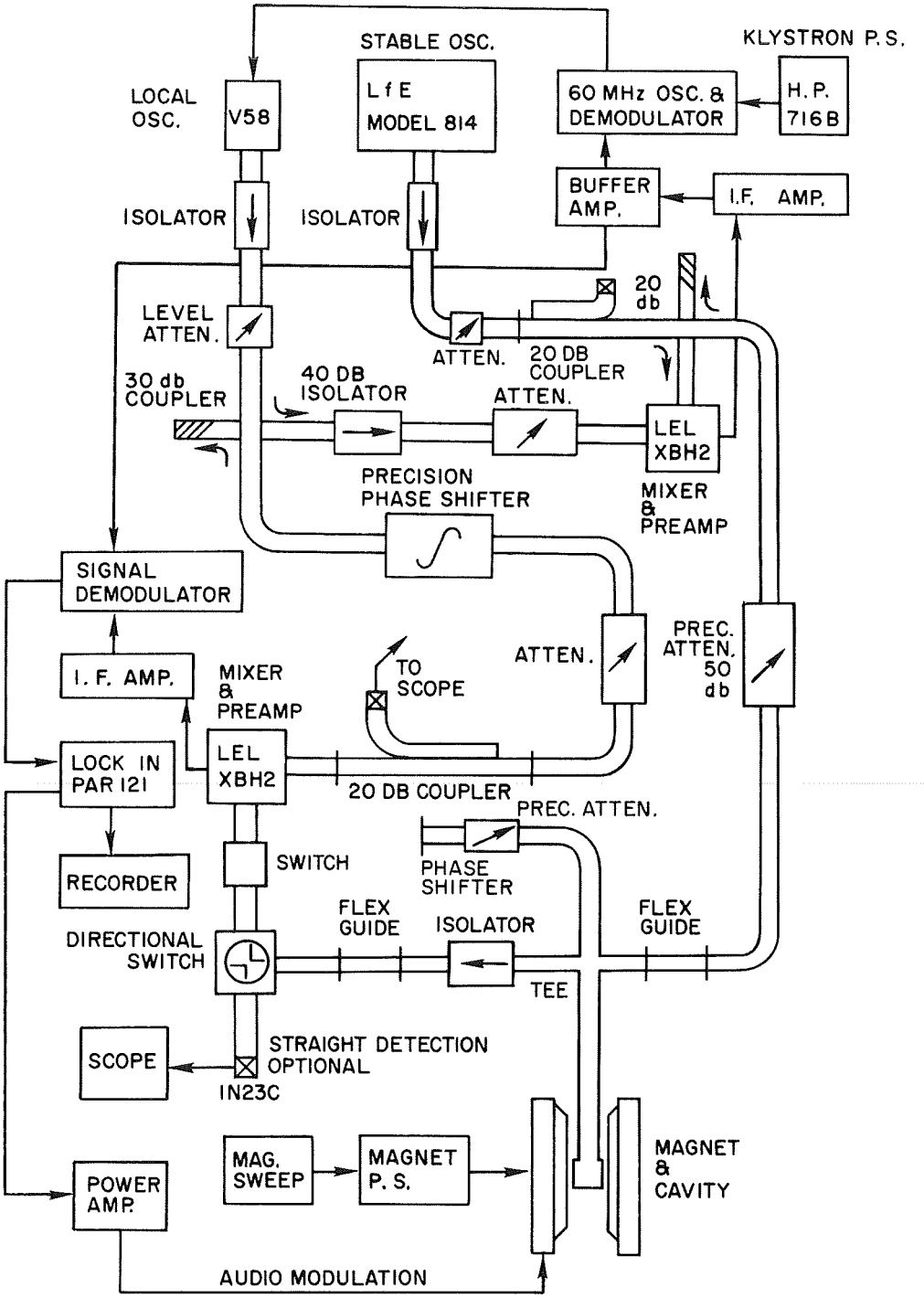


Fig. 30. ESR spectrometer for studies of lithium-doped silicon

is not observable by the ESR technique. The principal values for the diagonalized divacancy g-tensor (Si-G7) are $g_1$ = 2.0012, $g_2$ = 2.0135, and $g_3$ = 2.0150, with $\Phi$ = 29° from the [011] axis in the (011) plane.[35]

6.1.3.2. Si-G8 (Vacancy-Phosphorous). The vacancy-phosphorus is a recombination center which is thought to consist of one electrical level about 0.4 eV below the conduction band. If the Fermi level is above this level, the Si-G8 center is in a single negative charge state and is nonparamagnetic; however, if the Fermi level is below 0.4 eV, the center is in a neutral charge state and is paramagnetic. Thus, the Si-G8 center is better suited than the divacancy to study by ESR because it is paramagnetic over a much wider fluence range. The principal values in the diagonalized Si-G8 g-tensor are $g_1$ = 2.0005, $g_2$ = 2.0112, and $g_3$ = 2.0096, with $\Phi$ = 32° from the [011] axis in the (011) plane.[35]

### 6.1.4. Samples

Samples for the ESR studies were produced by the diffusion of lithium in float-zone n-type silicon. The lithium paint-on technique was used to diffuse lithium into the samples. Samples prepared ranged in resistivity from 0.11 to 0.66 ohm-cm, which corresponds to a room temperature carrier concentration from $10^{17}$ to $10^{16}$ carriers/cm$^3$.

The samples used during this work are described in Table 2. Irradiation was performed with 30-MeV electrons from the GGA Linac facility. All the ESR samples had volumes of about 0.023 cm$^3$ and were oriented (using light reflection patterns from an etched crystal face) along the <111> and <110> crystal axes.

### 6.1.5. Divacancy Study

Samples 1, 2, and 3 were irradiated with 30-MeV electrons to fluences of 1 x $10^{16}$, 2 x $10^{16}$, and 3 x $10^{16}$ e/cm$^2$. Immediately after the room temperature irradiations, the samples were stored in liquid nitrogen.

TABLE 2
SAMPLES USED IN ESR STUDIES

| Sample Number | Resistivity Before Lithium Diffusing (ohm-cm) | Resistivity After Lithium Diffusing (ohm-cm) | Irradiation Temperature ($^{o}K$) | Fluence at End of Irradiation No. 1 ($e/cm^2$) | Fluence at End of Irradiation No. 2 ($e/cm^2$) |
|---|---|---|---|---|---|
| 1 | $10^4$ (high-purity) | 0.66 | 300 | $1x10^{16}$ | --- |
| 2 | $10^4$ (high-purity) | 0.66 | 300 | $2x10^{16}$ | --- |
| 3 | $10^4$ (high-purity) | 0.66 | 300 | $3x10^{16}$ | --- |
| 4 | $10^4$ (high-purity) | 0.11 | 77 | $1.2x10^{17}$ | $2.8x10^{17}$ |
| 5 | $10^4$ (high-purity) | 0.11 | 77 | $1.6x10^{17}$ | $3.2x10^{17}$ |
| 6 | $10^4$ (high-purity) | 0.11 | 77 | $2.0x10^{17}$ | $4.0x10^{17}$ |
| 7 | 0.54 (phosphorus-doped) | --- | --- | --- | --- |
| 8 | 0.54 (phosphorus-doped) | 0.16 | --- | --- | --- |
| 9 | 0.54 (phosphorus-doped) | 0.16 | 77 | $0.9x10^{17}$ | $1.9x10^{17}$ |
| 10 | 0.54 (phosphorus-doped) | 0.16 | 77 | $1.2x10^{17}$ | $2.2x10^{17}$ |
| 11 | 0.54 (phosphorus-doped) | 0.16 | 77 | $1.5x10^{17}$ | --- |

The samples were briefly brought to room temperature for resistivity measurements using a four-probe apparatus. The room temperature resistivities, carrier concentrations, and Fermi levels are given in Table 3. The Fermi level and conduction electron density were determined from the postirradiation room temperature resistivity. Previous measurements[10] yield an approximate divacancy introduction rate of

$$\frac{\Delta n}{\Delta \Phi} = 0.1 \frac{\text{divacancies}}{\text{e-cm}} \quad . \tag{30}$$

The divacancy density was estimated from the introduction rate and the measured fluence. The density of paramagnetic divacancies at 20°K was also estimated. Any annealing of the divacancy because of lithium migration due to the room temperature irradiation was neglected in the above estimates since it was thought to be insignificant.

The results of the estimates predicted that at 20°K, sample 1 should have had about $1 \times 10^{15}$ divacancies/cm$^3$ in the double negative charge state, sample 2 should have had $1.85 \times 10^{15}$ divacancies/cm$^3$ in the single negative charge state, and sample 3 should have had only $3.6 \times 10^{14}$ divacancies/cm$^3$ in the single negative charge state. On this basis, only sample 2 contained enough paramagnetic divacancies to be seen in our ESR spectrometer, since the noise level of the spectrometer[39] is $4 \times 10^{14}$ spins/cm$^3$. However, when sample 2 was inserted into the ESR spectrometer and a careful search was made for the signal above the noise level of the spectrometer, no resonance peak was observed. Part of this search was concentrated at a magnetic field of 3312 gauss parallel to the <111> axis, where a predicted[39] signal with a signal-to-noise ratio of 3.6 should have been observed. No resonances were observed in any of the three samples when they were searched over several magnetic field directions and over a range of magnetic field strength corresponding to g values of $1.9825 \leq g \leq 2.0150$.

TABLE 3
ACCUMULATIVE ELECTRON FLUENCE FOR SAMPLES 1, 2, AND 3

| Sample Number | Fluence ($e/cm^2$) | Postirradiation Resistivity at 300°K (ohm-cm) | Carrier Concentration (number/$cm^3$) | Fermi Level (eV below conduction band) |
|---|---|---|---|---|
| 1 | $1x10^{16}$ | 2.9 | $1.5x10^{15}$ | 0.26 |
| 2 | $2x10^{16}$ | 35 | $1.5x10^{14}$ | 0.32 |
| 3 | $3x10^{16}$ | 9900 | $\sim10^{12}$ | $\sim$0.45 |

The results of these experiments point to three possible conclusions:

1. The divacancies had a lower introduction rate due to the effect of the presence of lithium.

2. The divacancies were in a nonparamagnetic charge state.

3. There was significant annealing of the divacancy during the irradiation due to migration of lithium to the divacancies.

To eliminate the possibility of thermal annealing due to the migration of lithium to the divacancy, it was decided to perform the irradiations at 77°K and to store the sample at this temperature. Three ESR samples (No. 4, 5, and 6) were prepared from $10^4$-ohm-cm, float-zone n-type silicon. After lithium diffusion, each had a room temperature resistivity of 0.11 ohm-cm corresponding to a carrier concentration of $10^{17}$ $cm^{-3}$. The total defect introduction rate and divacancy introduction rate are different at 77°K than at 300°K, so to establish these rates it was decided to irradiate samples 4, 5, and 6 in small fluence steps.

Samples 4, 5, and 6 were examined at 20°K in the ESR spectrometer following irradiations 1 and 2, but no paramagnetic resonances were detected. Thus, either (1) the introduction rate of the divacancies was too low, or (2) the divacancies produced were in the wrong charge state; i.e., they were nonparamagnetic instead of paramagnetic.

For the purpose of determining the introduction rate of paramagnetic divacancies, consider sample 6 at the end of irradiation 1 (total fluence of $2 \times 10^{17}$ $e/cm^2$). The calculated noise level for this sample is $5 \times 10^{14}$ $spins/cm^3$. Since no divacancy <111> axis signal was detected, the divacancy introduction rate must be less than 0.004 divacancy/e-cm. Otherwise, the <111> peak should have been detected. Previous data[36] on a 0.1-ohm-cm, phosphorus-doped float-zone silicon sample irradiated

at 77°K with 30-MeV electrons yielded a divacancy introduction rate of 0.04 divacancy/e-cm, which is well above the apparent introduction rate of paramagnetic divacancies in lithium-diffused silicon provided that all divacancies which are produced are paramagnetic. This implies that the divacancy introduction rate at 77°K is at least an order of magnitude lower for lithium-diffused silicon than in phosphorus-doped silicon.

Another possible reason for not observing divacancies is that although the introduction rate of divacancies may be the same for lithium-diffused silicon as for non-lithium-diffused silicon (0.04 divacancy/e-cm) at 77°K, the divacancies were not detected in the ESR spectrometer because they were in a nonparamagnetic charge state. Observation of the cavity Q (which is related to the sample resistivity) as a function of fluence indicated that a carrier removal rate of 0.5 $cm^{-1}$ or a fluence of 2 x $10^{17}$ $e/cm^2$ was required to substantially depopulate the conduction band, but no divacancies were observed up to this fluence. After irradiation to a fluence of 2.8 x $10^{17}$ $e/cm^2$, sample 4 was examined at 0°C with a two-probe resistivity measuring device and was found to have less than $10^{12}$ carriers/$cm^3$. This means that the Fermi level is below 0.4 eV, so that nearly all the divacancies in this sample were in a neutral charge state and, therefore, not paramagnetic at the 20°K ESR measurement temperature. Thus, for these samples, the divacancy is in the paramagnetic charge state for some fluence between 1.2 x $10^{17}$ and 2.8 x $10^{17}$ $e/cm^2$. Furthermore, the limited range of fluences (or window) over which the divacancies are paramagnetic must be less than the 4 x $10^{16}$ $e/cm^2$ fluence increments between the samples for irradiation 2, or less than the 8 x $10^{16}$ $e/cm^2$ between irradiation 1 (sample 6) and irradiation 2 (sample 4). An estimate of the probable fluence range is about 1.1 x $10^{16}$ $e/cm^2$ for samples 4, 5, and 6. With a fluence range of only about 0.11 x $10^{17}$ $e/cm^2$ for a fluence of 2 x $10^{17}$ $e/cm^2$, it is easy to miss the range on irradiations 1 and 2 for samples 4, 5, and 6.

The temperature of samples 4, 5, and 6 was not raised above 77°K because the elimination of the possibility of migration of lithium to the divacancies was important.

After irradiation 2, sample 6 was illuminated with an incandescent light for 3 hr while in the spectrometer cryostat at 20°K in an attempt to change the charge state of the divacancies from nonparamagnetic to paramagnetic. At temperatures near 20°K, the time constants for returning to equilibrium can be very long;[36] therefore, populated divacancies (paramagnetic) would exist for long periods of time. If this were true, then the ESR signals of these paramagnetic centers would be seen. However, in this experiment on sample 6, no resonance was observed after the illumination.

A final attempt to observe the divacancy in lithium-diffused silicon was performed. The sample which had been irradiated to a fluence of $4 \times 10^{17}$ e/cm$^2$ at 77°K was warmed to room temperature and held for 25 hr and again examined in the ESR spectrometer. Still no divacancy resonance was detected. This experiment was performed on the speculation that the divacancy would appear after sufficient annealing due to breakup of a complex containing lithium and the divacancy.

To make the ESR measurement when the divacancies are in the paramagnetic charge state for irradiation at 77°K would require continuous resistivity measurements on a sample of ever-increasing resistivity. Once all the divacancies were put into the paramagnetic charge state, no true annealing experiments could successfully be made, since other experiments[1,40] indicate an increase in resistivity upon annealing which lowers the Fermi level. This would make the divacancies nonparamagnetic and reduce the ESR signal. When this happened, it would not be possible to determine whether the divacancies disappeared due to the migration of lithium or due to the depopulation of vacancies by Fermi-level motion.

6.1.6. Vacancy-Phosphorus Study

At this point in the program, experimental attention was directed to an investigation of the Si-G8 (vacancy-phosphorus) center in lithium-diffused silicon. A thin slice was cut from a float-zone refined silicon boule which had been doped with $1.1 \times 10^{16}$ phosphorus atoms per cubic centimeter. This slice was carefully oriented along the <111> and <110> crystal axes, and an ESR sample (No. 7) was cut from it. The rest of the slice was lithium-diffused to a concentration of $3.6 \times 10^{16}$ lithium atoms per cubic centimeter, using the lithium-oil paint-on technique. This procedure gave a lithium-to-phosphorus concentration ratio of about 3.3. Four 0.0232-$cm^3$ ESR samples (No. 8-11) were cut from this material.

The effect of the lithium diffusion on the number of paramagnetic phosphorus donors was determined by comparing samples 7 and 8 in the ESR spectrometer at 20°K. It was found that the lithium diffusion reduced the number of paramagnetic phosphorus donors by about a factor of 3. We have no explanation for this reduction.

Samples 9 and 10 were irradiated in the Linac at 77°K to fluences of $0.9 \times 10^{17}$ and $1.2 \times 10^{17}$ $e/cm^2$, respectively. These fluences were chosen because the carrier removal rate at 77°K, obtained from the divacancy study, was 0.5 $cm^{-1}$, and because all free carriers must be removed from the conduction band for the Si-G8 center to be in the paramagnetic charge state. Examination of sample 10 in the ESR spectrometer indicated that not enough electrons had been removed from the conduction band to ensure that the Si-G8 center would be in the paramagnetic charge state.

Samples 9 and 10 were returned to the Linac and irradiated again at 77°K, which raised their accumulated fluences to $1.9 \times 10^{17}$ and $2.2 \times 10^{17}$ $e/cm^2$, respectively. At these fluence levels, both samples had high resistivities at 77°K, indicating that enough electrons had been

removed from the conduction band to place the Si-G8 center in its paramagnetic charge state. Based on previous experimental measurements,[1] the minimum Si-G8 center introduction rate was estimated to be 0.1 $cm^{-1}$ at 77°K. There can be no more Si-G8 centers than the initial phosphorus density of $1.1 \times 10^{16}$ $cm^{-3}$ permits, and our noise level was $5 \times 10^{14}$ $spins/cm^3$. Therefore, the above fluences were expected to give signal-to-noise ratios of about $1/2(1.1 \times 10^{16}$ $Si\text{-}G8/cm^3)/(5 \times 10^{14}$ $spins/cm^3) \approx 10$, including a factor of one-half to account for line splitting.

A careful search over the expected Si-G8 center g values of 1.99700 to 2.01400 revealed nothing. Thus, the presence of lithium in this phosphorus-doped sample has, at least, reduced the Si-G8 center introduction rate below

$$2 \times \frac{5 \times 10^{14} \text{ spins/cm}^3}{1.9 \times 10^{11} \text{ e/cm}^2} \simeq 0.005 \text{ cm}^{-1} \quad . \tag{31}$$

6.1.7. New Center

Continuing the examination of samples 9 and 10 at 20°K in the ESR spectrometer revealed an unknown paramagnetic radiation damage center whose range of g values was below that of the free electron (2.0023). This unknown center had a good signal-to-noise ratio; and comparison with a marker containing $5.14 \times 10^{14}$ spins gave a defect concentration of approximately $1 \times 10^{16}$ centers/$cm^3$. This indicates a 77°K introduction rate of approximately 0.04 $cm^{-1}$.

The strip-chart recording of ESR signal amplitude versus magnetic field (or g value) is presented in Fig. 31. Note that the individual lines of the spectrum are not resolved, but are broadened and merged into one general overall envelope. The most probable reason for this resonance-line broadening is nonhomogeneous broadening caused by the

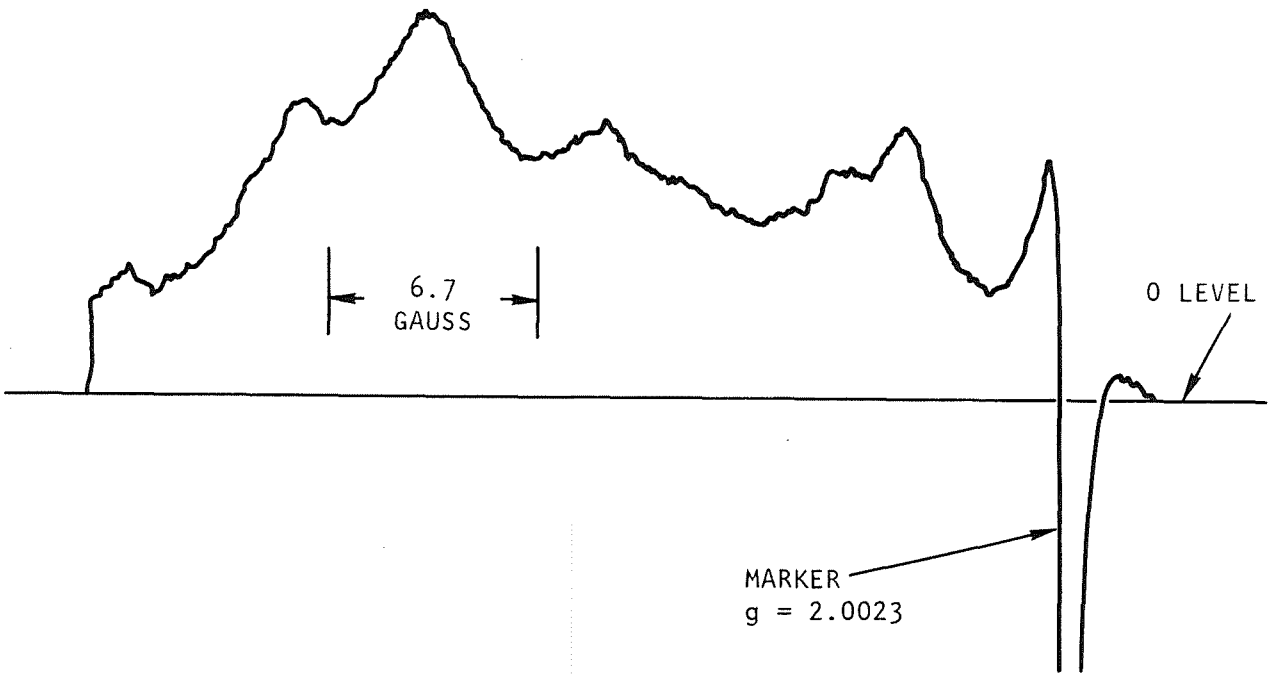


MAGNETIC FIELD ALIGNED ALONG THE <111> CRYSTAL AXIS

Fig. 31. Strip-chart recording of ESR signal amplitude versus magnetic field

overlapping of several individual resonance lines, which then merge into one overall envelope. An example of nonhomogeneous broadening is that caused by hyperfine structure, or line splitting, due to the magnetic interaction between the nuclear magnetic moment and the unpaired electron.[41]

It is possible that the spectrum of Fig. 31 was caused by the misorientation of the sample with respect to the magnetic field. However, this is considered unlikely since the sample orientation was checked by X-ray diffraction and was found to be within 3° of the desired <110> orientation.

In short, the broadening of the resonance lines in Fig. 31 makes it difficult to find the principal values and axis of the g-tensor (and the amount of hyperfine splitting described by the A-tensor).

This ESR spectrum was further investigated on the supposition that it is not just one center, but a superposition of more than one center. To investigate this possibility, one of the samples was annealed in stages to 473°K and examined after each stage in the hope that annealing would reduce the number of centers by causing some to become nonparamagnetic or to physically anneal. No change in either the magnitude or character of the resonance signal resulted from annealing to 423°K. The unknown center disappeared after a 15-min anneal at 473°K. It is tempting to assume that this center is a phosphorus-lithium complex, since it was not seen in the lithium-diffused high-purity silicon samples previously examined. However, one cannot rule out the possibility that the addition of the phosphorus had widened the fluence range in which this center is paramagnetic, allowing the center to be seen for the first time.

### 6.1.8. Conclusions

The study of the divacancy (Si-G7) in lithium-diffused silicon indicates that for room temperature (300°K) irradiations, the divacancy

is affected by the presence of lithium. The overall effect of lithium is to decrease the number of divacancies present after a 300°K irradiation. The lithium either lowers the introduction rate of divacancies or anneals the divacancies once they are formed. Earlier work[1] has shown that both of these mechanisms are present in B-1 center production and annealing.

The ESR measurements of the divacancy were performed after irradiations at 77°K in the hope of separating the mechanisms responsible for the decrease in the number of divacancies observed after room temperature irradiations of lithium-diffused n-type silicon. These experiments were inconclusive for the reasons described above.

The absence of the Si-G8 center for 30-MeV electron irradiations at 77°K leads to the conclusion that the presence of lithium is effective in decreasing the number of this center. Since lithium diffuses very slowly at 77°K, the decrease in the introduction rate of the Si-G8 center is not due to its annealing by lithium. The reasons for the lower introduction rate may be:

1. The vacancies produced by the irradiation are preferentially attracted to the lithium instead of the phosphorus because of the larger cross sections of the lithium than the phosphorus for the vacancies.

2. The phosphorus is paired with the lithium and therefore is not free to combine with the vacancies to produce Si-G8 centers.

The arguments for the decreased introduction rates of the Si-G8 centers are the same as those for Si-B1 centers.[1] However, in the Si-B1 center studies, oxygen was present in the samples instead of phosphorus.

The ESR studies of the Si-G7, Si-G8, and Si-B1 centers yield the same basic result. The introduction rate of these centers in lithium-diffused silicon is decreased for 300°K electron irradiations. However, the reason for the decrease is not completely understood for each center, and the reasons may even be different for each center.

Since these centers are considered as recombination centers in electron-irradiated non-lithium-diffused silicon, there is a possibility of decreasing the lifetime degradation in silicon due to the presence of lithium. However, experimental measurements of the lifetime degradation constant in heavily lithium-diffused silicon for 1-MeV[42] and 30-MeV[1] electrons yield values equal to or larger than those found for non-lithium-diffused silicon. This implies that in electron irradiations of heavily lithium-diffused silicon, a new recombination center is produced which degrades the lifetime at the same rate or faster than the Si-G7, Si-G8, or Si-B1 center. It is most probable that this new recombination center contains lithium or is affected in its production by lithium.

A new ESR center has been observed in lithium-diffused phosphorus-doped silicon irradiated with 30-MeV electrons. The nature of this center is not known at the present time.

## 6.2. INFRARED ABSORPTION STUDIES

As described in Section 6.1.5, ESR was used to search for the divacancy in lithium-diffused silicon. No resonance was observed. It was concluded that the reason for this failure was due to either a lower divacancy introduction rate in lithium-diffused silicon or the presence of divacancies in a nonparamagnetic charge state. To resolve this uncertainty, a short infrared absorption study was carried out.

The infrared absorption measurements were performed using a Perkin-Elmer Model 112 double-pass prism spectrometer. This instrument is

equipped with various light sources (a tungsten lamp and a Globar), prisms (glass, fused quartz, NaCl, and CsBr), and detectors (photoconductive cells and thermocouples) that allow it to cover the wavelength region from ultraviolet to about 30 μ. The spectrometer has been modified so that the monochromatic beam can be extracted and the sample positioned in either the monochromatic beam or the white light.

Infrared absorption is less sensitive than ESR, requiring approximately $10^{16}$ defects/cm$^3$ for bands to be observed. However, this technique has the advantage that the divacancy bands[43] are observed regardless of the divacancy charge state. The sample studied was the most heavily irradiated one, having received a dose of $4 \times 10^{17}$ e/cm$^2$. It was optically investigated at room temperature following a room temperature anneal of several days. The room temperature resistivity of the sample indicated that the Fermi level was deep enough so that the divacancy was not in its double-negative charge state, and thus the absorption band would be located at a wavelength of 1.8 μ.[43] The sample was placed in the white light beam of the Perkin-Elmer spectrometer and observed using fused quartz and NaCl prisms in the wavelength region from 1 to 4 μ.

The spectra taken in these measurements show no evidence of the divacancy absorption band. This means that less than $10^{16}$ divacancies/cm$^3$ are present in the sample. If no annealing occurred, the maximum divacancy introduction rate was 0.2 cm$^{-1}$, which is a factor of two lower than rates measured for non-lithium-diffused material.

It should be noted in this connection that there was an indication in the spectra of an absorption band at 1.4 μ which has been associated with lithium perhaps interacting with the divacancy.[44] This observation may indicate that some divacancies were eliminated by the room temperature anneal.

# 7. SUMMARY OF CONCLUSIONS

## 7.1. NEUTRON ACTIVATION ANALYSIS STUDY

Electrical resistivity measurements and NAA results tend to suggest that for the low-lithium-content (less than $10^{17}$ $cm^{-3}$) samples, the lithium is present in the samples as singly ionized donors. For the NAA study, the low-lithium-content samples were diffused by the lithium-tin bath technique. However, for the high-lithium-content (greater than $10^{17}$ $cm^{-3}$) samples, the NAA indicates that significantly more lithium may be present in certain samples than was determined by resistivity measurements. These high-lithium-content samples were produced by the lithium paint-on technique.

## 7.2. MINORITY-CARRIER LIFETIME STUDIES

### 7.2.1. 30-MeV Electron Irradiations

In the minority-carrier lifetime study of electron-irradiated, float-zone, lithium-diffused n-type silicon, the lifetime temperature dependence, degradation rate, and annealing characteristics were measured. Both lightly diffused ($n_0 \simeq 4.5 \times 10^{14}$ $cm^{-3}$) and heavily diffused ($n_0 \simeq 1.5 \times 10^{16}$) samples were investigated. From these studies, the following conclusions can be drawn:

1. The initial preirradiation lifetime of lightly diffused silicon is due to at least two centers. Its temperature dependence indicates that one center is near $E_c$ - 0.17 eV, and that the other is an attractive center deeper than 0.35 eV from either band edge. Because the initial conduction electron concentration

in the heavily diffused silicon was so high, the minority-carrier lifetime temperature dependence could not distinguish between the two centers if both were present. Our measurements on heavily diffused silicon indicate that an attractive center is deeper than $E_c$ - 0.17 eV.

2. At least two kinds of recombination centers are introduced in lightly diffused silicon by the 30-MeV electron irradiation: one dominant at temperatures above 150 to 200°K and the other dominant below 150 to 200°K. The recombination centers in heavily diffused silicon are not well located but are deeper than $E_c$ - 0.17 eV. The introduction rate of these individual centers cannot be determined until the charge state of the centers is established, since the capture cross section for neutral and attractive centers can differ by an order of magnitude.

3. The room temperature minority-carrier lifetime degradation constant for heavily diffused silicon was approximately three times that for lightly diffused silicon. The increased degradation constant of heavily lithium-diffused silicon compared with that of non-lithium-diffused silicon is interpreted to indicate that the presence of lithium is effective in the production of recombination centers in lithium-diffused silicon. These recombination centers either contain lithium or are affected in their production by lithium.

4. In lightly diffused silicon, the dominant postirradiation-preanneal center at low temperatures (less than 200°K) has an energy level near $E_c$ - 0.17 eV, and the dominant postirradiation-preanneal center at high temperatures (greater than 200°K) is deeper than 0.35 eV from either band edge.

5. The annealing of the recombination centers in lightly irradiated heavily diffused silicon is complete; i.e., all the recombination centers are annealed. The annealing times are consistent with results of previous work. However, after extended fluences the annealing of the recombination centers is not complete; i.e., not all the recombination centers are annealed.

6. In lightly diffused silicon, the radiation-induced center at $E_c$ - 0.17 eV which is dominant at low temperatures was not annealed in 1 hr at 390°K but appears to anneal, at least partially, over long periods at room temperature and seems to anneal completely in more highly diffused samples.

7. In lightly diffused silicon, the radiation-induced high-temperature center is significantly annealed in the presence of lithium.

8. Successive irradiations and anneals could shift the low-temperature portion of the minority-carrier lifetime curve downward and to higher temperatures. Thus, at some fluence, the dominant low-temperature center might become dominant at room temperature, perhaps changing the subsequent room temperature damage constants and annealing characteristics. This phenomenon may be related to the incomplete annealing observed in heavily irradiated heavily diffused silicon and electron-irradiated lithium-diffused silicon solar cells.

9. In general, it appears that in electron-irradiated, lithium-diffused, float-zone n-type silicon, both lithium-dependent and non-lithium-dependent recombination centers are produced. The number of each depends on the lithium concentration, with

the largest number of lithium-dependent centers being found in highly diffused silicon and the largest number of non-lithium-dependent centers being found in lightly diffused silicon.

10. No irradiation temperature dependence of the recombination center introduction rate for 30-MeV electrons in the 115 to 300°K temperature range was observed.

11. The minority-carrier lifetime degradation constant for lithium-diffused samples irradiated and measured at 300°K is an order of magnitude smaller than that for samples irradiated and measured at 115°K.

### 7.2.2. Fission Neutron Irradiations

A number of observations can be made concerning the results of minority-carrier lifetime studies in fission-neutron-irradiated lithium-diffused silicon. First, the degradation constants for this lithium-diffused n-type silicon irradiated at 273 and 302°K are equal and independent of the fluence to $2 \times 10^{11}$ n/cm$^2$. This value of the degradation constant is nearly the same as for silicon containing no lithium, which is consistent with the lack of impurity dependence for neutron damage and is in contrast to this laboratory's observation that the degradation constant for electron-irradiated n-type silicon depends on lithium concentration. These observations imply that the defects introduced by neutron irradiations are intrinsic defects, i.e., clusters, as expected. Second, more than 90% of the neutron damage was annealed at temperatures between 300 and 380°K. From Stein's data, one would expect less than 10% recovery for non-lithium-diffused n-type silicon subjected to the same annealing schedule. This is to be contrasted with the insignificant annealing impurity dependence observed for phosphorus- and arsenic-doped n-type silicon. Third, the effective

frequency factor of $\nu \sim 10^7$ $sec^{-1}$ for this annealing indicates a process involving long-range migration. Finally, the activation energies determined from isothermal and isochronal anneals agree and are very close to E = 0.66±0.05 eV for the energy of lithium diffusion in silicon. This strongly suggests that the anneal depends on the diffusion of lithium to the neutron-produced recombination centers.

## 7.3. ELECTRON SPIN RESONANCE AND INFRARED ABSORPTION STUDIES

The study of the divacancy (Si-G7) in lithium-diffused silicon indicates that the divacancy is affected by the presence of lithium. The overall effect of lithium is to decrease the number of divacancies present after irradiation. The lithium either lowers the introduction rate of divacancies or anneals the divacancies once they are formed. This conclusion was verified by the results of an infrared absorption study. Earlier work has shown that both of these mechanisms are present in the production and annealing of the B-1 center.

The absence of the Si-G8 center for 30-MeV electron irradiations at 77°K leads to the conclusion that the presence of lithium is effective in decreasing the number of these centers. Since lithium diffuses very slowly at 77°K, the decrease in the introduction rate of the Si-G8 center is not due to annealing of the center by lithium. The reasons for the lower introduction rate are:

1. The vacancies produced by the irradiation are preferentially attracted to the lithium instead of the phosphorus because of the larger cross sections of the lithium than the phosphorus for the vacancies.

2. The phosphorus is paired with the lithium and therefore is not free to combine with the vacancies to produce Si-G8 centers.

The arguments for the decreased introduction rates of the Si-G8 centers are the same as those for Si-B1 centers. However, in the Si-B1 center studies, oxygen was present in the samples instead of phosphorus.

The ESR studies of the Si-G7, Si-G8, and Si-B1 centers yield the same basic result. The introduction rate of these centers in lithium-diffused silicon is decreased for 300°K electron irradiations. Since these centers are considered as recombination centers in electron-irradiated non-lithium-diffused silicon, there is a possibility of decreasing the lifetime degradation in silicon due to the presence of lithium. However, experimental measurements of the lifetime degradation constant in heavily lithium-diffused silicon for 30-MeV electron irradiations yield values equal to or larger than those for non-lithium-diffused silicon. This result implies that in electron irradiations of heavily lithium-diffused silicon, a new recombination center is produced which degrades the lifetime at the same rate or faster than the Si-G7, Si-G8, or Si-B1 center. It is most probable that this new recombination center contains lithium or is affected in its production by lithium.

A new ESR center has been observed in lithium-diffused phosphorus-doped silicon irradiated with 30-MeV electrons. The nature of this center is not known at the present time.

## 8. RECOMMENDATIONS

The following activities are recommended in the continuing investigation of the radiation effects in silicon solar cells:

1. Continue the current investigation of minority-carrier lifetime in bulk, lithium-diffused, float-zone silicon of various resistivities before and after electron and neutron irradiations and anneals to determine (a) the density and nature of recombination centers before irradiation, (b) the nature and introduction rate of radiation-induced recombination centers, and (c) the annealing behavior of these centers.

2. Supplement this program with irradiations at reduced temperatures to determine the introduction rates, the annealing properties, and the nature of the defects produced by irradiations at temperatures between 77 and 450°K.

3. Investigate the annealing of electron and neutron radiation-induced recombination centers in lithium-diffused silicon at anneal temperatures above 400°K to explore the possibility of reverse annealing. If possible, relate this study to "redegradation."

4. Perform studies on lithium-diffused quartz-crucible-grown silicon as outlined in items 1, 2, and 3 for float-zone-grown silicon.

5. Continue the investigation of the radiation-induced defects by means of ESR studies. These studies would emphasize the nature and mechanisms for production and annealing in lithium-diffused silicon of defects known to be produced in non-lithium-diffused silicon. Where observable, the nature of lithium-related defects should be studied.

6. Use optical studies in conjunction with the ESR technique to obtain additional information on the nature of the defects, and their introduction and annealing, in lithium-diffused silicon.

7. Develop techniques making it possible to predict the performance of silicon solar cells in an irradiation environment. With minor modifications, available computer codes can be used to make these predictions from basic materials parameters and the effect of radiation on these parameters.

## 9. NEW TECHNOLOGY

No new technology is currently being developed or employed in this program.

## REFERENCES


1. Naber, J. A., H. Horiye, and V. A. J. van Lint, "Radiation Effects on Silicon. Final Report," NASA Report GA-8668, Gulf General Atomic Incorporated, August 20, 1968.
2. Reiss, H., and C. S. Fuller, J. Metals 8, 276 (1956).
3. Valdes, L. B., Proc. IRE 42, 420 (1954).
4. Berman, P. A., "Status of Lithium Solar Cell Development," in Record of the Seventh Photovoltaic Specialists' Conference, IEEE Publication No. 68C63ED, New York, 1968.
5. Lukens, H. R., and V. P. Guinn, "The Ultrasensitive Determination of Lithium by Neutron Activation Analysis," in Proceedings of the Second International Symposium on Nucleonics in Aerospace, Columbus, July 1967 (to be published).
6. Lukens, H. R., and J. K. MacKenzie, Trans. Am. Nucl. Soc. 10, 86 (1967).
7. Irvin, J. C., Bell System Tech. J. XLI, 387 (1962).
8. Ferman, J. W., and R. A. Swalin, in Proceedings of the Fourth International Conference on Reactivity of Solids, Elsevier, Amsterdam, 1961, J. H. DeBoer (ed.).
9. Kalenowski, J. J., and R. K. Thatcher (eds.), "TREE (Transient-Radiation Effects on Electronics) Handbook," Defense Atomic Support Agency Report DASA-1420, 1969.
10. Naber, J. A., H. Horiye, and E. G. Wikner, "Radiation Effects on Silicon. Summary Report, November 1, 1965 through April 20, 1967," NASA Report GA-8016, General Dynamics, General Atomic Division, June 20, 1967.
11. Kittel, C., Introduction to Solid State Physics, John Wiley & Sons, New York, 1963.
12. Nomura, K. C., and J. S. Blakemore, Phys. Rev. 112, 1607 (1958).
13. Nomura, K. C., and J. S. Blakemore, Phys. Rev. 121, 734 (1961).

14. van Lint, V. A. J., et al., "Radiation Effects on Silicon Solar Cells. Technical Summary Report, May 16, 1963 through October 15, 1963," NASA Report NASA-CR-56563, General Dynamics, General Atomic Division, December 4, 1963.
15. van Lint, V. A. J., et al., "Radiation Effects on Silicon Solar Cells. Final Report," NASA Report NASA-CR-50098, General Dynamics, General Atomic Division, February 15, 1963.
16. Shockley, W., and W. T. Read, Jr., Phys. Rev. 87, 835 (1952).
17. Leadon, R. E., and J. A. Naber, J. Appl. Phys. 40, 2633 (1969).
18. Lax, M., Phys. Rev. 119, 1502 (1960).
19. van Lint, V. A. J., and D. P. Snowden, "Radiation Effects on Silicon. Final Report, June 1, 1964 through May 31, 1965," NASA Report NASA-CR-69568, General Dynamics, General Atomic Division, July 21, 1965.
20. Damask, A. C., and G. J. Dienes, Point Defects in Metals, Gordon and Breach, New York, 1963.
21. Nakashima, K., and Y. Inuishi, Japan. J. Appl. Phys. 7, 965 (1968).
22. Bochet, J. C., et al., "Photoconductivity Study of Annealing of Radiation Defects in Lithium-Doped Silicon," in Record of the Seventh Photovoltaic Specialists' Conference, IEEE Publication No. 68C63ED, New York, 1968.
23. Brucker, G. J., T. Faith, and A. Holmes-Siedle, "Injection Level Effects in Irradiated Lithium-Containing Solar Cells," in Record of the Seventh Photovoltaic Specialists' Conference, IEEE Publication No. 68C63ED, New York, 1968.
24. Stein, H. J., and F. L. Vook, "Electron-Induced Defects in n-Type Silicon," in Proceedings of the Santa Fe Conference on Radiation Effects in Semiconductors, Plenum Press, New York, 1968, p. 115.
25. Vook, F. L., and H. J. Stein, "Production of Defects in n-Type Silicon," in Proceedings of the Santa Fe Conference on Radiation Effects in Semiconductors, Plenum Press, New York, 1968, p. 99.
26. Stein, H. J., and F. L. Vook, Phys. Rev. 163, 790 (1967).
27. Gregory, B. L., and C. E. Barns, "Defect Reordering at Low Temperatures in Gamma Irradiated n-Type Silicon," in Proceedings of the Santa Fe Conference on Radiation Effects in Semiconductors, Plenum Press, New York, 1968, p. 124.

28. Curtis, O. L., Jr., R. F. Bass, and C. A. Germo, "Impurity Effects in Neutron-Irradiated Silicon and Germanium," U.S. Army Materiel Command, Harry Diamond Laboratories, Report NARD-65-20R, Northrup Nortronics Applied Research, November 1965.
29. Stein, H. J., J. Appl. Phys. 37, 3382 (1966).
30. Curtis, O. L., Jr., IEEE Trans. Nucl. Sci. NS-13, 33 (1966).
31. Pell, E. M., J. Appl. Phys. 31, 291 (1960).
32. Fuller, C. S., and J. C. Severiens, Phys. Rev. 96, 21 (1960).
33. Maita, J. P., J. Phys. Chem. Solids 4, 68 (1958).
34. Passenheim, B., and J. Naber, "Minority-Carrier Lifetime Degradation and Anneal in Neutron-Irradiated Lithium-Diffused n-Type Silicon," Radiation Effects (to be published).
35. Watkins, G. D., "A Review of EPR Studies in Irradiated Silicon," in Proceedings of Seventh International Conference on the Physics of Semiconductors, Radiation Damage in Semiconductors, Dunod, Paris, 1965, p. 97.
36. Wikner, E. G., et al., "Transient Radiation Effects. Final Report," U.S. Army Materiel Command, Harry Diamond Laboratories, Report GA-7607, General Dynamics, General Atomic Division, 1967 (AD-808-797).
37. Flanagan, T. M., et al., "Transient Radiation Effects. Final Report," U.S. Army Materiel Command, Harry Diamond Laboratories, Report GA-8338, Gulf General Atomic Incorporated, December 1967, p. 76 (AD-838-975).
38. Leadon, R. E., et al., "Research on the Physics of Transient Radiation Effects," U.S. Army Materiel Command, Harry Diamond Laboratories, Report GA-9334, Gulf General Atomic Incorporated, 1969.
39. Berger, R. A., et al., Gulf General Atomic Incorporated, "Study of Radiation Effects in Silicon Solar Cells," unpublished data.
40. Naber, J. A., et al., "Production and Annealing of Defects in Lithium-Diffused Silicon after 30-MeV Electron Irradiation at 30°K," in "Proceedings of the Conference on Effects of Lithium Doping on Silicon Solar Cells, May 9, 1969," Jet Propulsion Laboratory Report JPL-TM-33-435, August 15, 1969.
41. Watkins, G. D., and J. W. Corbett, Phys. Rev. 121, 1601 (1961).
42. Wysocki, J. J., IEEE Trans. Nucl. Sci. NS-14, 103 (1967).

43. Cheng, L. J., et al., Phys. Rev. 152, 761 (1966).
44. Young, R. C., J. W. Westhead, and J. C. Corelli, J. Appl. Phys. 40, 271 (1969).